National Library of Canada
Acquisitions and Bibliographic Services Branch
395 Wellington Street
Ottawa, Ontario
K1A 0N4

Bibliothèque nationale du Canada
Direction des acquisitions et des services bibliographiques
395, rue Wellington
Ottawa (Ontario)
K1A 0N4

NOTICE

The quality of this microform is heavily dependent upon the quality of the original thesis submitted for microfilming. Every effort has been made to ensure the highest quality of reproduction possible.

If pages are missing, contact the university which granted the degree.

Some pages may have indistinct print especially if the original pages were typed with a poor typewriter ribbon or if the university sent us an inferior photocopy.

Reproduction in full or in part of this microform is governed by the Canadian Copyright Act, R.S.C. 1970, c. C-30, and subsequent amendments.

AVIS

La qualité de cette microforme dépend grandement de la qualité de la thèse soumise au microfilmage. Nous avons tout fait pour assurer une qualité supérieure de reproduction.

S'il manque des pages, veuillez communiquer avec l'université qui a conféré le grade.

La qualité d'impression de certaines pages peut laisser à désirer, surtout si les pages originales ont été dactylographiées à l'aide d'un ruban usé ou si l'université nous a fait parvenir une photocopie de qualité inférieure.

La reproduction, même partielle, de cette microforme est soumise à la Loi canadienne sur le droit d'auteur, SRC 1970, c. C-30, et ses amendements subséquents.

Canada

The Structural, Thermal, and Magnetic Properties of Mn_2SiS_4.

by

Christopher J. Church

Thesis submitted to the School of Graduate Studies of the University of Ottawa in partial fulfillment of the requirements for the degree of Master of Science.

Department of Physics
Faculty of Science
University of Ottawa
Ottawa, Canada

1994

© University of Ottawa,1994


Christopher J. Church, Ottawa, Canada, I994

National Library of Canada
Acquisitions and Bibliographic Services Branch
395 Wellington Street
Ottawa, Ontario
K1A 0N4

Bibliothèque nationale du Canada
Direction des acquisitions et des services bibliographiques
395, rue Wellington
Ottawa (Ontario)
K1A 0N4

Your file Votre référence

Our file Notre référence

THE AUTHOR HAS GRANTED AN IRREVOCABLE NON-EXCLUSIVE LICENCE ALLOWING THE NATIONAL LIBRARY OF CANADA TO REPRODUCE, LOAN, DISTRIBUTE OR SELL COPIES OF HIS/HER THESIS BY ANY MEANS AND IN ANY FORM OR FORMAT, MAKING THIS THESIS AVAILABLE TO INTERESTED PERSONS.

L'AUTEUR A ACCORDE UNE LICENCE IRREVOCABLE ET NON EXCLUSIVE PERMETTANT A LA BIBLIOTHEQUE NATIONALE DU CANADA DE REPRODUIRE, PRETER, DISTRIBUER OU VENDRE DES COPIES DE SA THESE DE QUELQUE MANIERE ET SOUS QUELQUE FORME QUE CE SOIT POUR METTRE DES EXEMPLAIRES DE CETTE THESE A LA DISPOSITION DES PERSONNE INTERESSEES.

THE AUTHOR RETAINS OWNERSHIP OF THE COPYRIGHT IN HIS/HER THESIS. NEITHER THE THESIS NOR SUBSTANTIAL EXTRACTS FROM IT MAY BE PRINTED OR OTHERWISE REPRODUCED WITHOUT HIS/HER PERMISSION.

L'AUTEUR CONSERVE LA PROPRIETE DU DROIT D'AUTEUR QUI PROTEGE SA THESE. NI LA THESE NI DES EXTRAITS SUBSTANTIELS DE CELLE-CI NE DOIVENT ETRE IMPRIMES OU AUTREMENT REPRODUITS SANS SON AUTORISATION.

ISBN 0-612-00524-0

Canada

UNIVERSITÉ D'OTTAWA
UNIVERSITY OF OTTAWA

ABSTRACT

Mn_2SiS_4 is a synthetic Olivine in which we have discovered an exceptional temperature dependent magnetic behavior that may lead to interesting applications. A state of spontaneous magnetization was found to exist in this material, but only between 83 and 86.5 K.

In order to explain this unusual magnetic phenomena, polycrystalline samples of Mn_2SiS_4 were first prepared from the elements and studied by SQUID magnetometry in low fields, by X-ray and neutron diffraction, by electron spin resonance (ESR) and by specific heat calorimetry. The origin of this rare magnetic behavior was completely uncovered by analyzing in detail the neutron diffraction spectra obtained at 29 different temperatures between 4.2 and 150 K to reveal and explain the magnetic phase diagram of Mn_2SiS_4. Up to 83 K, the Mn^{++} ions are ordered antiferromagnetically. At 83 K there is an abrupt transition to a weak-ferromagnetic arrangement resulting from small angle canting of the two spin sublattices giving rise to the observed spontaneous magnetization. There is another transition some 3 degrees higher at 86.5 K, where the spins become disordered. Above 86.5 K the material is in the paramagnetic phase.

The transition at 86.5 K is a commonly encountered order-disorder transition but the one at 83 K consists of a rarely observed transition between two different magnetically ordered phases not accompanied by any crystal structure change; only the magnetic space group changes at that point from Pnma to Pn'm'a. It was considered important to investigate the effects that two such transitions, coexisting near each other, may have on other physical properties.

In such magnetic materials, Mn^{++} ions are known to give rise to a wide ESR line in the high temperature paramagnetic region. In general the linewidth increases in an exponential fashion as the transition to the ordered phase is approached from above. In a series of measurements done from room temperature down to 77 K it was observed that the

linewidth increased as the order-disorder transition was approached, passed through a maximum slightly above the 86.5 K transition and then decreased rapidly below the spontaneous magnetization region. This observation has not yet received an explanation on a microscopic scale since the theory of these wide ESR lines has not been successfully developed yet.

As for the specific heat, it is well known that its measurement is a powerful means of studying magnetic transitions. The transition at 86.5 K corresponding to an order-disorder transition is expected to give a lambda-type anomaly whose detailed analysis yields some information on the dimensionality and nature of the magnetic spin system while the transition at 83 K between two ordered phases would be expected to be of the first order and allow an evaluation of its latent heat which may be important from the point of view of applications.

This research, in which the author was a member of a team, is described. His specific contributions include among others; the debugging and extension of some of the computer programs used to analyze the neutron diffraction results, the interfacing of the Bruker ESR spectrometer to a IBM compatible computer and the development of the computer programs to acquire the resonance curves and analyze the line spectra, the analysis of the ESR results, the assembly of parts of an apparatus and the development of a procedure to measure the specific heat of small samples in the 77 to 150 K range as well as some preliminary measurements on a sample of Mn_2SiS_4. These contributions are emphasized in this thesis.

ACKNOWLEDGMENTS

I would like to acknowledge Dr. Gilles Lamarche, my supervisor and Madame Anne-Marie Lamarche and Dr. John Woolley for their contibutions of knowledge, guidance, and support; Dr. Thomas Holden whose contribution was as our liaison to the Chalk River facility; Dr. Ian Swainson who assisted in the manipulation of neutron diffraction spectra; Dr. Alain Junod et al. of the University of Geneva, for performing specific heat measurements and analysis on our sample; Roger Chagnon for all his help with desktop publishing and word processing software; and my wife Karen Currie Church, whose love and support made the completion of this thesis possible. Partial fininancial support from Dr. Lamarche's NSERC grant is gratefully acknowledged.

Table of Contents

Introduction 1

Chapter 1 STRUCTURE & SUSCEPTIBILITY 4
- 1.0 Introduction 4
- 1.1 Crystal structure 4
- 1.2 Sample Preparations 7
- 1.3 Magnetic Susceptibility 7
- 1.4 Conclusion 11

Chapter 2 NEUTRON DIFFRACTION 13
- 2.0 Introduction 13
- 2.1 Apparatus 13
- 2.2 Theory 13
- 2.3 Experimental Details 16
- 2.4 Symmetry 19
- 2.5 Results 20
- 2.6 Conclusion 30

Chapter 3 SPECIFIC HEAT 32
- 3.0 Introduction 32
- 3.1 Theory 32
- 3.2 Apparatus & Preliminary Results 35
- 3.3 Results from the University of Geneva 41
- 3.4 Conclusion 45

Chapter 4 ELECTRON SPIN RESONANCE 46
- 4.0 Introduction 46
- 4.1 Lorentzian Lineshape 46
- 4.2 Apparatus 50
- 4.3 ESR Results and Analysis 53
- 4.4 Conclusion 61

Conclusion 63

Reference 65

Appendix A 68
Appendix B 69
Appendix C 71

Table of Figures

Chapter 1

Fig 1.1a 3-d perspective of unit cell showing Octahedra 5
Fig 1.1b Isolated Octahedra 5
Fig 1.2 Orthographic projection of unit cell.....6
Fig 1.3 Susceptibility vs. Temperature (4.2- 250 K).....9
Fig 1.4 Inverse Susceptibility vs. Temperature 10
Fig 1.5 Susceptibility vs. Temperature (80- 90 K).....12

Chapter 2

Fig 2.1 Dualspec Spectrometer.....14
Fig 2.2 Scattering Geometry 16
Fig 2.3 Shubnikov Groups 19
Fig 2.4 International Atom Numbering.....20
Fig 2.5 Neutron Diffraction Profiles 21
Fig 2.6 Profile at 180 K.....22
Fig 2.7 Profile at 4.2 K.....24
Fig 2.8 Intensity vs. Temperature for 001 and 100 lines.....26
Fig 2.9 Intensity vs. Temperature for 110 and 310 lines.....27
Fig 2.10 Profile at 84 K.....28
Fig 2.11 2-Dimensional View of Unit Cell.....31

Chapter 3

Fig 3.1 1-Dimensional Model of Heat Flow 33
Fig 3.2 Apparatus of Calorimeter 36
Fig 3.3a Input Power vs. Temperature 39
Fig 3.3b dT/dt Decay as a Function of Temperature.....39
Fig 3.4 Specific Heat vs. Temperature 42
Fig 3.5 Derivative of Specific Heat vs. Temperature.....43
Fig 3.6 Magnetic Specific Heat vs. Temperature.....44

Chapter 4

Fig 4.1 Lorentzian Derivative Lineshape 47
Fig 4.2 ESR Profile at 106 K.....55
Fig 4.3 ESR Profile at 83 K.....56
Fig 4.4 ESR Linewidth vs. Temperature.....58
Fig 4.5 ESR Amplitude vs. Temperature.....59

The Structural, Thermal, and Magnetic properties of Mn_2SiS_4.

INTRODUCTION

Magnetic ternary and quaternary compounds are known to be materials showing a variety of magnetic properties such as ferro, ferri and antiferro magnetism and have shown potential for applications in the field of semiconductors. In the course of our research group's systematic investigations on polycrystalline quaternary compounds of the form I_2.Mn.IV.VI_4 an unusual magnetic susceptibility behavior was noticed as a function of temperature for a compound prepared as Ag_2MnSiS_4. Through the process of elimination it was later determined that the least common constituents that were responsible for the anomalous behavior was in fact Mn_2SiS_4.

From its similarity with Mg_2SiO_4 whose structure shows an orthorhombic unit cell [22], Mn_2SiS_4 was expected to show analogous structure. By the use of Debye-Scherrer X-rays analysis the crystalline structure of Mn_2SiS_4 was confirmed as being orthorhombic and similar to Mg_2SiO_4.

After having established that it was Mn_2SiS_4 that was responsible for the unusual magnetic behavior in the temperature range of 83 - 86 K, it was also discovered that another compound of similar composition gave similar results: Mn_2GeS_4.

At first the hypotheses put forward to explain the narrow peak in susceptibility observed between 83 and 86 K were: 1) the occurrence of a change of crystal structure at 83 K causing some form of ferri- or weak-ferromagnetism, followed 3 degrees higher by a magnetic transition to paramagnetism or else 2) some form of ferrimagnetism in which the two equal and opposite sublattices have different transition temperatures giving rise to the observed peak in magnetization. Both models had weaknesses, since: 1) a crystal structure change would generally show some sort of magnetic hysteresis on cooling and warming while the experimental

measurements showed essentially no such hysteresis, the field cooled and the zero field cooled measurements showing no appreciable differences. As for the other, 2) the particular form of ferrimagnetism imagined here has never been observed before and it is hard to imagine how one lattice could order, while the other sublattice would not, at any given temperature. The explanation was likely something else.

Since equipment for X-ray investigation as a function of temperature was not available, and more importantly, would not reveal much in term of magnetic structure, it was decided instead to make use of the neutron diffraction technique which is capable of yielding crystallographic and magnetic structure information simultaneously. Another approach, readily available to the research group, was the Electron Spin Resonance technique, in which the linewidth of the signal has been shown to be sensitive to magnetic transitions. Also the lineshape can indicate important changes in the g-factor that occur as a result of changes in crystalline fields due to distortions in the structure. Finally measurements of specific heat would certainly provide some insight on the nature of the transitions at 83 and 86 K and reveal if other transitions, not seen by magnetic susceptibility, were present, at any other temperatures. This last approach required development of a small sample calorimeter.

In this thesis we discuss the structural, thermal and magnetic properties of Mn_2SiS_4 as they became known by use of various methods of investigation. The first chapter gives a description of the crystal structure of this olivine and gives 3 dimensional views of a model of the atom positions in the unit cell. Then some details of the preparation of Mn_2SiS_4 are given, followed by the results of magnetic susceptibility measurements obtained with a SQUID magnetometer. The second chapter contains an account of the neutron diffraction experiment done at Chalk River, the analysis of the data, and includes a brief description of the computer programs used to predict the diffraction lines positions and intensities and to refine the parameters of the crystallographic and magnetic structures.

The specific heat measurement experiment is described in the third chapter. It gives details of the apparatus assembled and the procedures

developed as well as preliminary results obtained. Unfortunately it was not possible to obtain the thermometric resolution necessary for conclusive results. The delay expected to remedy this problem was much longer than acceptable for the completion of a master thesis. It was decided, nevertheless to include this section in the thesis as the apparatus built and the procedures developed will be used later, once the proper equipment becomes available. To complete the description of the thesis subject a brief account of the specific heat results obtained elsewhere on our sample is given, since it has not yet been published as of the time of the writing of this thesis.

The fourth chapter contains the details of the experiment and analysis of the ESR study done on Mn_2SiS_4. It includes a description of the software and hardware developed to digitize and analyze the ESR signal as well as the results obtained with this approach.

In this thesis all the results obtained by the research group, and not necessarily by the author, are summarized mainly to make the description coherent and to explain the context in which the author's contributions have been made. The contributions consists mainly in the design and implementation of the data acquisition system for the ESR, data analysis of the ESR signal, design, construction, and implementation of the apparatus to measure specific heat, analysis of specific heat data, authoring or co-authoring analysis software for crystal, ESR, and Neutron diffraction data.

Chapter 1

STRUCTURE & SUSCEPTIBILITY

1.0 Introduction:

In this chapter the crystal structure is described giving details of the lattice parameters and atom positions. A 3-dimensional orthographic representation of the unit cell is illustrated. Also the method used in the preparation of the Mn_2SiS_4 sample is outlined. Finally the result of magnetic susceptibility measurements are given.

1.1 Crystal Structure:

Initially X-ray powder diffraction revealed that the compound has the orthorhombic symmetry Pnma and that the lattice parameters corresponded with those found by Fuhrman and Pickardt [18]. The lattice parameters at room temperature are: a = 12.688, b = 7.427, and c = 5.946 Å .

There are 8 Mn++ ions per unit cell which are divided into two sites unrelated by symmetry. Both Mn sites are octahedrally coordinated with the sulphur but each is distorted in different ways (see fig 1.1,1.2). There are the 4a sites which have inversion symmetry and are located at {x,y,z} = {0,0,0}, {0,0.5,0}, {0.5,0,0.5}, {0.5,0.5,0.5} within the unit cell. The 4c sites have mirror symmetry with coordinates {x,y,z} = {0.2295,0.25,0.5105}, {0.7705,0.75,0.4895}, {0.2705,0.75,0.0105}, {0.7295,0.25,0.9895}.

The sides of the octahedra surrounding the 4a atoms have a mean length of 3.6648 Å giving a volume of the octahedra of 23.183 $Å^3$. Conversely, the sides of the octahedra surrounding the 4c atoms have a mean length of 3.7003 Å, giving a volume of the octahedra of 23.884 $Å^3$. The isolated polyhedra are shown in fig 1.1b. In the 4a octahedra the length of the S-S bonds are more uniform than in the 4c case. There are three planes in an octahedra defined by ABCD, EBGD, and AECG for the 4c Mn's, and HLJN, HIJK, and INKL for the 4a Mn's (fig 1.1a). The distortion in the 4c

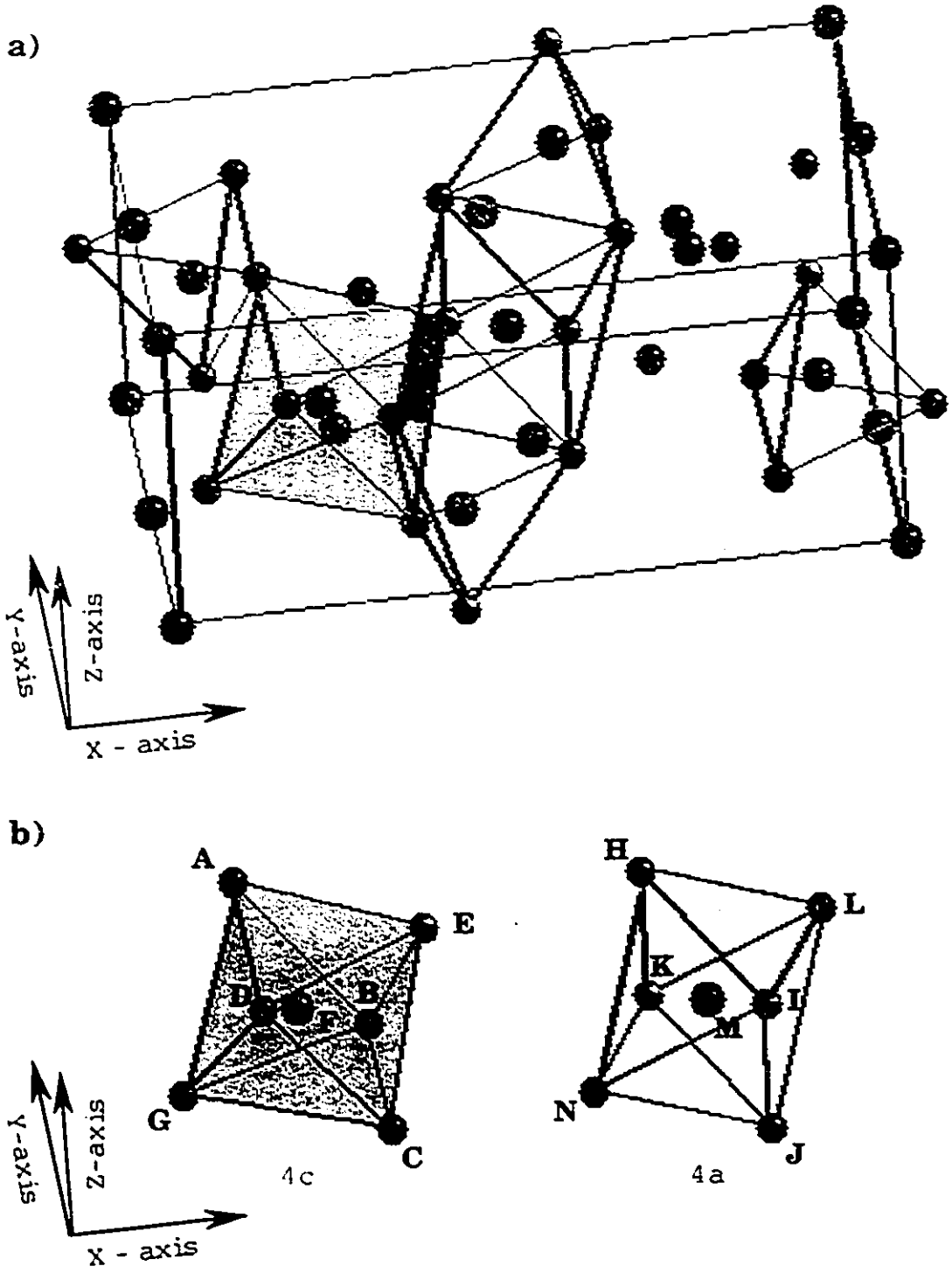

Fig 1.1 a) The orthorhombic structure of Mn_2SiS_4 depicting the octahedra of the 4a and 4c Manganese atoms, b) isolated 4a and 4c octahedra.

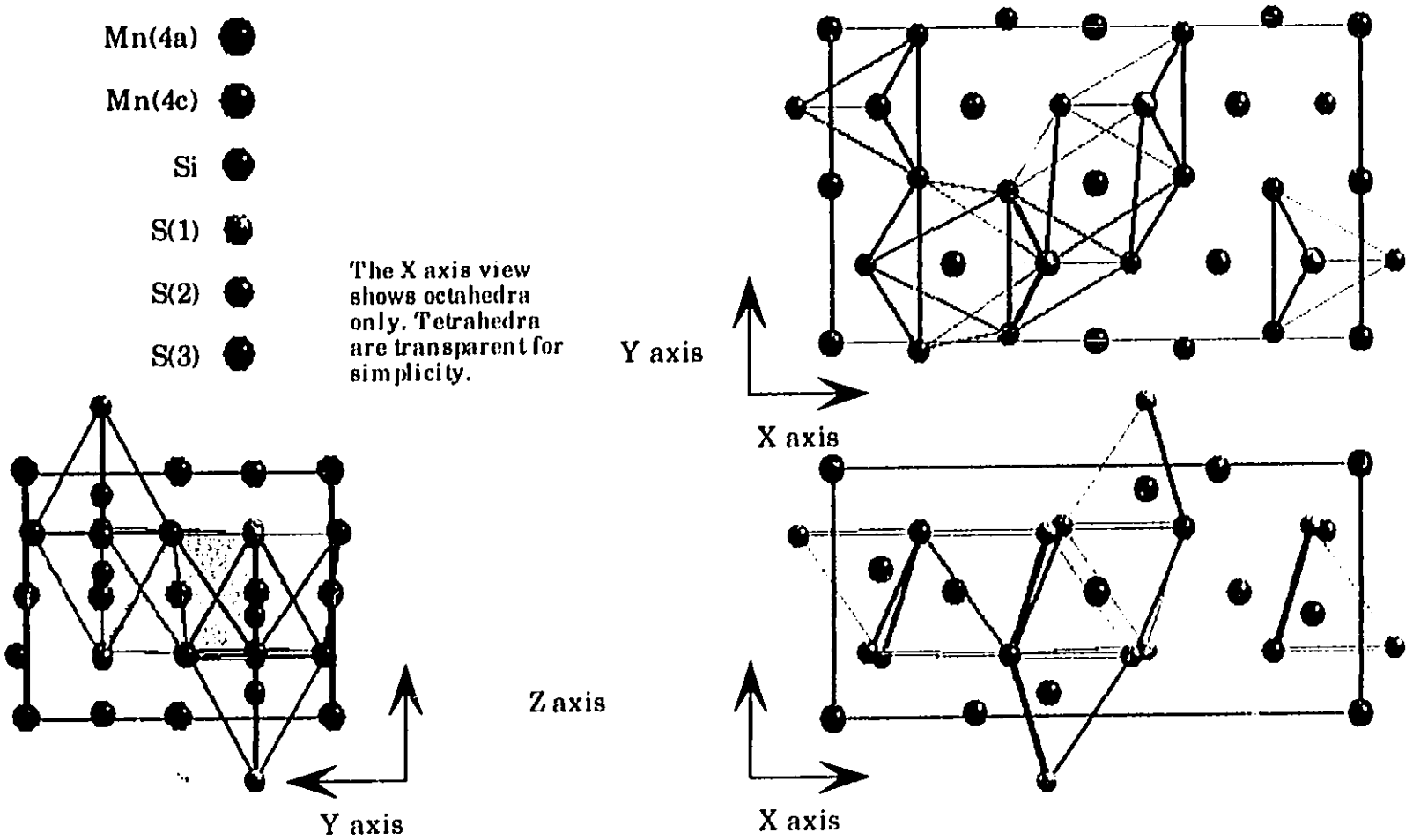

Fig. 1.2 Axial perspectives of crystal structure of M n2SiS4.

octahedra is such that there are no 2 equal lengths within any given plane. In the 4a octahedra there are two pairs of equal lengths forming parallelograms in each of the 3 planes. For the 4c the largest variation in the S-S bond lengths occurred in the ABCD plane ranging from 4.073 to 3.3643 with an average value of 3.703 Å and a standard deviation, $\sigma = 0.25$. The nearest magnetic neighbor for the 4a is another 4a atom with a distance of 3.715 Å while the nearest neighbor for a 4c atom is a 4a atom with a distance of 3.875 Å. The 4c-4c distance is 4.610 Å.

The sulphur atoms have a hexagonal closed packed arrangement that form in layers located at z = 0.25 and z= 0.75 [3]. The 4 silicon atoms in the unit cell are tetrahedrally coordinated by the sulphur atoms.

A program called BONDLNTH was developed for the calculation of the bond lengths. It produces a list of lengths for all the possible atom to atom combinations.

1.2 Sample Preparation:

The Mn_2SiS_4 samples were prepared by combining the powdered elements in stoichiometric proportions in evacuated quartz tubes. These tubes were always carbonized first to prevent the interaction of the manganese with the quartz. The total weight of the combined elements was 1 gram. The sample was slowly heated to a temperature of 1150°C. Through this procedure it was found that an impurity, MnS, was almost invariably produced. In order to compensate for this a silicon excess of 10% was introduced to initial constituents or it was added to the product of the first run. In either case the constituents were subject to the initial process. The samples were then annealed at 540°C for approximately 3 weeks and then quenched at 0°C.

1.3 Magnetic Susceptibility:

The normal or expected values for the susceptibility of transition group elements as a function of temperature follow the Curie or Curie-Weiss laws. Curie's law is obeyed provided it is assumed that the orbital

angular momentum is quenched i.e. L = 0. This phenomenon of quenched orbital angular momentum is a result of crystal field splitting which produces a ground state singlet and excited states which are higher in energy than room temperature.

One of the necessary parameters for a permanent magnetic moment is the existence of uncompensated electrons in an inner shell. This condition is present when a 3d group ion is in a regular or nearly regular octahedral. In addition manganese has an odd number of electrons which is also responsible for a permanent magnetic moment.

It is known that a departure from the Curie and Curie-Weiss laws is possible due to the effects of placing the magnetic ions in a crystalline field where the 3d electrons that are responsible for the paramagnetism of manganese are greatly affected. Crystalline fields have the effect of separating the degenerate levels.

The magnetic susceptibility of samples were measured by the SQUID magnetometer [12]. The measurements were carried out in both zero-field-cooled and field-cooled conditions. The magnetization of Mn_2SiS_4 was measured in the temperature range of 4.2 to 250 K. In fig 1.3 the magnetic susceptibility as a function of temperature in the range stated above is shown.

In fig 1.4 the linear relationship between $1/\chi$ vs. T is easily observed above the Néel temperature T_n, where the sample follows the Curie-Weiss law for paramagnetic materials (eqn 1.1). The Néel temperature is the transition temperature between ordered and disordered states in the case of an antiferromagnetic.[10]

$$\chi = \frac{C}{T - \theta} \qquad 1.1$$

Through linear extrapolation the θ, the paramagnetic Curie-Weiss point is determined to be -200+/-50 K and the Curie constant is 0.013+/-0.002 emu/g. As the temperature decreases towards T_n of 86.5 +/- 0.5 K a

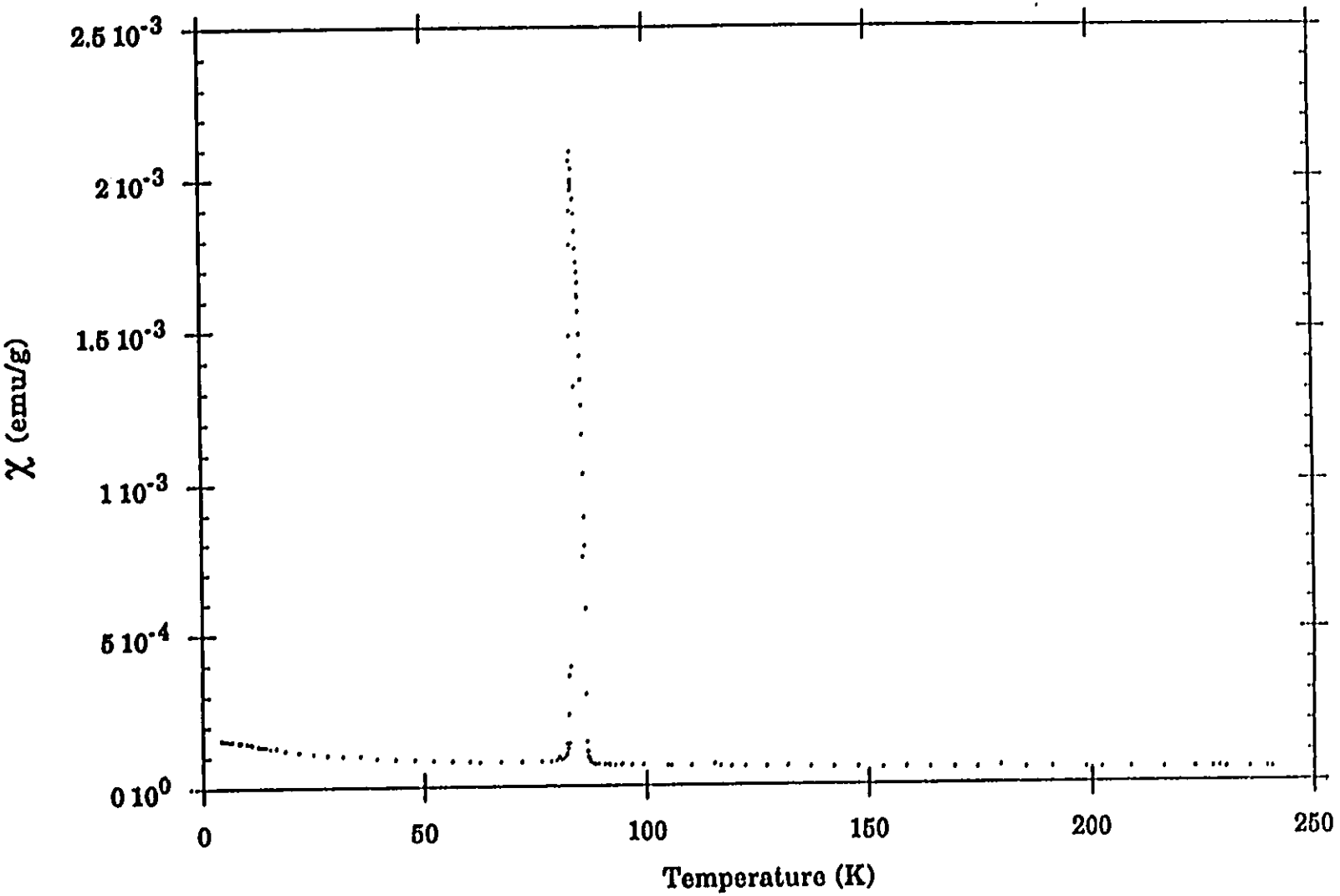

Fig 1.3 Magnetic Susceptiblity of Mn_2SiS_4 as a function of temperature.

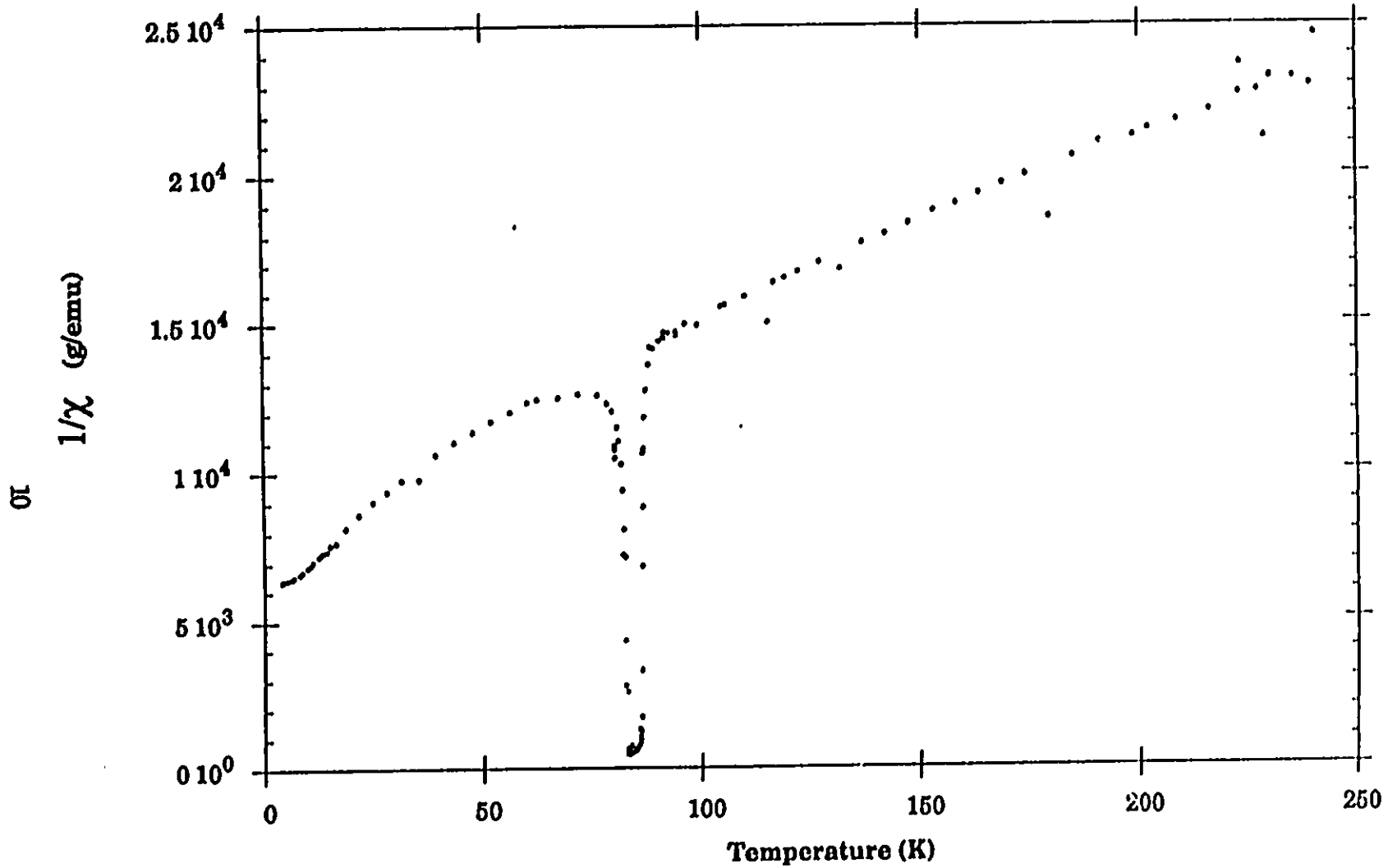

Fig. 1.4 Inverse Susceptibility of Mn_2SiS_4 as a function of temperature.

hyperbolic behavior is observed that is characteristic of a ferri or weak-ferro magnetic transition.

At 86.5 +/- 0.5 K spontaneous magnetization occurs producing an abrupt spike in the susceptibility (see fig 1.5). The magnitude of this susceptibility is ~ 2.1x10-3 emu/g which is of the order of magnitude expected of a ferri or weak ferro-magnetic material. At approximately 83 K the susceptibility drops to a low. This material behaves as an antiferromagnet from 83 K down to 4.2 K showing a negligible susceptibility. This anomalous phenomenon occurred in both zero field cooled and field cooled conditions with no discernible differences.

1.4 Conclusion:

It has been shown that the material Mn_2SiS_4 has an orthorhombic structure having a symmetry of Pnma. There are 8 Mn^{++} ions per unit cell which are divided into two sites, 4a and 4c, unrelated by symmetry. The 4a and 4c Mn++ ions are both octahedrally coordinated and form two interpenetrating substructures, which is one requirement for antiferromagnetism. The lattice parameters of Mn_2SiS_4 are a = 12.688, b = 7.427, and c = 5.946 Å. Based on the magnetic susceptibility results, it can be inferred that the material is in a paramagnetic phase above 86.5 K and that between 83 and 86.5 K it is in a weakly ferromagnetic state and below 83 K the material displays the small susceptibility of an antiferromagnet.

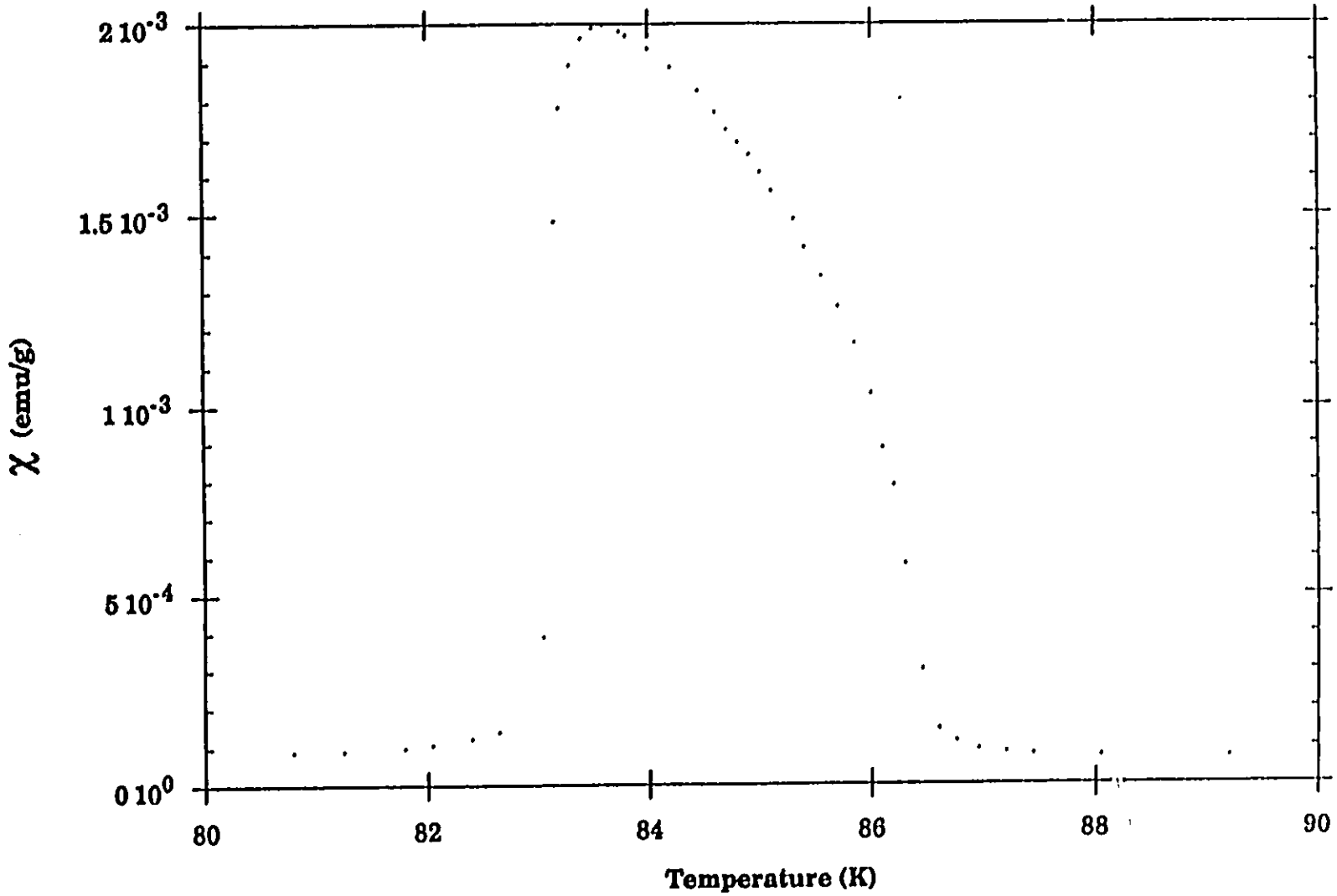

Fig 1.5 Magnetic Susceptiblity of Mn_2SiS_4 as a function of temperature.

Chapter 2

NEUTRON DIFFRACTION

2.0 Introduction:

In order to investigate the possibility of crystal structure changes at 83 - 86 K and to examine the details of the magnetic properties of Mn_2SiS_4 as a function of temperature a powder sample was prepared for neutron diffraction. The neutron diffraction experiments were conducted at the Chalk River Laboratories of the Atomic Energy of Canada Limited in Chalk River Ontario, Canada, using the Dualspec powder diffractometer [24].

2.1 Apparatus:

The basic components of the Dualspec powder diffractometer are illustrated in fig 2.1. The thermal neutrons enter through the aperture in the reactor shielding and then pass through an initial collimator and onto the monochromator. The monochromator, through the Bragg condition, $\lambda = 2d \sin \theta_M$, diffracts a monoenergetic beam of neutrons that have a take-off angle from the incident neutron beam $2\ \theta_M$. The monoenergetic beam then passes through another collimator and then the powder sample which is continuously rotated to ensure isotropic exposure by averaging out the crystal orientations. The sample is suspended inside a cryostat so that the measurement of diffraction spectra can be performed at various temperatures. The diffracted neutrons then go to one of 800 detectors dependent on their angle of diffraction. This produces a spectra like the one shown in fig 2.5.

2.2 Theory:

In the diffraction experiment at Chalk River the sample was exposed to unpolarized neutrons which produce scattering intensities that are the sum of the nuclear and magnetic scattering intensities. The total scattered

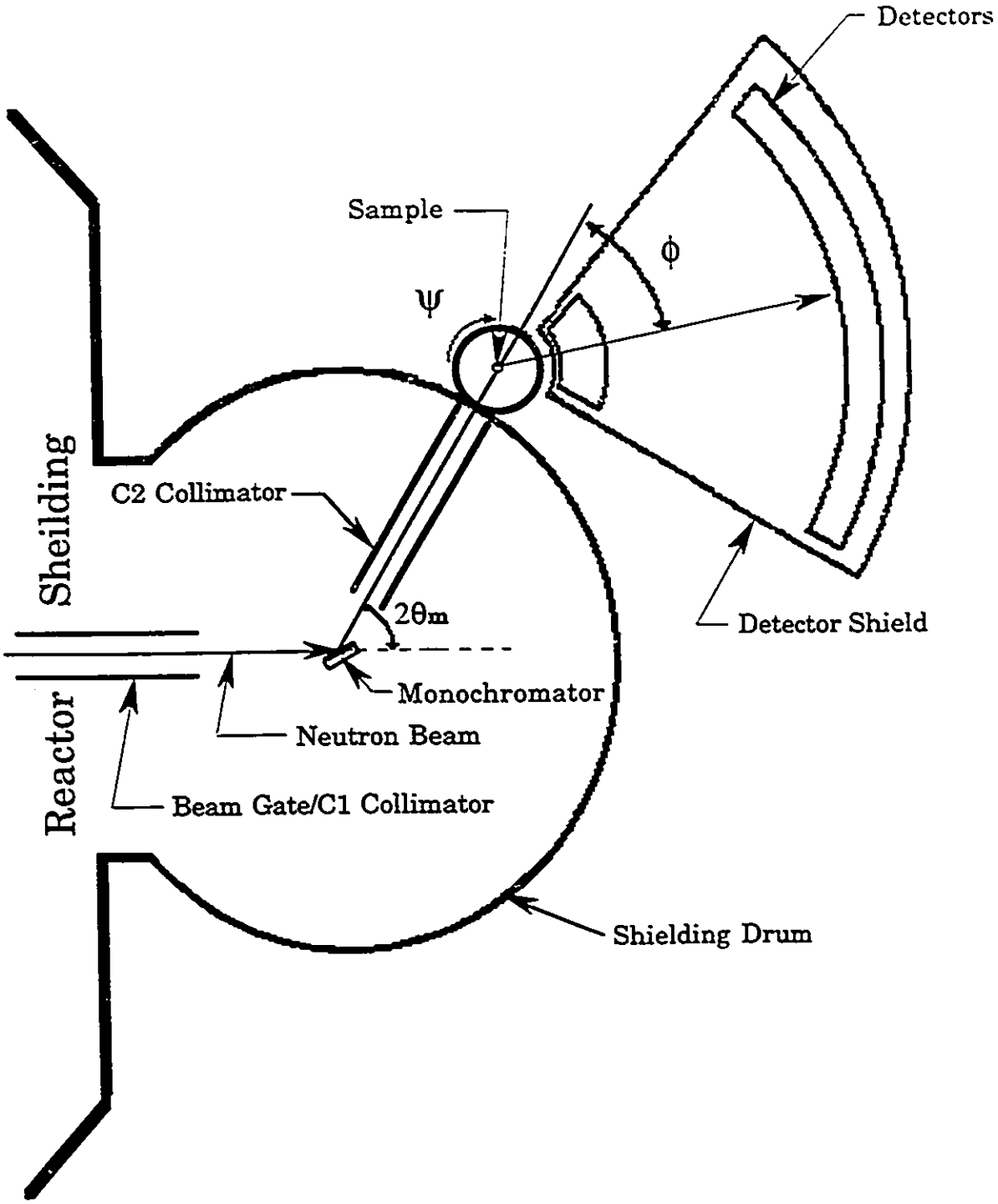

Fig 2.1 Schematic diagram of Dualspec neutron diffraction spectrometer at Chalk River, Ont.

intensity for any reflection can be determined by calculating the effective structure factor $\mathbf{F}^2$ for a unit cell.

$$\mathbf{F}^2=\mathbf{F}^2_{\text{nucl}}+q^2\mathbf{F}^2_{\text{magn}} \qquad 2.1$$

where q is the magnetic interaction vector such that

$$\vec{q}=\vec{\varepsilon}\left(\vec{\varepsilon}\cdot\vec{K}\right)-\vec{K} \qquad 2.2$$

where ε is the scattering vector and $\mathbf{K}$ is the magnetization vector (see fig 2.2) and

$$\mathbf{F}^2_{\text{nucl}}=\left|\sum_{1}^{\text{\# of atoms}} b\,e^{2\pi i\left(\frac{hx}{a_0}+\frac{ky}{b_0}+\frac{lz}{c_0}\right)}\right|^2 e^{-2W} \qquad 2.3$$

and

$$\mathbf{F}^2_{\text{magn}}=\left|\sum_{1}^{\text{\# of magnetic atoms}} p\,e^{2\pi i\left(\frac{hx}{a_0}+\frac{ky}{b_0}+\frac{lz}{c_0}\right)}\right|^2 e^{-2W} \qquad 2.4$$

Here b is the nuclear scattering amplitude, p is the magnetic scattering amplitude and W is the Debye-Waller factor. It should be noted that p can be calculated from magnetic and spectroscopic data while b can only be found experimentally. A listing of values of nuclear scattering is available [28].The magnetic scattering amplitude is given by

$$\mathrm{p}=2\,\mathrm{Sf}(\theta,\lambda)\left(\frac{e^2\gamma}{2mc^2}\right) \qquad 2.5$$

where $f(\theta,\lambda)$ is the form factor and for manganese is equal to

$$f(\theta,\lambda)=e^{-.0561\left(\frac{4\pi\sin\theta}{\lambda}\right)^2} \qquad 2.6$$

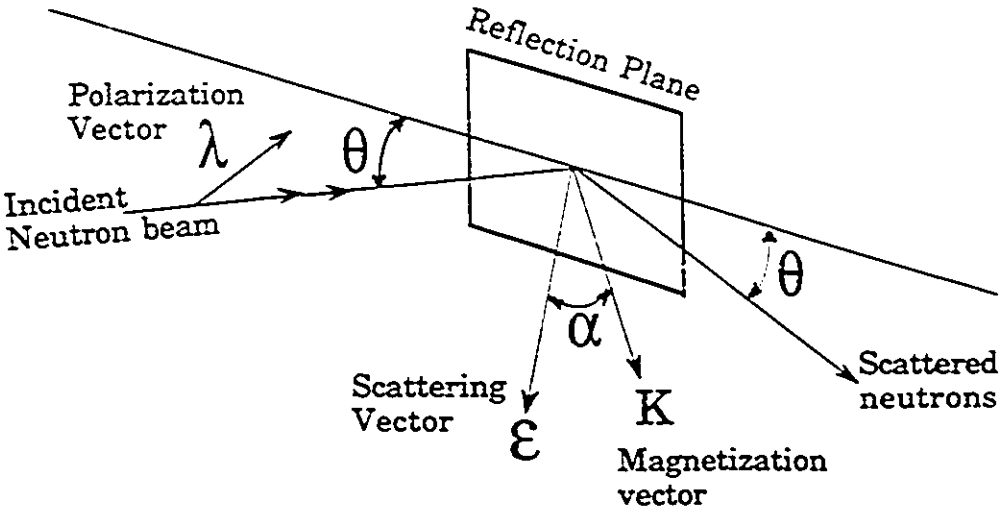

Fig 2.2. Diagram illustrating the geometry of scattering.

2.3 Experimental Details:

There were two separate series of measurements performed at Chalk River. The first series obtained spectra at 4.2, 70, 77 ,79, 80 , 82, 83, 84, 85, 86, 87, 100, 180 K. During this series of measurements the wavelength of the thermal neutrons was 2.6707Å. The temperature variation was performed within a helium bath cryostat. The detection was done in 2 runs; one with the detectors spanning 5 - 85° of arc, and the other spanning 40 - 120° of arc. With 800 detectors this gives an angular resolution of 0.1°.

The second series of measurements were carried out on the same Mn_2SiS_4 powder sample in a closed cycle helium refrigerator. This series of measurements were designed to fill in the gap between 4.2 and 70 K and to get more data in the range of 80 - 86 K. Neutron diffraction was carried out at 12, 30, 40, 50, 60, 70, 80, 83.5, 84.0, 84.5, 85.0, 85.5, 86.0, 86.5, 140 K. The neutron wavelength for this series was 2.6822 Å. To obtain greater resolution some of the measurements were performed twice for the same temperature. In one run the detectors spanned 5 - 85°, and in the second run the detector array was precisely shifted 0.05°. During the second run the same # of total counts were detected with the detector array spanning

5.05 - 85.05°. The data from these two runs were interleaved into one data file that had 1600 points spanning 5 - 85.05°.

These spectra were then used to refine the lattice parameters, atomic positions, and determine magnetic moment orientations. Most of the results were obtained from hand calculation performed by Anne-Marie Lamarche [27]. A relative peak intensity calculation program called POWDER, written by John Roots at AECL Chalk River and the General Structure Analysis System(GSAS) written by Allen C. Larson and Robert B. Von Dreele at Los Alamos National Laboratory were used to assist in the analysis of the spectra.

The analysis of certain spectra were performed using GSAS which is a collection of programs designed to process single crystal and powder diffraction data obtained with x-rays or neutrons [23]. GSAS performs a least squares fit to the observed profile through an iterative process.

GSAS uses Reitveld refinement techniques to analyze the powder diffraction data. Reitveld refinement is a form of least squares minimization based on the difference of the experimental spectra and a theoretical spectra [14]. The theoretical spectra is derived from

$$I_c = I_b + \Sigma Y_h \qquad 2.8$$

where I_b is the intensity due to the background and ΣY_h is the contributions from each of the Bragg reflections (Y_h). Each of these components is based on mathematical models that encompass the crystalline, noncrystalline, and magnetic features of a powder diffraction experiment. Within these mathematical models are parameters that describe the physical system which are refined in order to reduce the least-squares difference between the experimental and theoretical intensities. As a result the final product is a list of parameters, ie., lattice parameters, atom positions, coefficients of background polynomial, profile coefficients, nuclear and magnetic structure factors, etc. that combine in the mathematical models to produce a calculated spectra that is compared to the observed spectra. For a more detailed explanation refer to H. M. Rietveld, J. App. Cryst 2, 65, 1969.

Originally it was expected that the orientation of the magnetic spins of the Mn atom would be easily extracted by running GSAS with the correct input parameters. This was not the case and as such a manual approach was adopted. The determination of relative intensities of observable peaks were performed by combining the results of the program POWDER and manual calculations [27] using eqns 2.1- 2.4 [2], see appendix A for the expanded form of eqn 2.1.

It should also be noted that both the program POWDER and GSAS utilize these same equations for the determination of the theoretical spectra. Both GSAS and POWDER require the input of approximate starting values for the atom positions, lattice parameters, crystallographic angles α,β, and γ, and magnetic orientations. The difference between GSAS and POWDER is that while POWDER takes this input data and calculates the nuclear and magnetic intensities of a powder pattern, GSAS also accepts experimental data to which it will fit and refine these parameters. By using the program POWDER the peak intensities were calculated and then compared to the experimental line intensities. The experimental line intensities were determined by summing up the number of counts under a peak or by treating the peak profile as a gaussian.

The program POWDER was received in the Beta test version and was debugged and modified to facilitate its use within the Ottawa University group. The 3 primary modifications were: to allow the magnetization vector to incorporate non-parallel spin orientations, to change the method of data entry from command line mode to batch file mode, and to change the language of the source code from FORTRAN to QUICKBASIC so that it could be integrated into the Labwindows environment. The rest of these modifications allowed for multiple batch processing, eliminated the need to re-enter material parameters by reading in batch files, reduced the number of keystrokes to perform redundant operations, displayed realtime processed information and allowed optional renaming of the output file.

2.4 Symmetry:

There are four possible space groups relating to the spin arrangement, called Shubnikov groups, which can apply to the case of Mn_2SiS_4 (fig 2.3). Unlike ordinary point group symmetry, the magnetic point group symmetry used to describe magnetic crystals must also be able to describe non vanishing time-averaged distribution of current density J(r) and spin density S(r) [11]. The total magnetic moment density is defined as $\mu(r) = J(r) + S(r)$ and has a symmetry that is characterized by an anti symmetry operator R which reverses vector direction. This antisymmetry operator, sometimes referred to as a Shubnikov spin reversal operator, reverses the sign of the magnetic moment at each point in space but does not perform any spatial transformation.

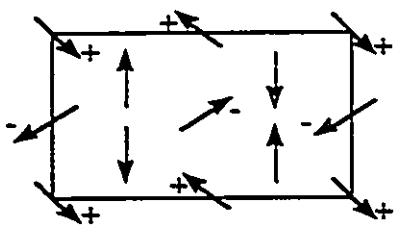

Pnma G(x) + C(y) + A(z) + C´(y)

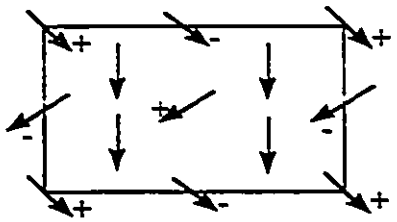

Pn´ma´ A(x) + F(y) + G(z) + F´(y)

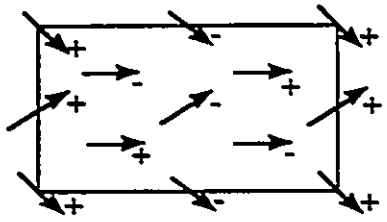

Pnm´a´ F(x) + A(y) + C(z) + C´(z)

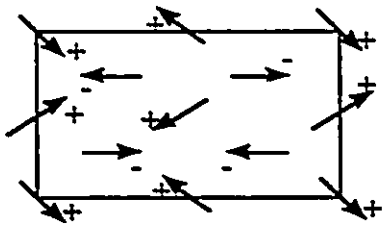

Pn´m´a C(x) + G(y) + F(z) + F´(z)

Fig 2.3 Possible Shubnikov Groups for Mn_2SiS_4

The operators used above are as described here: $C = S_1 + S_2 - S_3 - S_4$, $G = S_1 - S_2 - S_3 + S_4$, $A = S_1 - S_2 + S_3 - S_4$, $F = S_1 + S_2 + S_3 + S_4$. The prime (´) indicates that the operators are applied to the 4c atoms. The notation for spin vectors is from Vincent and Bertaut[16,17] adapted for an atom numbering conforming to the International Tables for Crystallography (see

fig 2.4). The groups containing the F or F´ modes can show spontaneous magnetization, while the group Pnma can only be antiferromagnetic.

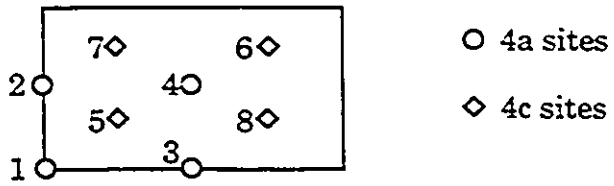

Fig 2.4 International atom numbering.

2.5 Results:

The complete result of the neutron diffraction experiment [25] is summarized in fig 2.5. The main point of interest in this diagram is the temperature dependence of the intensities of the 100 and 001 lines. The observed spectra indicate an olivine pattern which is independent of temperature. GSAS refinement of the experimental profile taken at 180 K (fig 2.6) produced values for the atom positions, lattice parameters, bond angles and bond lengths. At this temperature the sample is paramagnetic so it is not complicated by magnetic contributions. The values are reported in table 2.1. These atom positions and lattice parameters were used to calculate the intensities of the nuclear reflections and thereby establish a scaling factor for the fixed-count runs.

	X	Y	Z
Mn (4a)	0.0000	0.0000	0.0000
Mn (4c)	0.2325	0.2500	0.5807
Si (4c)	0.4074	0.2500	0.1046
S (4c)	0.4012	0.2500	0.7410
S (4c)	0.5621	0.2500	0.2508
S (8d)	0.3343	0.0236	0.2390

Table 2.1: Atom parameters, given in fractions of unit cell dimensions, derived from the refinement of the 180K data, yielding R = 0.058.

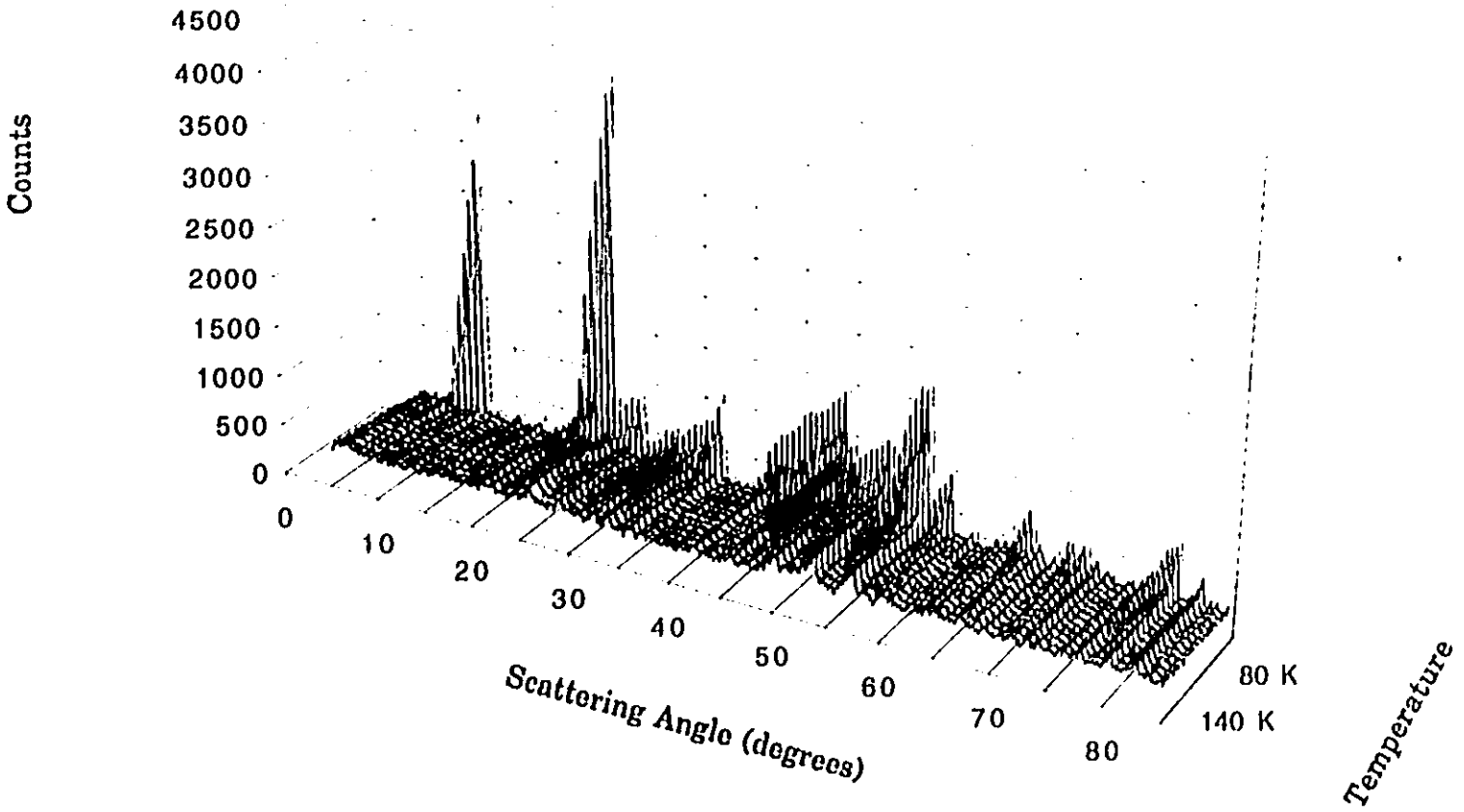

Fig. 2.5 Neutron diffraction profiles for Mn2SiS4 as a function of Temperature.

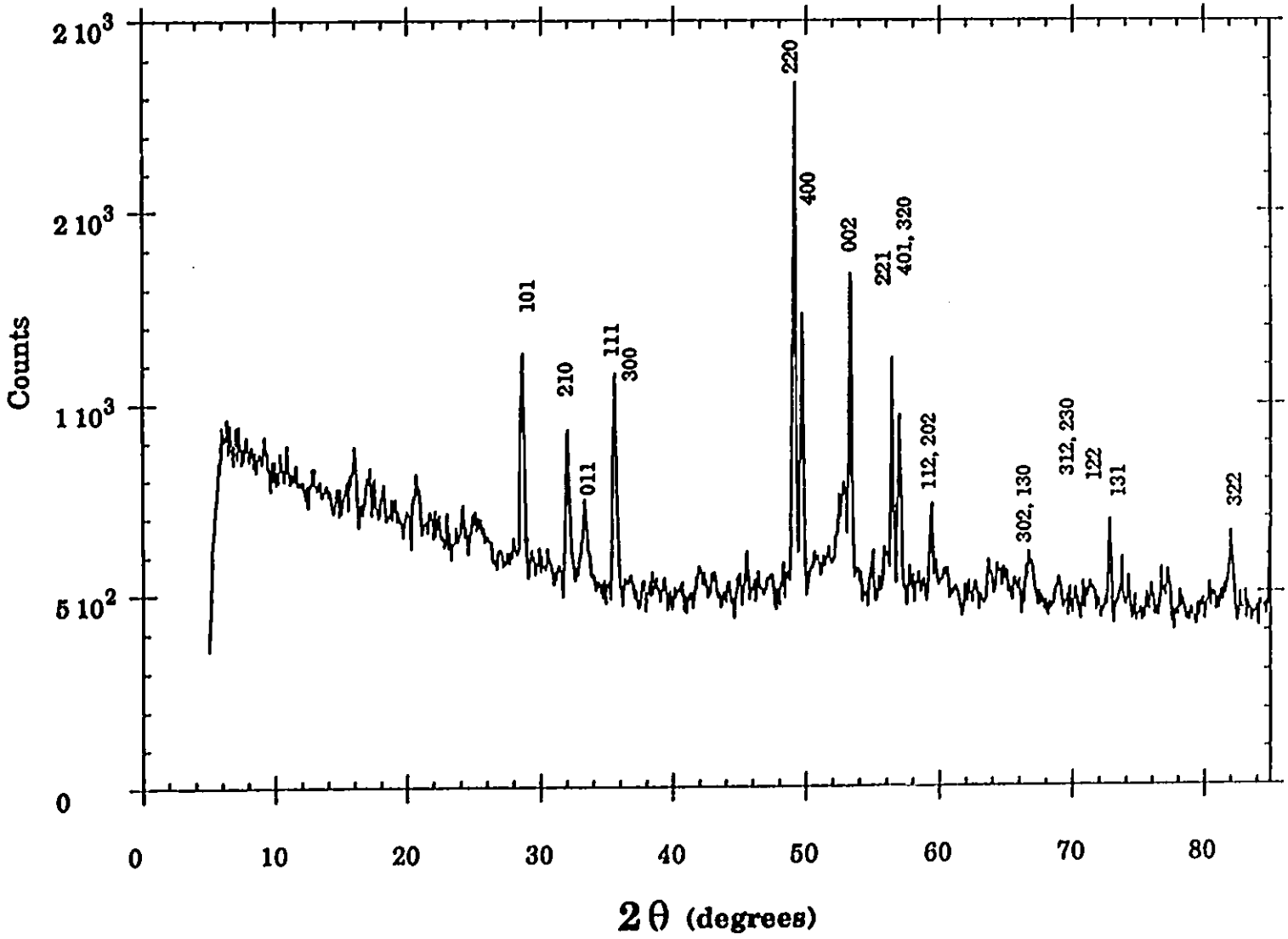

Fig. 2.6 Diffraction pattern of Mn_2SiS_4 at 180 K with a wavelength of 2.6707Å.

The diffraction pattern obtained at 4.2 K is shown in fig 2.7. The magnetic lines are indexed in the chemical cell and have $h + l = 2n + 1$. The indexation of these peaks suggests antiferromagnetic ordering along the y axis. The spins on the 4c sites were obtained from the reflections where only the 4c atoms contribute to the observed intensities, namely $k = 2n + 1$. Once the spins on the 4c atoms were ascertained then the spins and their orientation of the 4a atoms was deduced. It became evident that the coupling of the magnetic moments of Mn^{++} is C(y) - C´(y) in the Shubnikov group Pnma. The introduction of the G(x) and A(z) modes for the 4a spins did not improve the refinement.

The results of the program POWDER is listed in table 2.2 showing the combined nuclear and magnetic intensities along with the corresponding hkl for a given scattering angle. By comparing the theoretical values with the diffraction spectra the most likely set of direction cosines of the individual Mn spins was obtained.

hkl	d(a)	I(calc)	I(obs)
100	12.659	1460	1473
110	6.403	198.6	203
001	5.937	1411	1485
300	4.22	308.9	293.3
310	3.668	137.5	130.0
120	3.562	21.2	20.2
102	2.890	93.1	99.1
221	2.818	248.9	370.7
401	2.793	370.5	
320	2.787	19.7	377.0
112	2.693	149.7	140.7
500	2.532	14.6	13.8
302	2.428	129.3	
130	2.428	2.3	131.0
312	2.308	83.6	87.3
122	2.280	89.0	80.7
330	2.134	9.2	10.7
520	2.092	71.6	72.7
003	1.979	66.2	63.7

Table 2.2. Calculated and observed(integrated) intensities for collinear antiferromagnetism at 4.2 K, using values for S = 2.28, S' = 2.18, x = 0.23, and z = 0.51. Only observed lines with h + l = 2n + 1 are given. Calculated correspondence factor R = 0.037.

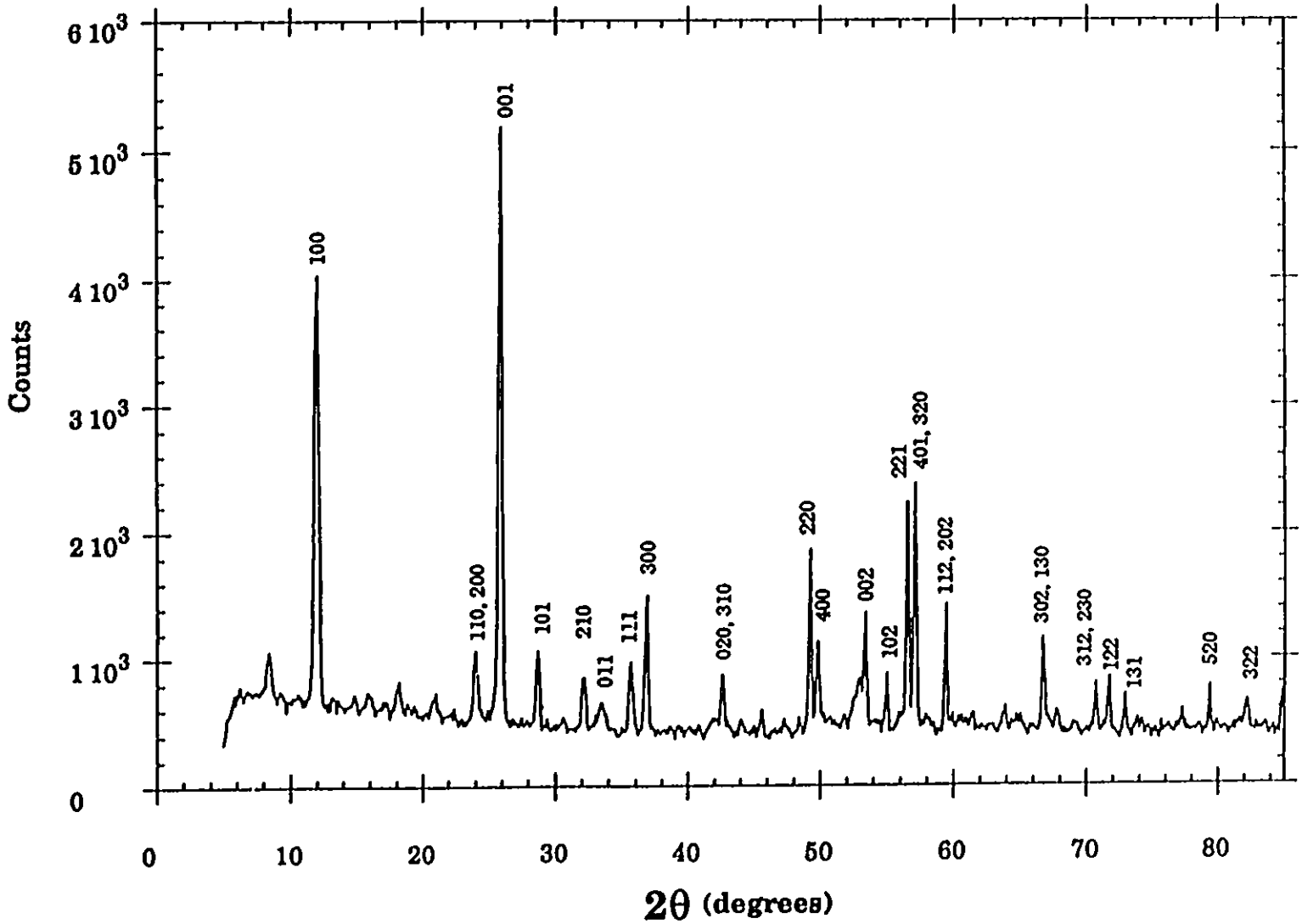

Fig. 2.7 Diffraction pattern of Mn_2SiS_4 at 4.2 K with a wavelength of 2.6707Å.

The comparison between the observed intensities for the lines 001 and 100 (fig 2.8) with the lines 110 and 310 (fig 2.9) as a function of temperature, can be used as an indication of the progressive canting of the spins on the 4a sites with increasing temperature. The 001 and 100 reflections are sensitive to the canting angles. The intensities of the 100 reflection are a function of the canting mode C(y), while the intensities of the 001 reflection have equal contributions from the C(y) and C´(y) modes.

The plots of the intensities of 110 and 310 show a Brillouin-like saturation curve. For both of these lines there is a negligible contribution from the G(x) mode of the 4a spins and the 4c spin contributions from the C´(y) mode are constrained to the *y* axis. These type of saturation curves were also found for collinear and canted spins in magnetic silicates of the olivine structure by Lottermoser and Fuess [22].

The diffraction pattern for the temperature range of 83 - 86 K indicate that the 4a and 4c spins are principally oriented on the x-axis. This is illustrated in the very low intensity of the 100 line which is of the order of magnitude of peaks in the background scattering.

The diffraction pattern obtained at a temperature of 84 K is shown in fig 2.10. Calculated intensities for the different models of spin arrangements that satisfied the four possible Shubnikov space groups were compared to the observed intensities at 84 K. The only model that correctly predicted the observed intensities was the Pn´m´a model. Not all the spins are ferromagnetically aligned so the small values of spin will be effective spins S_{eff}. By evaluating the magnetic contributions, of the 111 line which has a contribution from the F´(z) mode only and the 110 line which is derived solely from the C´(x) mode, it was possible to determine the z-component α'_z and the magnitude S'_{eff} of the effective spin on the 4c atoms. Values for α_z and S_{eff} for the 4a sites were determined by substituting the already obtained values for α'_z and S'_{eff} into F(z) + F´(z) mode which comprises the magnetic contribution to the 020 line. Several other lines were used to evaluate α_z and are listed in table 2.3. Incorporating a small y component in the 4a spins did not improve the agreement.

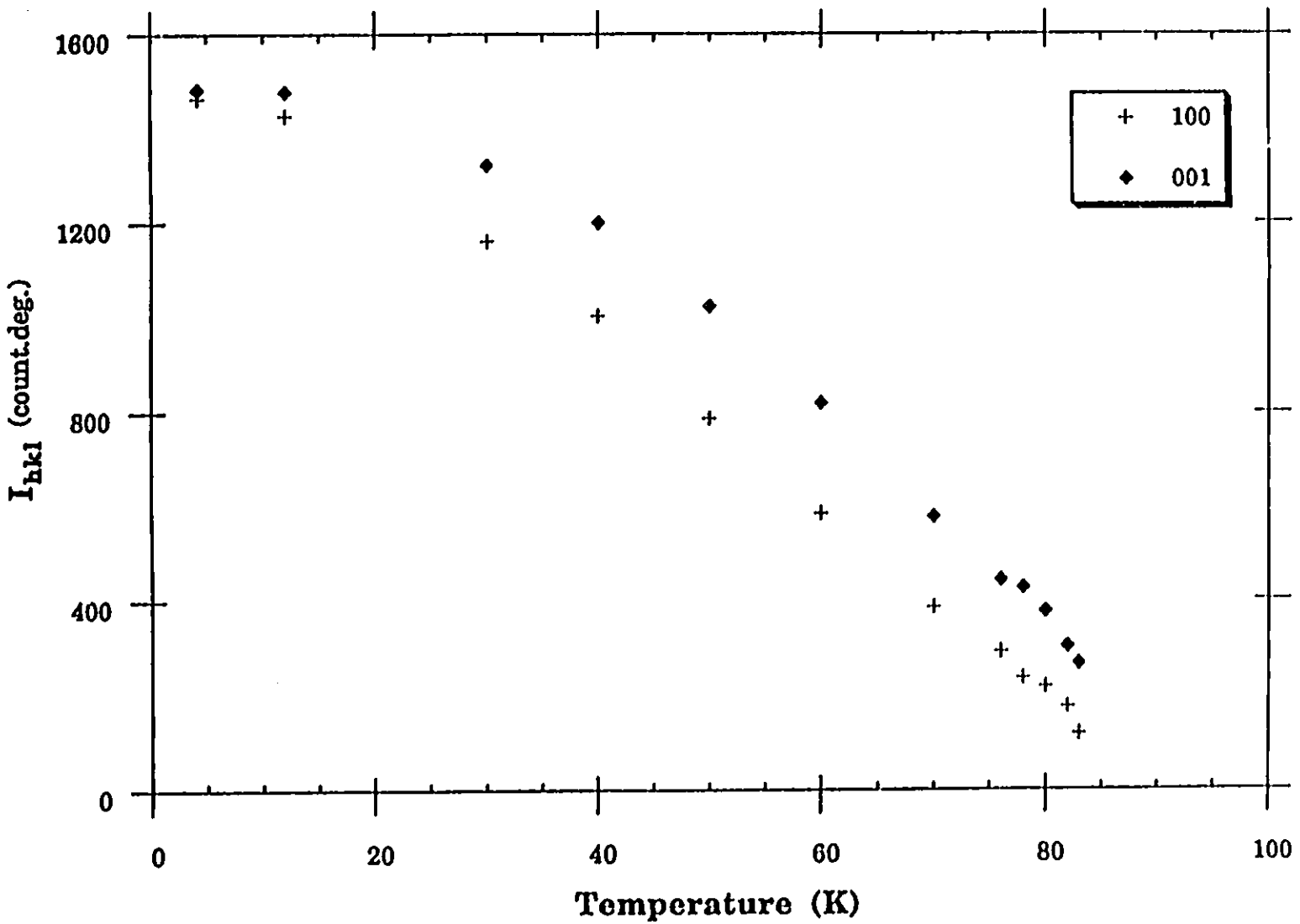

Fig. 2.8 Observed intensities of the 100 and 001 lines as a function of temperature.

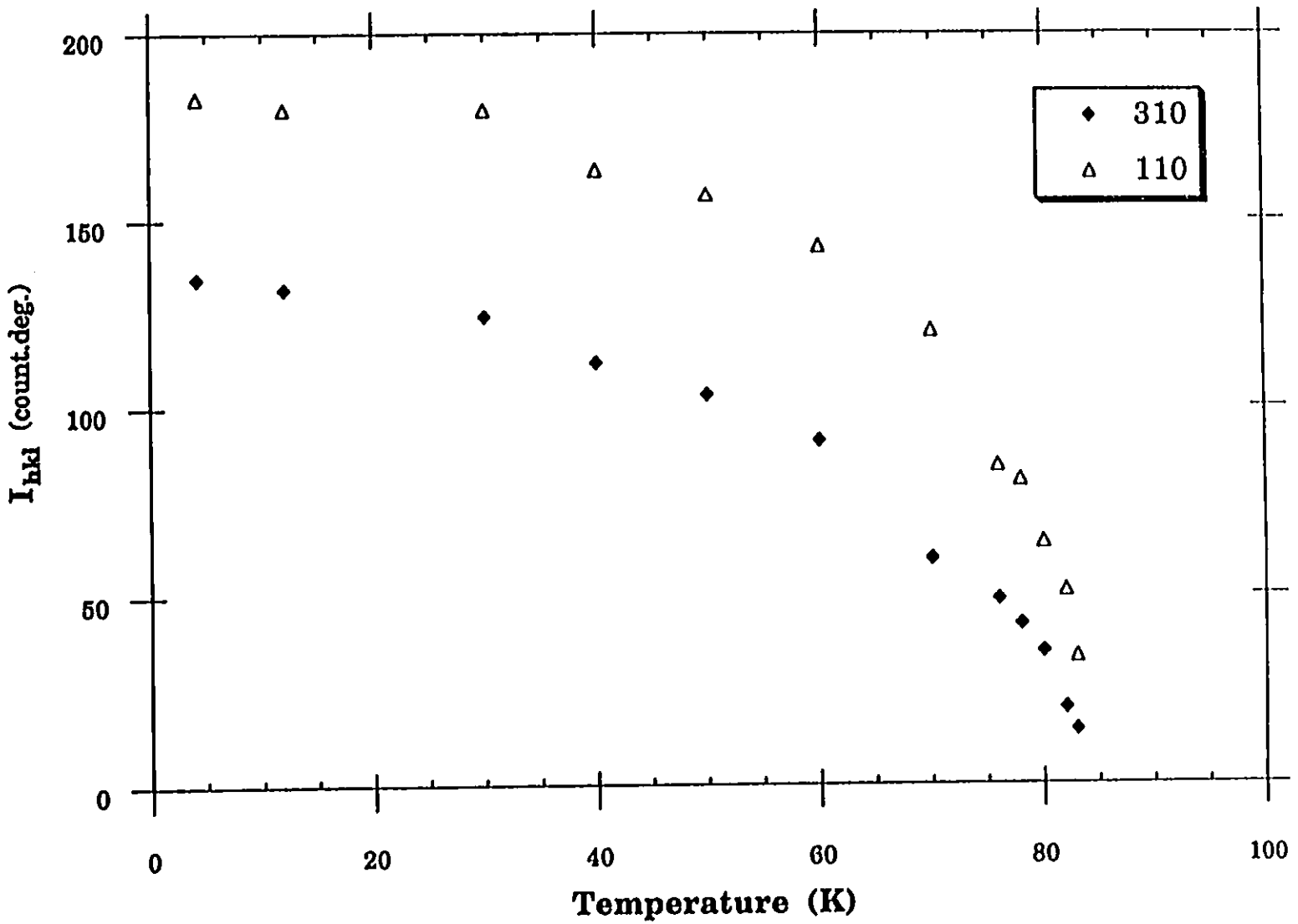

Fig 2.9 Observed intensities of lines 110 and 310 as a function of temperature.

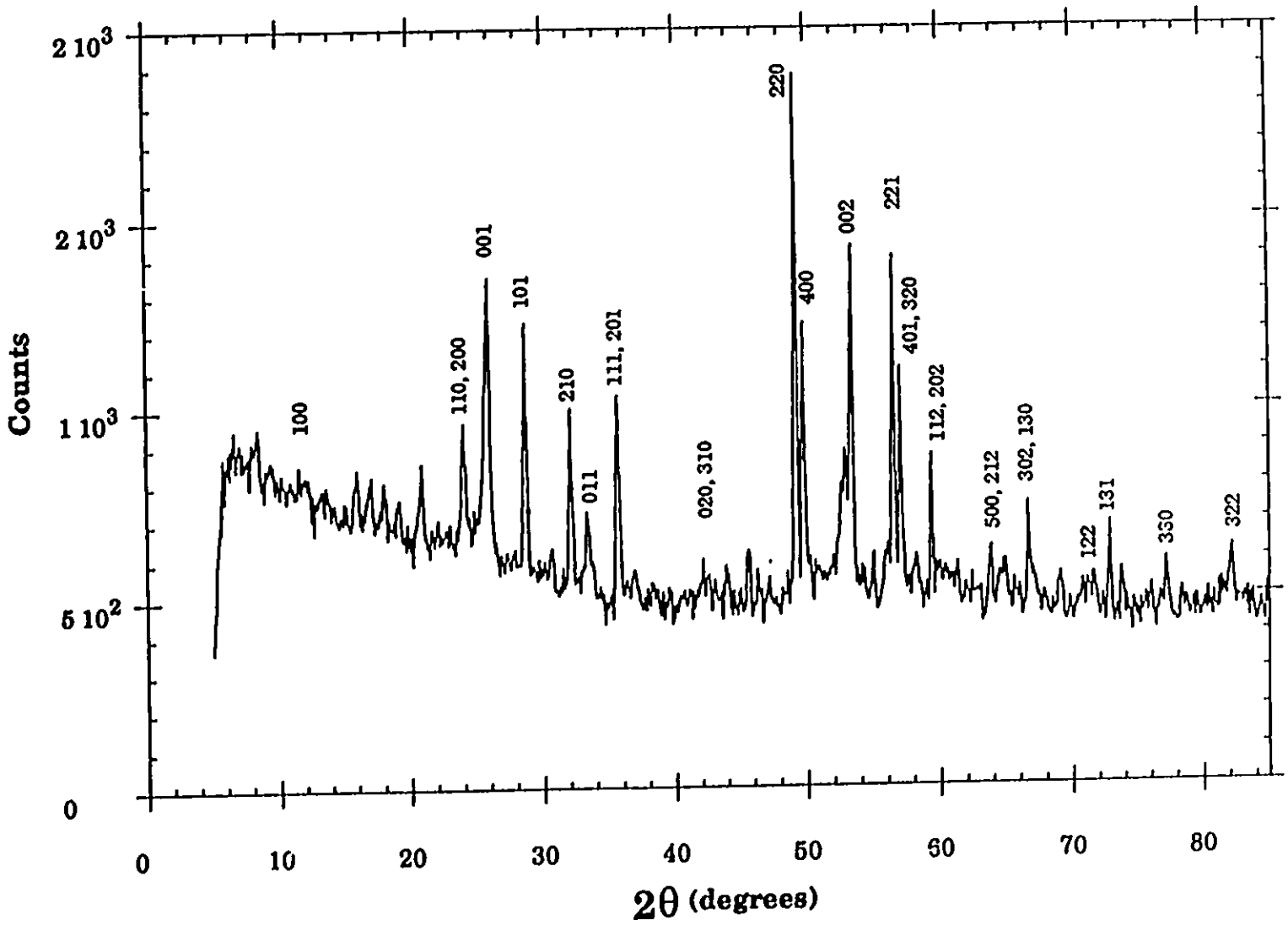

Fig. 2.10 Diffraction pattern of Mn_2SiS_4 at 84 K with a wavelength of 2.6707Å.

h k l	d(A)	sI(calc)	I(obs)	modes
100	12.677	24.9	23.8	C, C'
110	6.409	93.4	95.8	C'
200	6.339	4.8	—	F, F'
001	5.932	199.8	203	C, C'
101	5.373	10.7	13.1	C', F, F'
011	4.635	0.3	—	C', F'
111	4.353	13.1		C', F'
201	4.331	0.8	12.0	C, C', F'
300	4.226	6.1	7.2	C, C'
211	3.742	2.5	—	C', F'
020	3.714	10.5	10.0	F, F'
310	3.673	11.2	12.5	C'
120	3.564	42.9	44.7	C, C'
311	3.123	2.7	—	C', F'
121	3.055	7.2	6.7	C', F, F'
102	2.888	14.1	16.5	C, C', F'
221	2.819	105.9	100.4	C, C', F'
401	2.795	11.6		C, C', F'
320	2.790	5.2	15.0	C, C'
112	2.692	21.5		C'
202	2.686	1.4	20.5	C', F'
130	2.430	9.2		C'
302	2.428	12.8	21.5	C, C', F'
122	2.280	22.0	22.8	C, C', F'

Table 2.3: Calculated and observed intensities for ferrimagnetism at 84 K with S = 1.01, $\alpha_x = 0.944$, S' = 0.91, $\alpha'_x = 0.925$. Calculated correspondence factor R = 0.047.

2.6 Conclusion:

The following model is proposed to summarize the neutron diffraction results presented in this chapter. At 4.2 K Mn_2SiS_4 has a crystallographic and magnetic symmetry of Pnma. The spins on the 4a and 4c sites are collinear with the y-axis (see fig 2.11a). As the temperature rises, the 4c spins remain antiferromagnetically aligned along the y-axis, while the spins of the 4a atoms gradually rotate their antiferromagnetic axis away from the y-axis (fig 2.11b). The alignments of the 4a spins are still in the x-y plane and the maximum angle achieved from the y-axis is 32° and occurs at 83 K. Between 83 and 86 K both the 4a and 4c atom are predominantly aligned along the x-axis. There is some canting of the spins occurring in the x-z plane (fig 2.11c). As a product of this canting the 4a and 4c sites each develop a non-zero magnetization in the z-axis. The magnetization of the 4a sites oppose the magnetization of the 4c sites but the magnitudes of their magnetizations are not equal and hence there is a small non-zero difference which is the origin of the small spontaneous magnetization observed by the SQUID measurements in chapter 1.

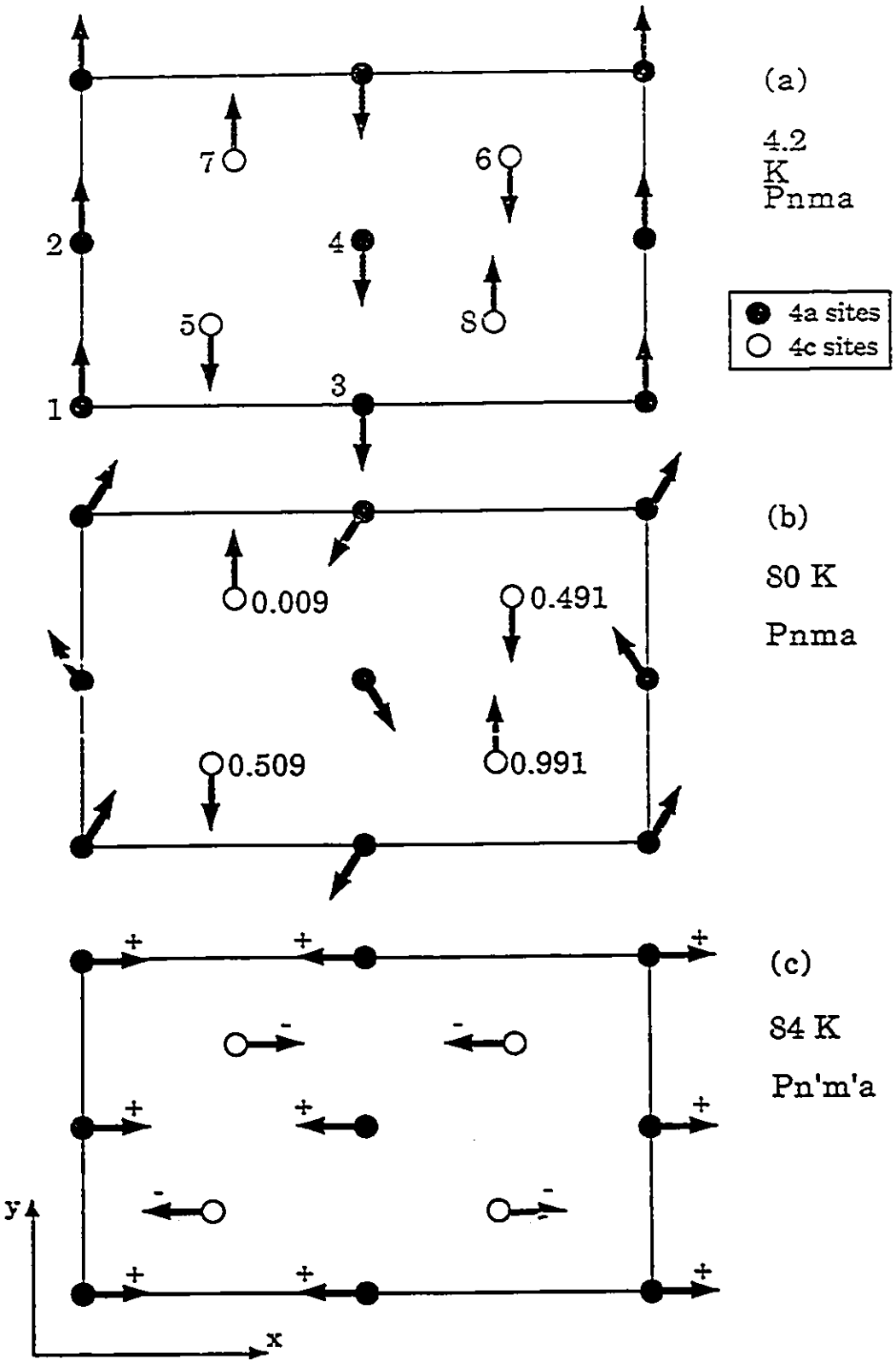

Fig 2.11 2-dimensional view of unit cell of Mn2SiS4; a) shows the 4a and 4c positions, the international numbering and the spin directions at 4.2 K, b) shows spin directions at 80 K and atomic positions in the z-axis (the default is in the x-y plane), c) shows the canting in the positive and negative z-axis.

Chapter 3

SPECIFIC HEAT

3.0 Introduction:

One of the traceable response functions of a phase change in a solid state sample is the specific heat. Any kind of atomic or magnetic variation as a function of temperature will produce variations in the specific heat of the sample. In a phase transition there is a change in the order of the system. The change in the system order can be attributed to a structural and/or magnetic alteration as the system tries to satisfy the requirements of the state of lowest energy. The specific heat of a substance is defined as TdS/dT, temperature multiplied by the rate of change of entropy with respect to the rate of change of temperature. Hence in the temperature region where the phase change is occurring it is expected that an anomaly in the specific heat will occur concurrently.

3.1 Theory:

To measure the specific heat of Mn_2SiS_4 the sweep thermal relaxation technique [19] was utilized. The underlying theory of this method is centered around the adjustability of the thermal relaxation time constant τ_1 of the system. The thermal relaxation time constant τ_1 is given by $\tau_1 = C/k$, where k is the thermal conductance linking the sample to the heat reservoir. In designing the apparatus and choosing the sample's geometry, it is important to minimize the internal relaxation time τ_2. The internal relaxation time τ_2, given by $\tau_2 = C/k_{int}$, relates to the lateral diffusion rate within the sample. As τ_2 increases a thermal gradient will occur within the sample and thereby cause the instantaneous measurement of the sample's temperature to be inaccurate. In addition if τ_2 is of the order of τ_1 then it is obvious that the resultant time constant would not truly reflect the heat capacity of the sample That is why it is assumed that $\tau_2 \ll \tau_1$.

To begin, the following assumptions have been adopted to facilitate the explanation and the implementation of the theory: 1) a one dimensional

model is assumed and the heat flows only in the direction of the z axis; 2) the lateral diffusion of the heat ($\propto 1/\tau_2$) within the sample is considerably faster than the longitudinal diffusion rate ($\propto 1/\tau_1$) of which will be measured; 3) the thermal conductivities used are linear with respect to temperature if the temperature interval is small enough; 4) radiation effects are negligible.

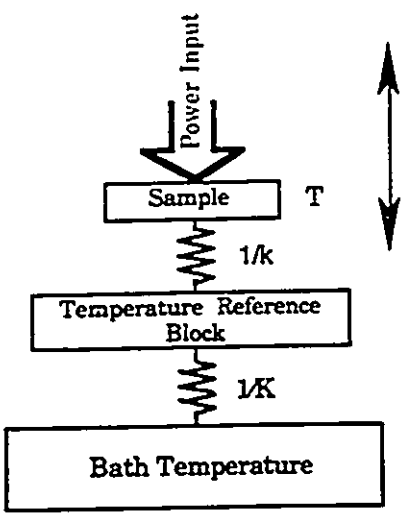

Fig 3.1 One dimensional model illustrating the direction of heat flow.

From the diagram depicting the model, Fig 3.1, it is apparent that for a steady state the power that is added to the system will equal the power removed from the system plus the power retained by the system. In other words

power in = power out + power absorbed.

The power absorbed will take the form of an increase in temperature. By measuring the power in and the power out the heat absorbed can be calculated. If the power is abruptly cut the elevated temperature T_1 will decay to the block reference temperature T_0 with a time constant of $\tau_1=C/k$. If ΔQ is the heat applied to the sample given by

$$\Delta Q = C\Delta T \qquad 3.1$$

and the power P going into the sample is

$$P = A\kappa\, \partial T/\partial z + C(T)\partial T/\partial t \qquad 3.2$$

then the specific heat as a function of temperature is

$$C(T) = \frac{dt}{dT}\left(P - A\kappa\frac{\partial T}{\partial z}\right) \quad . \qquad 3.3$$

where A = the cross sectional area of the wire linking sample to RTB

κ = the thermal conductivity of the wire

z = is the direction of heat flow

By integrating over the length of the wire L:

$$C(T) = \frac{dt}{dT}\left(P - \int_{T_0}^{T} k(T')dT'\right) \qquad 3.4$$

where k(T) is the thermal conductance of the wire as a function of temperature given by $k(T) = \kappa(T) \times A/L$.

Note that for this approximation it is assumed that the wire has no heat capacity. Also in a steady state, power in equals power out, so:

$$P(T_1) = \int_{T_0}^{T_1} k(T)dT \; . \qquad 3.5$$

Thus the integral on the right hand side of eqn 3.5 can be evaluated between T_0 and T_1 by measuring the power P as a function of T_1.

In the sweep method the input power is increased in intervals and maintained until equilibrium is obtained. The resultant temperature of the sample is recorded. The cycle is then repeated at the next increment of power. This gives the relationship of temperature as a function of power. When the maximum temperature is obtained the power input is abruptly terminated and the temperature decay from T_1 to T_0 is measured. The maximum temperature is determined by the thermal conductance of the heat leak to the bath such that the maximum T_1 does not effect the reference block temperature T_0. The change in the block reference temperature is given by,

$$\Delta T_0 = (k/K)(T_1 - T_0) \qquad 3.6$$

where K is the thermal conductance linking the block to the bath.
The heat capacity is then given by

$$C(T) = \left(\frac{dt}{dT}\right)\int_{T_0}^{T_1} k dT' = \left(\frac{dt}{dT}\right)P(T) \qquad 3.7$$

The k was calculated by assuming that the copper wires used to support the sample acted as the only heat leak and their conductivities were assumed to be close to that of pure copper.

3.2 Apparatus and Preliminary Results:

Measurements pertaining to the specific heat of the Mn_2SiS_4 sample were performed by using both the step and sweep methods described in Bachman et al.[19]. The apparatus designed for this experiment is illustrated in fig 3.2. The thermometer used consisted of a glass covered platinum thin film deposited on a ceramic substrate. This thermometer was a commercially available prefabrication and was designed to follow the calibration curve outline in Din 43760.

The heater consisted of a small contoured copper block with maximum extraneous mass removed. A 42 gauge Manganin wire with a resistivity of 18 ohms per foot is wound in a bifillar fashion around the block such that the total resistance is 3.3±0.05 ohms.

The Mn_2SiS_4 sample is polycrystalline and in the shape of a truncated disk. The mass of the sample is 43 mg which represents 1.615 x 10^{-4} moles. The shape was dictated by the compromise of having the largest contact surface area, the least amount of superfluous mass, and the limits of the fabrication process.

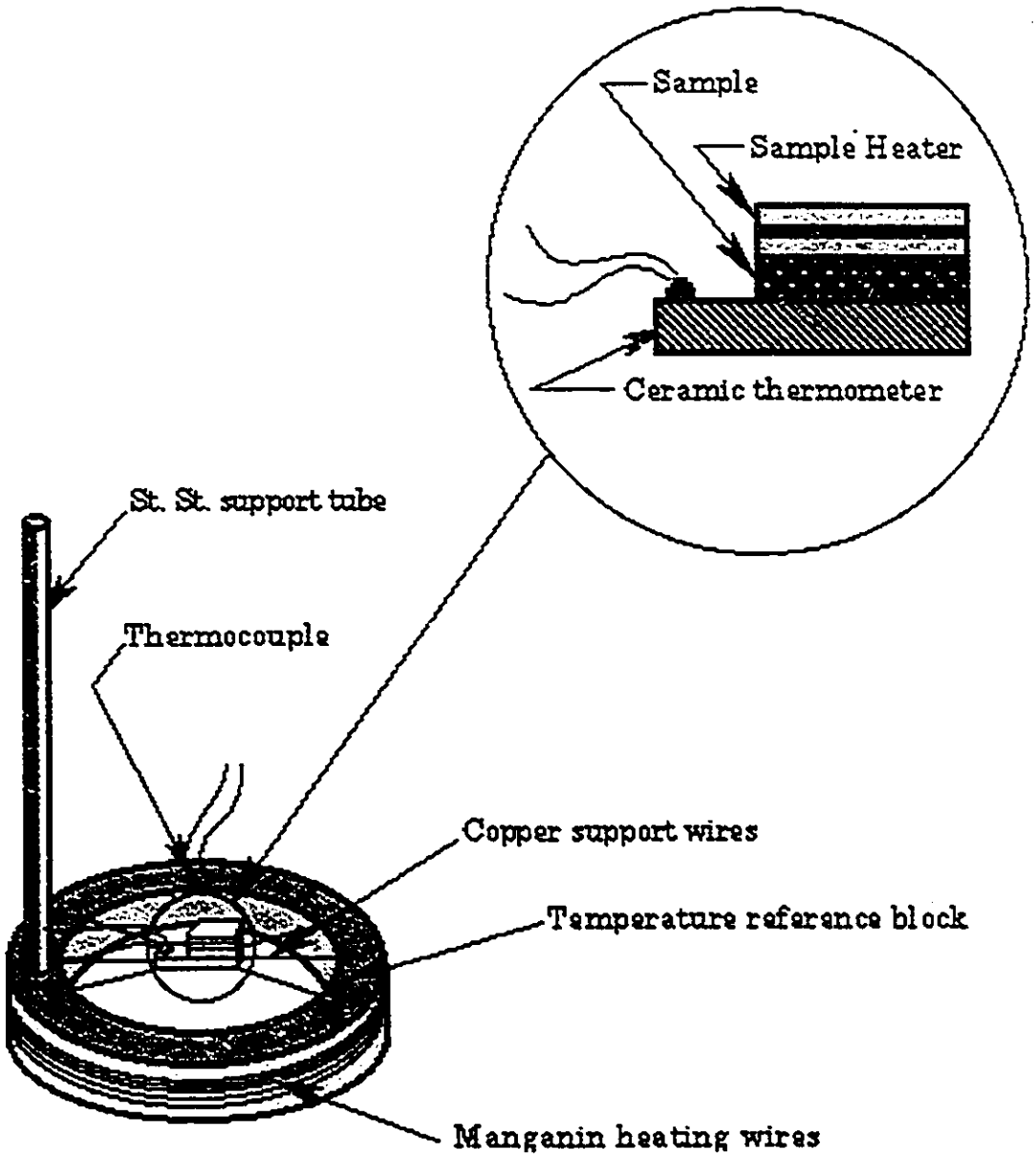

Fig 3.2 Illustration of apparatus used in calorimetery measurements.

The sample was sandwiched between the copper heater block and the ceramic-platinum thermometer. Thermal contact was ensured by using thin layers of Apeizon M vacuum grease which also served as an adhesive.

The variable reference temperature was produced by using a relatively large copper block which was heated by a manganin bifillar wound heater wire wrapped around it to supply the input energy. The block also has a semiconductor diode thermocouple mounted on it to feedback the temperature to the Palm Beach temperature controller model #4025 which maintains the temperature set point by metering out current to the heater windings.

The heat leak that produces a continuous drain on the accumulated heat reservoir is a 14 gauge copper wire that is soldered to the reference temperature block(RTB) and the liquid nitrogen bath.

In order to measure a flow of heat it was necessary to create a controlled heat leak. The heat leak from the ceramic platinum thermometer to the reference temperature block is achieved by the 3 supporting 36 gauge copper wires that span the diameter of the RTB.

Equation 3.7 states that the specific heat can be determined by evaluating the power as a function of temperature and the derivative of the temperature decay curve.

The power is increased in discrete steps of 100 - 200 mW in the range of 200 - 1800 mW. After a period of a few minutes equilibrium was attained and the sample temperature reading was taken. After equilibrium was reached, at the highest power setting, the power was cut-off and the temperature vs. time decay curve was obtained. This data was acquired using 2 Fluke model # 8842a DVM's connected to the computer through an IEEE 488 bus. The time was measured via the internal clock onboard the computer. The measurements are approximately 1.5 to 2 seconds apart depending on the instruction processing timing interval. The total length of the measuring interval was on average 350 seconds.

The results of the relationship between power and resulting temperature were plotted and fit with a linear equation with a Pearson's correlation of at least 0.999 (see fig 3.3). This correlation factor is calculated using

$$R = \frac{\sum_{i=1}^{n} \left(Y_{i(theo)} - \overline{Y_{(theo)}}\right)\left(Y_{i(obs)} - \overline{Y_{(obs)}}\right)}{\sqrt{\sum_{i=1}^{n} \left(Y_{i(theo)} - \overline{Y_{(theo)}}\right)^2} \sqrt{\sum_{i=1}^{n} \left(Y_{i(obs)} - \overline{Y_{(obs)}}\right)^2}} \qquad 3.8$$

where R = Pearson's R value (Chi square)
c = Chi square value
Yi = Actual value of data point
$\overline{Y}$ = the mean of actual values.

The equations found from this linear curve fitting were used to determine the interpolated values of the Power as a function of Temperature, 'P(T)'. The derivative of the temperature decay curve was calculated numerically using the formula:

$$\frac{dT_n}{dt_n} = \frac{T_{n+1} - T_n}{t_{n+1} - t_n} . \qquad 3.9$$

The sensitivity of the ceramic thermometer was such that the derivative was not monotonically decreasing. The fluctuations in the temperature measurements produced a wide spread in the values for the derivative. Hence the temperature data had to be smoothed by taking a moving average over five values at a time in order to extract any meaning (see fig 3.3b). The inverse of the derivative multiplied by the P(T) for a given temperature will give the heat capacity for that temperature.

$$C(T) = \left(\frac{dT}{dt}\right)^{-1} P(T) \qquad 3.10$$

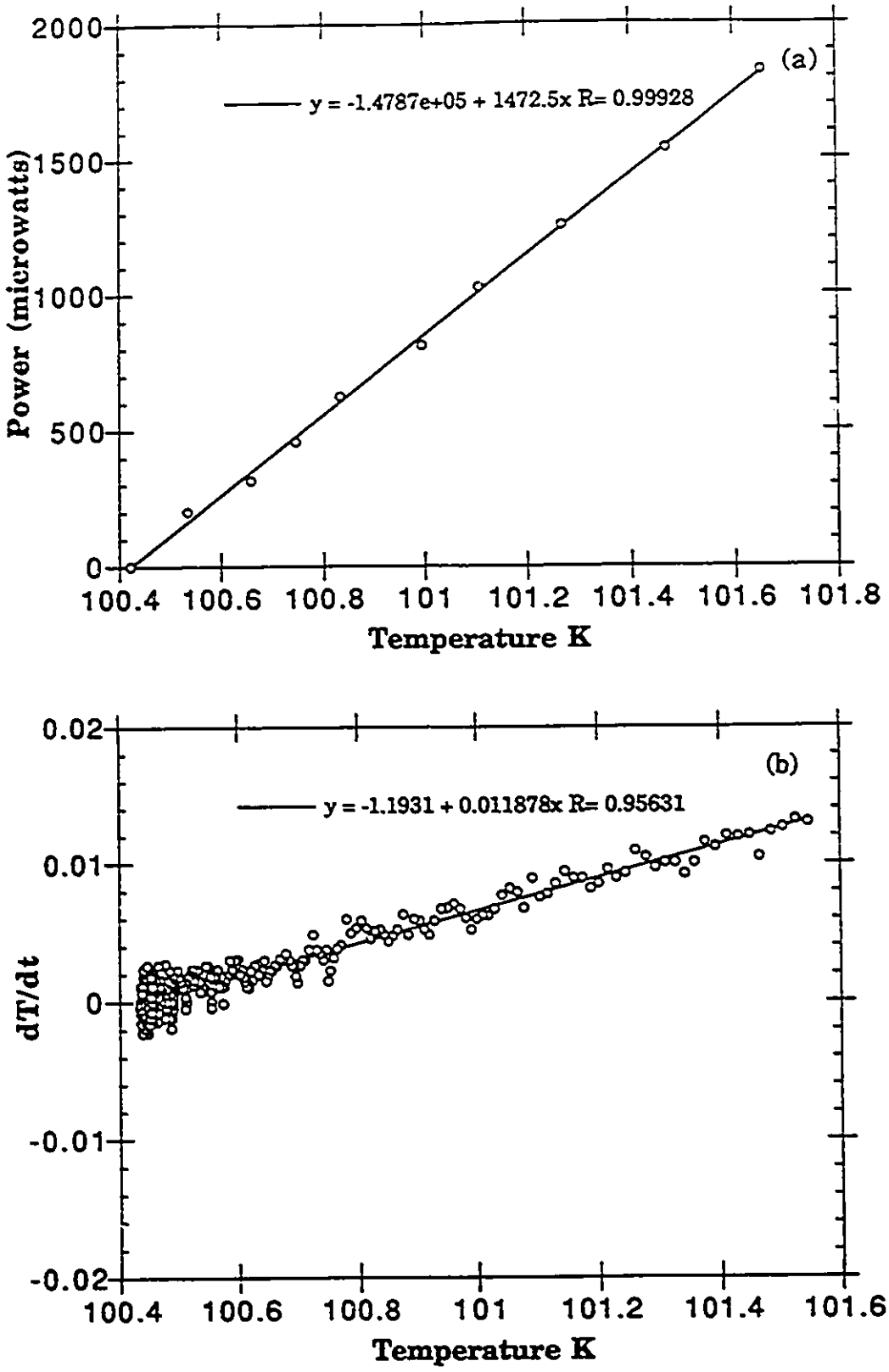

Fig 3.3 a) Input power vs. resulting temperature.
b) dT/dt of decay as a function of temperature.

The results of our experiment do not reveal the anomalous behavior expected from the magnetic susceptibility results. It is believed that, although the data indicates that there is a trend of increasing heat capacity with increasing temperature, the resolution of the ceramic platinum thermometer is not high enough to provide any details by differentiating the minute fluctuations in temperature with the randomness of background noise in the detection system.

The methodology of this technique is sound, but this particular implementation needs to be improved. Some of the problems encountered and the possible improvments are outlined below.

The small copper block used as the sample heater had a mass approximately seven times that of the sample. This requires corrections that are possibly an order of magnitude higher than the specific heat of the sample. An alternative heater should be realized, lower mass and lower heat capacity.

The heat capacity and the thermal diffusivity for the ceramic platinum thermometer are unknown. Until measurements of the sample holder, heater, and thermometer are done to determine the overall system effects, the value of the heat capacity of the sample will continue to be obscured. This problem and the low thermometric resolution of the ceramic platinum thermometer are sufficient reasons to consider an alternative method or device to measure the sample temperature. It should be noted here that the original reason for choosing this particular thermometer was its low mass and compact regular geometry.

Doing the above mentioned modifications would also be necessary to examine the sample geometry and dimensions to reduce the effects of lateral diffusion and the reaction of the sample and apeizon M grease.

3.3 Results from the University of Geneva:

In collaboration with Alain Junod at the University of Geneva [31] the measurement of the specific heat in the ranges of interest was obtained. Junod's specific heat measurements are performed in an adiabatic continuous heating calorimeter which allows for a resolution of 0.02%. His apparatus is based on P = CdT/dt, where P is the constant heating power and C is the heat capacity at temperature T. The heat capacity can be deduced if the heating power is kept constant and the rate of change of temperature with respect to time, dT/dt, of the sample is measured. The external environment temperature is maintained at as close to the sample temperature as possible to eliminate heat dissipation through radiation. The heat capacity of the sample holder is measured separately and subtracted from the total heat capacity.

Their results are depicted in fig 3.4 - 3.6. Fig 3.4 shows the specific heat of Mn_2SiS_4 as a function of temperature in the range of 70 - 100 K. There is a specific heat anomaly that occurs at approximately 85.9 K. The discontinuous nature of the first derivative shown in fig 3.5 is indicative of an order-disorder or lambda transition [7]. At this temperature the sample changes magnetic ordering from paramagnetic to ferrimagnetic or weak ferromagnetic.

The magnetic contribution to the specific heat, shown in fig 3.6, was calculated by subtracting the phonon contribution from the total specific heat. There is a small bump at approximately 83 K that coincides with the transition of the magnetic symmetry of Pn'm'a to Pnma and with the transition of ferrimagnetism to antiferromagnetism. This anomaly is a first order transition broadened by experimental resolution and by inhomogeneity of the sample. By subtracting a smooth baseline produced by the fit of the λ-anomaly at 85.9 K from the curve, the latent heat of the magnetic symmetry change can be estimated as a value of 0.09±0.01 J/mole.

From the small magnitude of the specific heat anomaly and the high resolution of the Geneva measurements, it is apparent why the attempts made in our lab to see this effect were unsuccessful. It is interesting to note

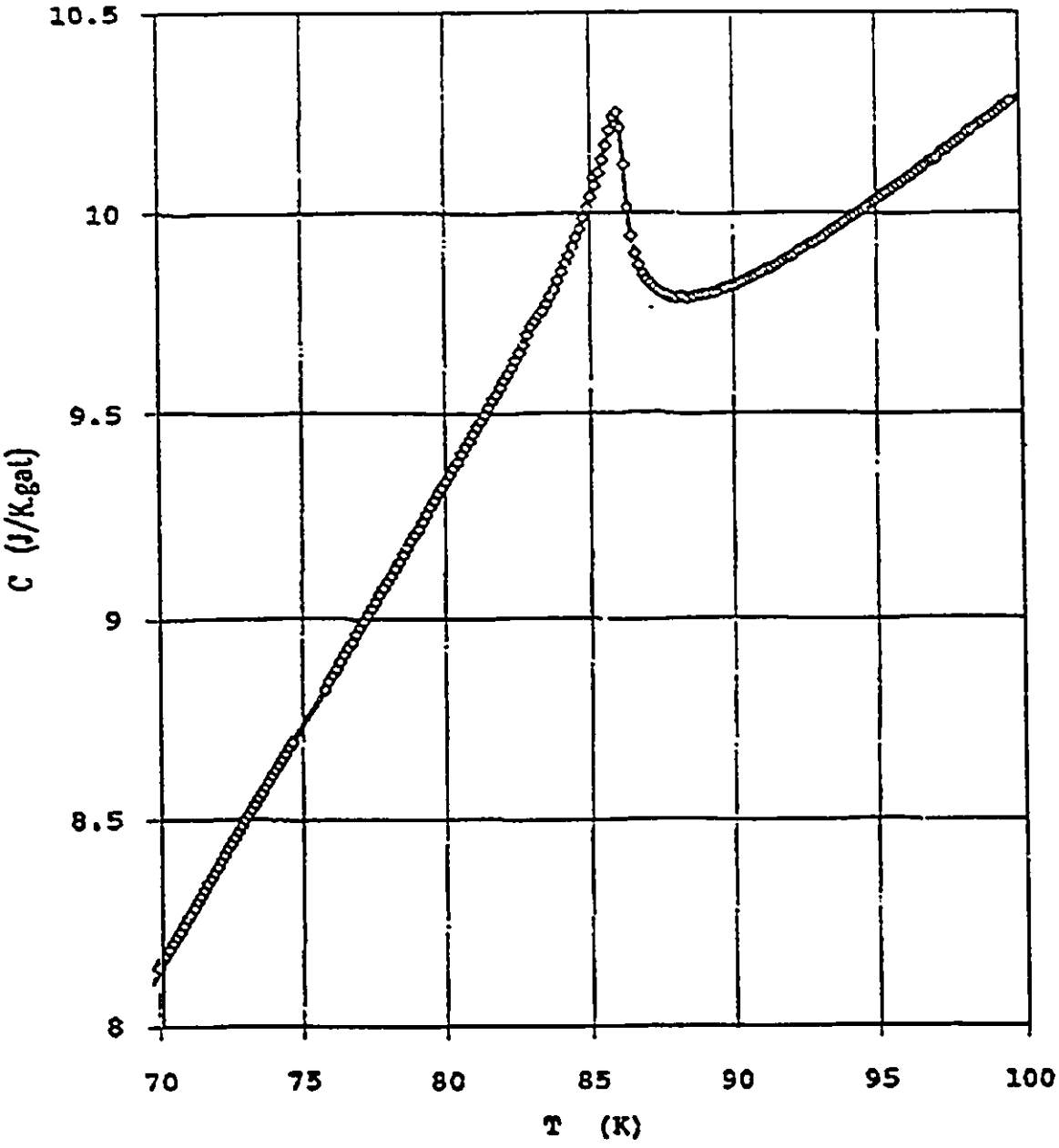

Fig 3.4 Specific Heat of Mn2SiS4 as a function of temperature[31]. Sample is 286.1 mg, 1 gat = 38.0288 g, measurement rate 10mK/s.

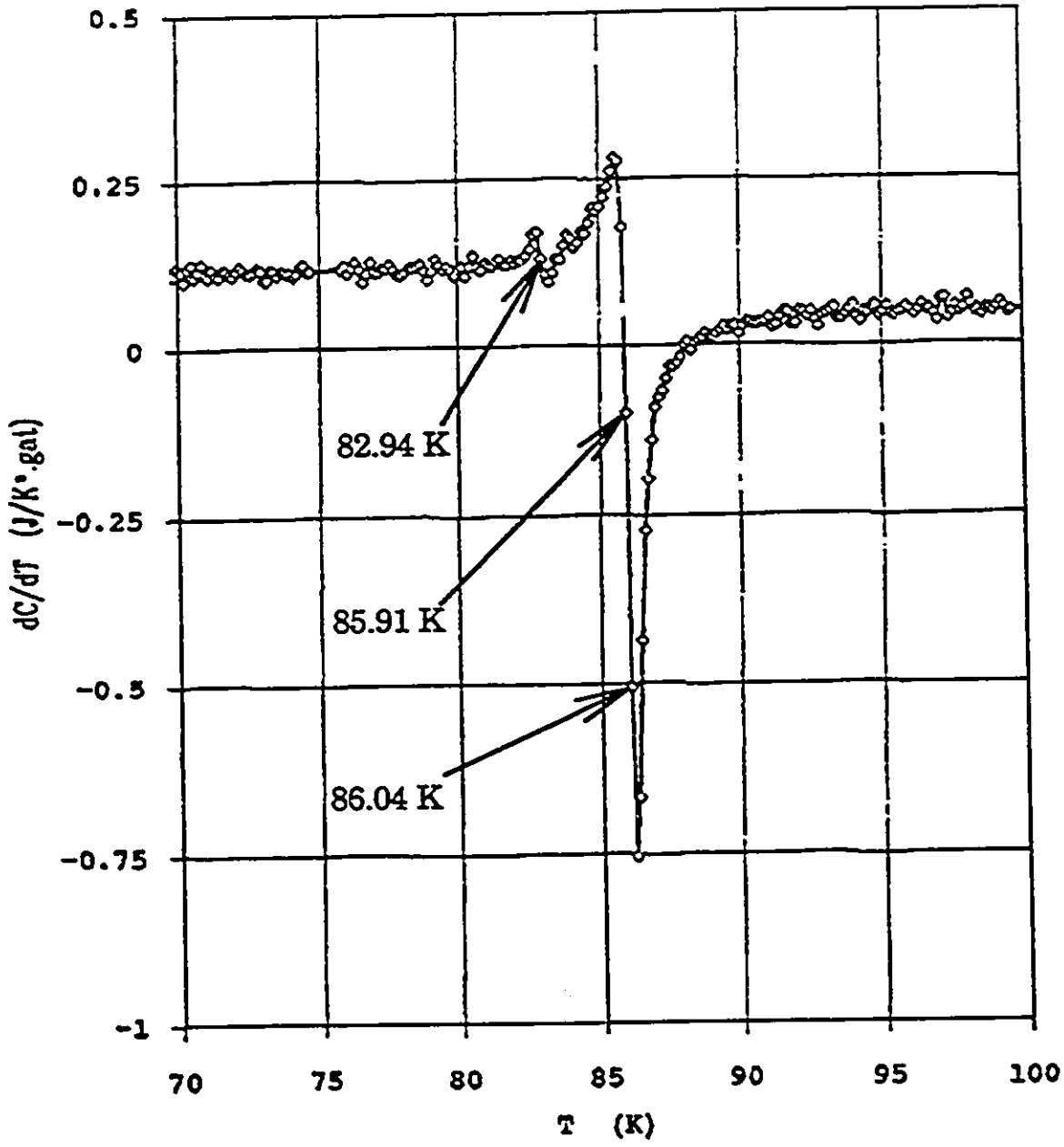

Fig 3.5 Derivative of Specific Heat as a function of temperature.

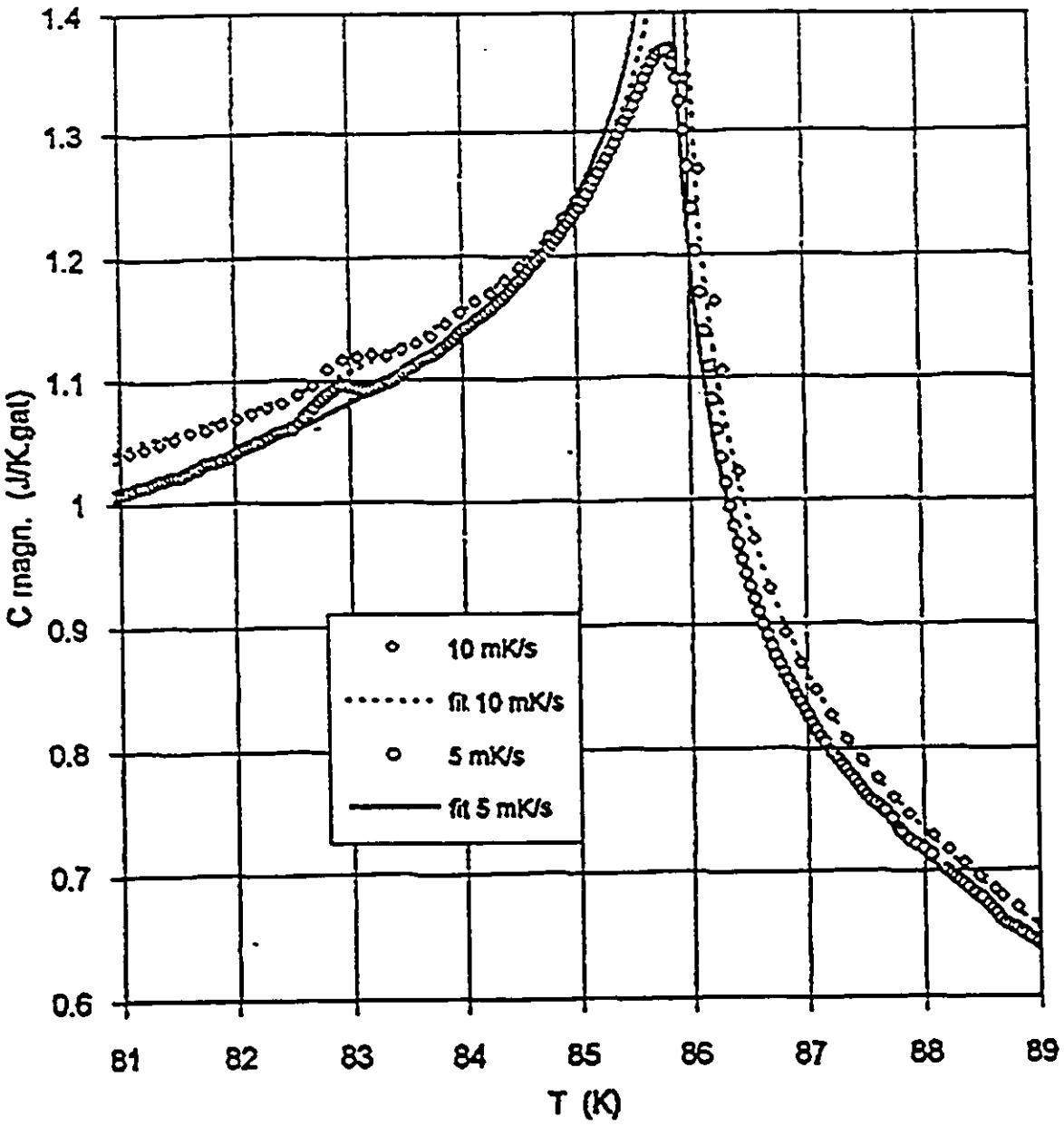

Fig 3.6 Magnetic contribution to the Specific Heat.

that the graphs of heat capacity vs. temperature vindicate the calibration of the thermometry used in other experiments described in previous chapters. In particular the transition temperatures gathered from the graph shown in fig 3.5 coincide with the magnetic susceptibility measurements described in chapter 1 and the neutron diffraction data in chapter 2.

3.4 Conclusion:

Although the theory and the procedure of the sweep method of heat capacity measurements were sound, there were some difficulties with their implementation, especially the fine tuning of the system. To achieve reliable results it may be necessary to increase the sensing voltage in the thermometer so that there will be greater resolution in the current measurement and hence the platinum thermometer resistance. Hopefully the required voltage will not produce a significant amount of self heating. An alternative method is to modify the system to be an adiabatic constant power calorimeter similar to the one in Geneva [31].

The results from our collaboration with Junod et.al. has shed some light on the nature of the transitions at 83 and 86.5 K. The peak in the specific heat corresponds to an order-disorder transition as Mn_2SiS_4 goes from paramagnetic to ferrimagnetic ordering. The magnetic contribution to the specific heat is identified. This is obtained by subtracting the Einstein lattice specific heat from the total specific heat. It proposed that the anomaly at 83 K is a first order transition broadened by experimental resolution and by inhomogeneity of the sample. By subtracting a smooth baseline produced by the fit of the λ-anomaly at 85.9 K from the curve of the first-order transition, the latent heat of the magnetic symmetry change is estimated to be 0.09 ± 0.01 J/mole.

Chapter 4

ELECTRON SPIN RESONANCE

4.0 Introduction:

Magnetic resonance forms a branch of spectroscopy that utilizes an oscillating field, which when superimposed on a static field perpendicular to it, induces transitions between the energy levels of the magnetic dipoles [1,4,8]. These permanent magnetic dipoles are associated with the motion of a charged particle. In electron paramagnetic resonance (EPR) the charged particle under study is the electron and the magnetic dipole consists of both orbital angular momentum, L and spin angular momentum, S giving a total momentum, J=L+S. Electron spin resonance (ESR) is a subset of EPR where the magnetic dipole is made up of only spin angular momentum J=S. This nomenclature is not always adhered to.

Poole and Farach [7] state that near a structural phase transition the resonance linewidth and intensity of an ESR profile may exhibit anomalous behavior; these effects are associated with changes in the spin-lattice and spin-spin relaxation times near the transition temperature. By examining the ESR spectra of Mn_2SiS_4 it was hoped that an anomalous behavior would be detected in the temperature range of interest.

To examine the ESR spectra of Mn_2SiS_4 with enough detail to extract information, it was necessary to computerize the data acquisition of the ESR signal. One of the main objectives of this thesis work was to develop a data acquisition system for the Bruker ESR spectrometer.

4.1 Lorentzian Lineshape:

Some spectrometers give a signal which is proportional to the energy absorbed by the spin system while others give a signal which is proportional to the 1st derivative of the absorption curve. In the cases of interest in this thesis the signals observed are essentially of Lorentzian shape [13,15,29] and the output of the Bruker spectrometer is a Lorentzian Derivative(LD) shape

as shown in fig 4.1. Thus each line can be characterized by: a peak to peak width (ΔH_{pp}),a maximum amplitude (Ymax), and a resonant field or crossover point (Ho). Fitting the ESR lineshape to a LD allows the values of ΔH_{pp}, Ymax, and Ho to be determined.

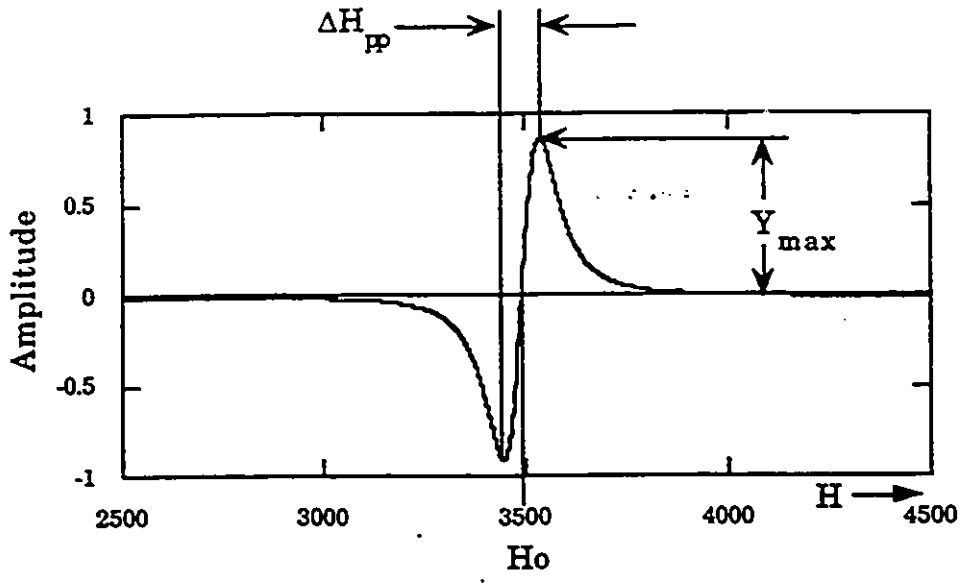

Fig 4.1 Lorentzian derivative (LD) lineshape.

If the lorentzian lineshape is perfect then its derivative (LD) can be expressed as:

$$LD(H) = \frac{16\, Y_{max}\left[(H - Ho)/\frac{1}{2}\Delta H_{pp}\right]}{\left\{3 + \left[(H - Ho)/\frac{1}{2}\Delta H_{pp}\right]^2\right\}^2} \qquad 4.1$$

This equation is for a normalized LD [5], and is used in the minimization subroutine described later.

A lorentzian lineshape can be justified by considering the following simplified model. In a static field, H_o, the bulk magnetization, M, of a sample made up of one type of spin has a Larmor precession frequency ω_o given by γ Ho, since the magnetization in the absence of saturation effects obeys the equation

$$d\vec{M}/dt = \gamma \vec{M} \times \vec{H}_o \ . \qquad 4.2$$

If relaxation effects are taken into account, then the result is the well known Bloch Equations which can be expressed as

$$dM_x/dt = \gamma(M_y H_{o_z} - M_z H_{o_y}) - (M_x/T_2) \qquad 4.3$$

$$dM_y/dt = \gamma(M_z H_{o_x} - M_x H_{o_z}) - (M_y/T_2) \qquad 4.4$$

$$dM_z/dt = \gamma(M_x H_{o_y} - M_y H_{o_x}) - (M_z/T_1) \qquad 4.5$$

where the longitudinal or spin-lattice relaxation time is T_1 and T_2 is the transverse or spin-spin relaxation time. If both the magnetization and the magnetic field vectors are in the z direction, then these equations reduce to the single expression

$$dM_z/dt = -(M_z - M_o)/T_1 \qquad 4.6$$

which may be integrated to give:

$$M_z = M_o e^{-t/T_1} \ . \qquad 4.7$$

The solution of the Bloch equations for the conditions that are present in this experiment, that is, having a strong Ho along the z direction and a weak radio frequency field $2H_1 \cos\omega t$ in the x direction, such that:

$$\vec{H} = (2H_1 \mathrm{Cos}\ \omega t)\vec{i} + H_o\vec{k} \qquad 4.8$$

gives a magnetization in the x direction that has a real and an imaginary part corresponding to the dispersion and absorption respectively of the microwave energy

$$M_x = 2H_1(\chi'_{(\omega)}\cos\omega t - \chi''_{(\omega)}\sin\omega t) \qquad 4.9$$

where the complex susceptibility

$$\chi_{(\omega)} = \chi'_{(\omega)} - i\chi''_{(\omega)} \qquad 4.10$$

is introduced.

These susceptibilities have lorentzian lineshapes as illustrated in eqn 4.11 and eqn 4.12. Both of these susceptibilities can be obtained with the Bruker ESR spectrometer, but in the experiments done for this thesis only the absorption mode was used.

$$\chi'_{(\omega)} = \frac{1}{2}\chi_o\omega_o T_2 \frac{(\omega-\omega_o)T_2}{1+(\omega-\omega_o)^2T_2{}^2+\gamma^2H_1{}^2T_1T_2} \qquad 4.11$$

$$\chi''_{(\omega)} = \frac{1}{2}\chi_o\omega_o T_2 \frac{1}{1+(\omega-\omega_o)^2T_2{}^2+\gamma^2H_1{}^2T_1T_2} \qquad 4.12$$

where χ_o is the static susceptibility which was measured and described in chapter 1. If there is no saturation, i.e. for small values of H_1 so that

$$\gamma^2H_1{}^2T_1T_2 \ll 1 \qquad 4.13$$

and as such can be neglected, then the dispersion and absorption become

$$\chi'_{(\omega)} = \frac{1}{2}\chi_o\omega_o T_2 \frac{(\omega-\omega_o)T_2}{1+(\omega-\omega_o)^2T_2{}^2} \qquad 4.14$$

$$\chi''_{(\omega)} = \frac{1}{2}\chi_o \omega_o T_2 \frac{1}{1+(\omega-\omega_o)^2 T_2^2} \qquad 4.15$$

respectively [4]. This particular dependence on field or frequency is referred to as a Lorentzian lineshape [9].

4.2 Apparatus:

One of the main objectives of this thesis work was to develop a data acquisition system for the Bruker ESR spectrometer. In order to do a detailed mathematical analysis of the ESR spectra it was necessary to computerize the data acquisition of the ESR signal. The goal was to make the ESR results easily available to a computer so that numerical analysis could be made more quickly and more accurately than the present manual method.

Prior to the installation of the data acquisition set-up all ESR spectra were recorded on a X-Y plotter. As such, all of the extracted information was the result of many man-hours of interpolation and calculation. All of the theoretical data points were manually calculated and subtracted from the empirical data points . This procedure was time consuming and made the accuracy of the results difficult to estimate. If the ESR spectra were digitized and subsequently analyzed by computer there should be improvements in the reliability and accuracy of the analysis.

The hardware used was an IBM compatible 386 computer (PC) in conjunction with a National Instruments(N.I.) LAB-PC data acquisition card. For specification and capabilities of the LAB-PC board refer to the National Instruments technical reference manual[30]. The acquisition card was installed in one of the expansion slots of the PC and was connected to the external environment through a multi connector interface box. The interface box has a BNC connector for each of the LAB-PC board's 8 analog channels.

In addition to the hardware there were also certain software requirements. First there was N.I.'s LABWINDOWS software which was specifically designed to facilitate the development of user friendly applications. LABWINDOWS, in turn, used a subset of function calls from either QUICK C or QUICKBASIC, so it was necessary to have all of the subroutine libraries of one of these two languages. MICROSOFT QUICKBASIC was chosen as the programming language. MINUIT is a minimization program that was written at CERN expressly for the purpose of handling multiple parameters simultaneously. MINUIT was written in FORTRAN, so in order to write a subroutine that would be compatible with it, it was necessary to install MICROSOFT FORTRAN.

Two of the LAB-PC's analog inputs were connected to the pen driver motors on the Bruker X-Y plotter. The Y axis corresponds to the voltage output of the Y axis plotter driver which is always proportional to the amplitude of the ESR signal. The X axis is a measurement of the horizontal driver voltages which always span 0 - 2.05 ± 0.05 V regardless of the actual magnetic field sweep range it represents. The ramping of the X axis voltage is linear throughout the range. The resultant magnetic field calibration is performed by a simple mathematical operation: each horizontal point is an increment

$$\Delta x = \frac{\text{Sweep Range}}{\text{Number of Points}} \qquad 4.16$$

At the initialization of an acquisition run the sweep range is known and at the end of a run the number of data points is known. For the LAB-PC board there is no built in method of timing sequential acquisitions, so there is a software loop that accomplishes the necessary delay to acquire data at every 'n' seconds. The disadvantage of a software loop is that the running time between each loop is not exactly constant. However the difference between subsequent loop periods can be measured in a few 1/100 th's of a second and as such do not significantly contribute to the error in the 'Magnetic Field' axis. The overall average period is constant. On a 200 second scan at an acquisition setting of 2000 points the system virtually runs free of any software timers or delays. This allows the system to acquire

1740 points 9 times out of ten. One out of ten scan will have 1739 data points. Using a sweep range of 6000 gauss the error potential in the discrepancy of number of data points translates into 0.002 gauss per data point. This error is much smaller than the X-axis voltage resolution and can be neglected.

Another source of error in the acquisition system is the manual method of synchronization between the Bruker spectrometer and the acquisition computer. Due to the complexities of the Bruker's subsystems it not possible to find a triggering response that was simultaneously abortable in the case of early termination. The simplistic method adopted was the verbal and visual synchronization of two human operators. The worst case scenario for error estimation would create a temporal difference of 0.5 sec. All of the acquisition scans were performed for at least 200 seconds, so 200±0.5 sec = 0.25% error.

The Y-axis motor driver relayed the information of the intensity of the dM/dH that is being measured by the spectrometer. The magnitude of this field variable intensity depends on several of the spectrometer's set-up parameters, such as gain, modulation, offset, etc.. These parameters were logged so that relative scaling could be accomplished at a later date.

The resolution of analog to digital conversion is ± 0.0024 volts. In the case of the Y-axis, at full scale deflection, this limit in resolution would correspond to 0.0024/5.00 V = 0.05% error.

The actual acquisition for a single data point consists of 20 sequential readings alternating between the X-voltage and Y- voltage taken at a rate of 15000/sec. This results in 10 measured values for each coordinate of this data point which are then averaged to give a single voltage value. The acquisition time for each point is 0.0013 seconds which corresponds to a point width of 0.04 gauss on the X-axis. The data acquired is then stored in tabular ascii format for subsequent analysis.

The ESR profiles were obtained at different temperatures. The temperature control was performed by using a nitrogen gas flow technique.

Under ideal conditions the temperature variation at equilibrium was ± 0.1 K.

4.3 ESR Results and Analysis:

ESR spectra were obtained for the same Mn_2SiS_4 sample that was used in the neutron diffraction experiments described earlier. The temperatures at which the spectra were obtained are mostly in the range of interest. These temperatures are 82, 83, 84, 85, 86, 87, 88, 89, 90, 91, 93, 106, 110, and 297 K.

Once the ESR data is acquired it is analyzed in order to extract information. The analysis consists of a comparison between the experimental data and a mathematical model. This comparison is performed by the program MINUIT.

Prior to running MINUIT, the raw ESR spectra is passed through a pre-analysis program. This program is called ANALYSIS and is a graphical user interface (GUI) that allows the user to find approximate values for the parameters used to describe the number of LD's expected. The output of ANALYSIS is a data file that is in the input format required by MINUIT. The input file for MINUIT contains a list of parameters, the raw data, and a few minimization instructions.

A front end program is needed to utilize MINUIT. This program is used to customize the operation of MINUIT. For fitting one LD to the experimental data the program was called MIN-1. In the analysis provided below several different versions of this program [see appendix B] were used to describe systems with 1,2,3 and 4 LD's.

MIN-1 declares variables, reads in the data file, calls MINUIT as a subroutine to carry out the minimization, and then outputs the results. MIN-1 also describes the relationship between the parameters used to fit the data. Within this short program a function is defined that MINUIT will minimize. This function is usually something that will encompass the 'goodness of fit' like a Chi square variable. In all the results quoted below

there is a correlation factor which is a measure of the 'goodness of fit' and is determined by:

$$C.F. = 1 - \frac{\sum (Y_{exp} - Y_{theo})^2}{\sum (Y_{exp} - Y_{avg})^2} \qquad \text{eqn 4.17}$$

The value of Y_{avg} was assumed to be zero due to the symmetry of the LD lineshape.

The data was analyzed in terms of several different models and possible physical conditions. There were four models each having 1,2,3 or 4 LD's, another model had 2 LD's each having equal area under their curves, and 2 models having specific LD's for MnO and MnS. In the analysis of the ESR spectra many combinations of the above models were tried. In each case the results were interpreted such that the smaller the least squares fit between the experimental and theoretical curves the higher the probability of that condition being present or that model being correct.

One set of analysis consisted of fits with 1, 2, 3, and 4 LD's without constraints except for numerical limits. In most cases fitting the experimental data with 2, 3, and 4 LD's did not significantly improve the correlation obtained by fitting to 1 LD. Another set of analysis involved constraining several parameters that would represent possible physical situations.

The graphs showing the recorded ESR signals and 1 LD fits for all 14 runs can be found in appendix C. In all cases but one the 1 LD fit gave the best least squares result. A typical result is shown in fig 4.2. Each of the fitted LD's is described by the parameters named in section 4.1. These parameters are collated to determine their variation as a function of temperature. The correlation factor for the profile at 83 K did improve noticeably when fitted with 2 LD's. Fig 4.3 shows the two LD's, their total, and the experimental data.

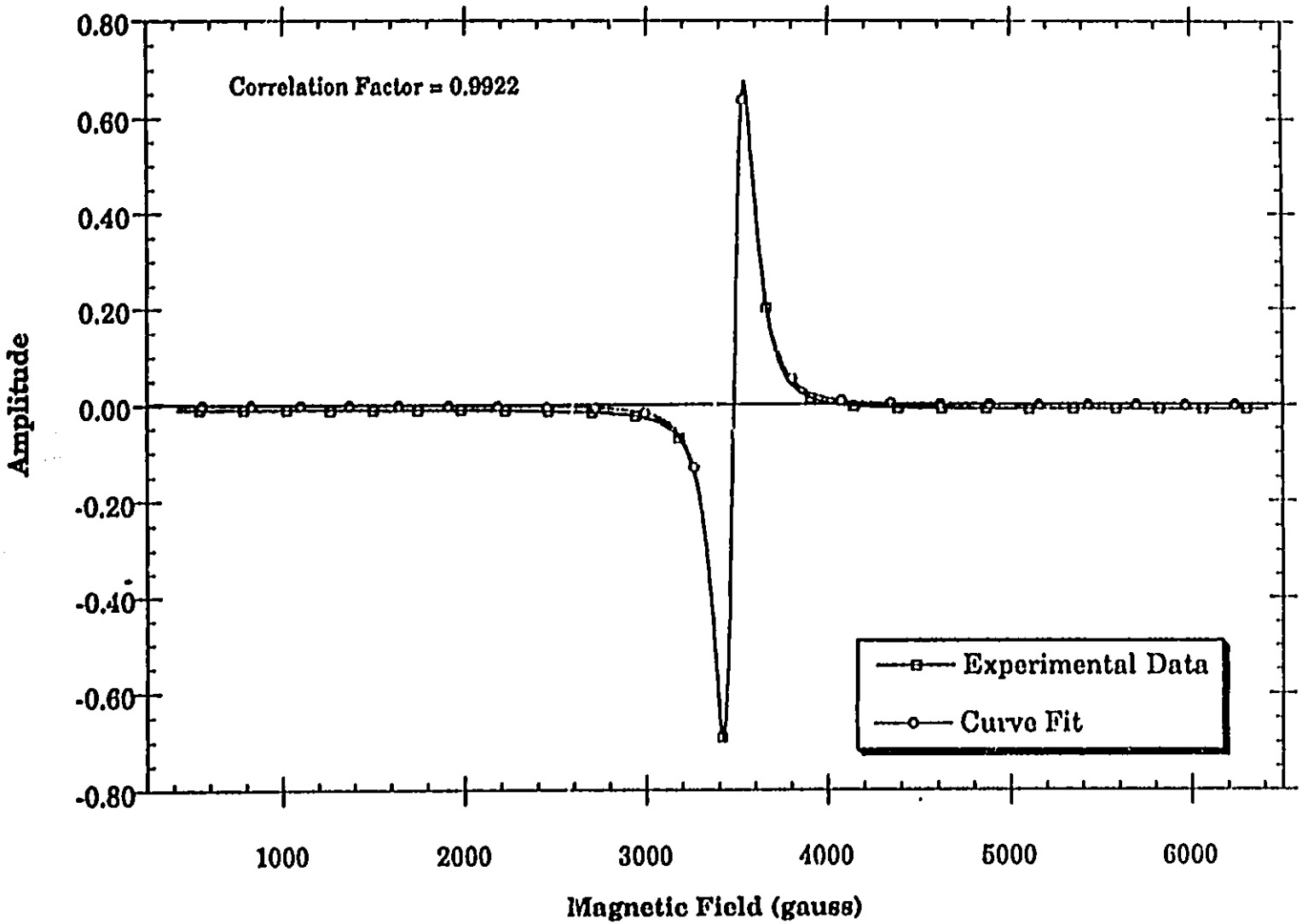

Fig 4.2 ESR linshape of Mn_2SiS_4 at 105.7 K fitted with 1 LD.

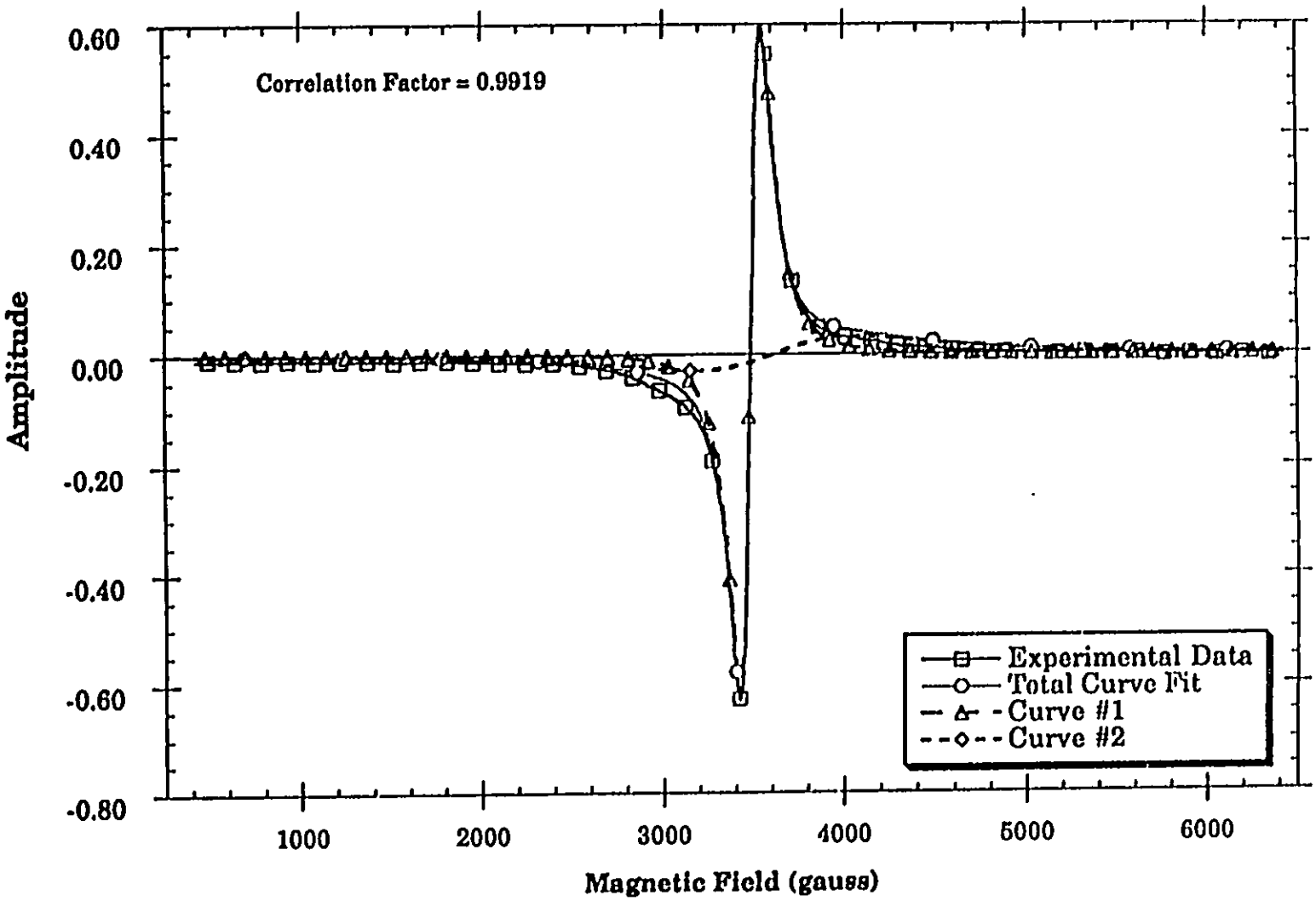

Fig 4.3 ESR profile of Mn_2SiS_4 at 83.3 K fitted with 2 LD's.

The first general trend noticed is the broadening of the linewidth with decreasing temperature in the range of 110 to 88 K. The maximum linewidth of 154 gauss occurs at 87.7 K which is slightly above the temperature of the magnetic phase transition from paramagnetic to ferrimagnetic. In the temperature range of 87 to 82 K the linewidth decreases with decreasing temperature. The linewidth of Mn_2SiS_4 is shown in fig 4.4. The shape of the curve in fig 4.4 resembles that of the curve showing χ vs T, fig 1.5 with the exception of a shift in the temperature. This may be due to the difficulty in measuring the temperature of the sample within the dewar in the resonant cavity of the ESR spectrometer.

These results are comparable with those found by Goede et.al.[13] and Trounson et.al.[26] where the ESR linewidth vs T(K) of polycrystalline samples show a sharp peak somewhat above the Néel temperature. Also the relationship between the maximum amplitude Y_{max} and temperature, shown in fig 4.5, is quite similar to the one Goede depicts. Y_{max} strongly decreases as the temperature approaches the Néel temperature, but the amplitude does not vanish below T_n.

According to Goede the broadening of the ESR profile could be due to: 1) a spin-spin relaxation rate which increases as the temperature approaches T_n, or 2) an inhomogeneous broadening mechanism attributed to the random distribution of internal fields.

In the fabrication of Mn_2SiS_4, MnS can form. Using the results quoted by Okamura et.al.[20], in which the resonant field and the temperature dependence linewidth of MnO, MnS were described, it was possible to check for the presence of these compounds within our sample.

The values of Ho and ΔH_{pp} for MnS and MnO were inputted as fixed parameters for fits with 2 or more LD's. The ESR profile taken at 110 K was used because at this temperature the sample is far from the transition temperature range. The results of the minimization failed to indicate a significant presence of MnS or MnO.

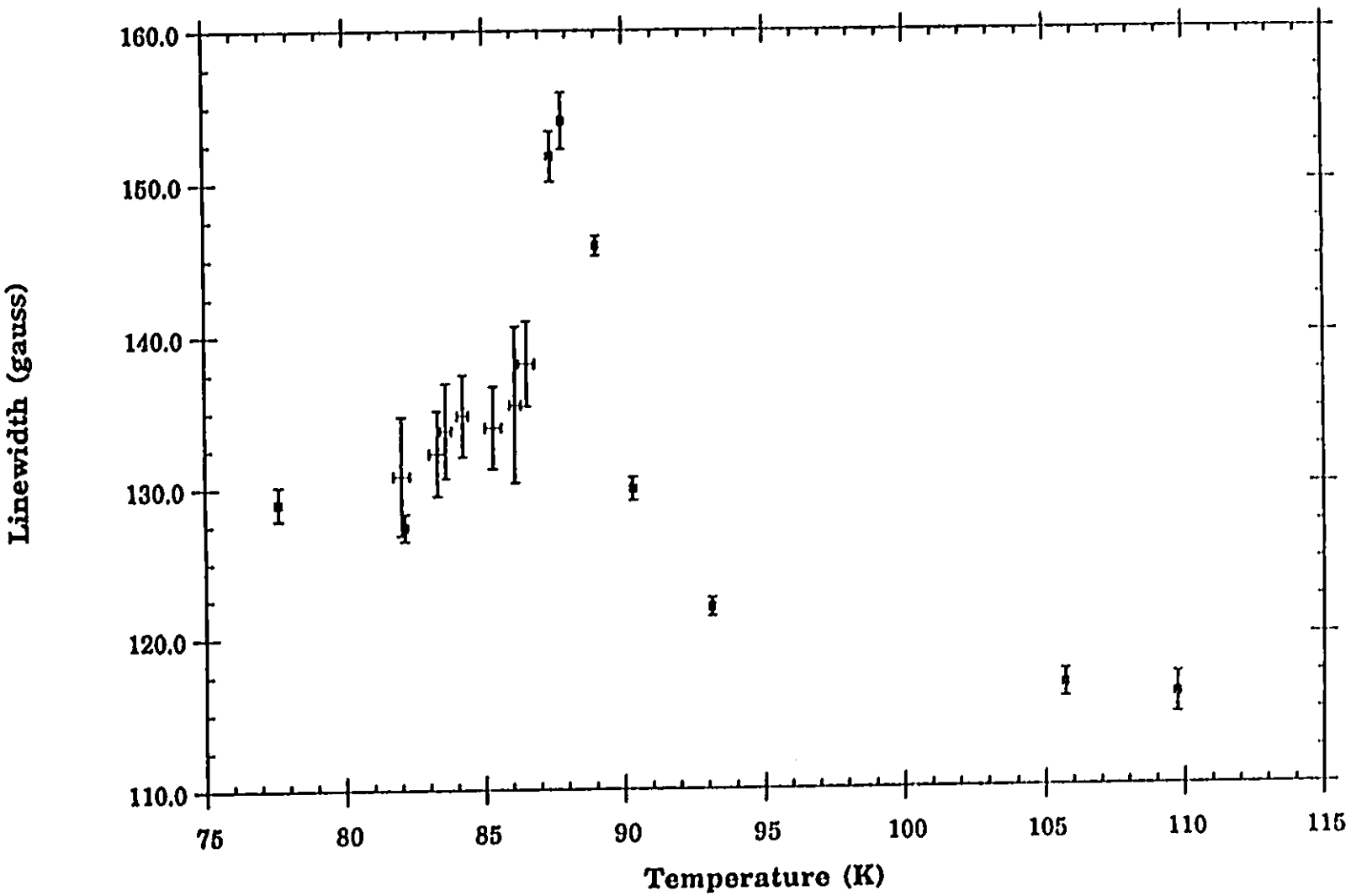

Fig 4.4 Linewidth of Mn_2SiS_4 as a function of temperature.

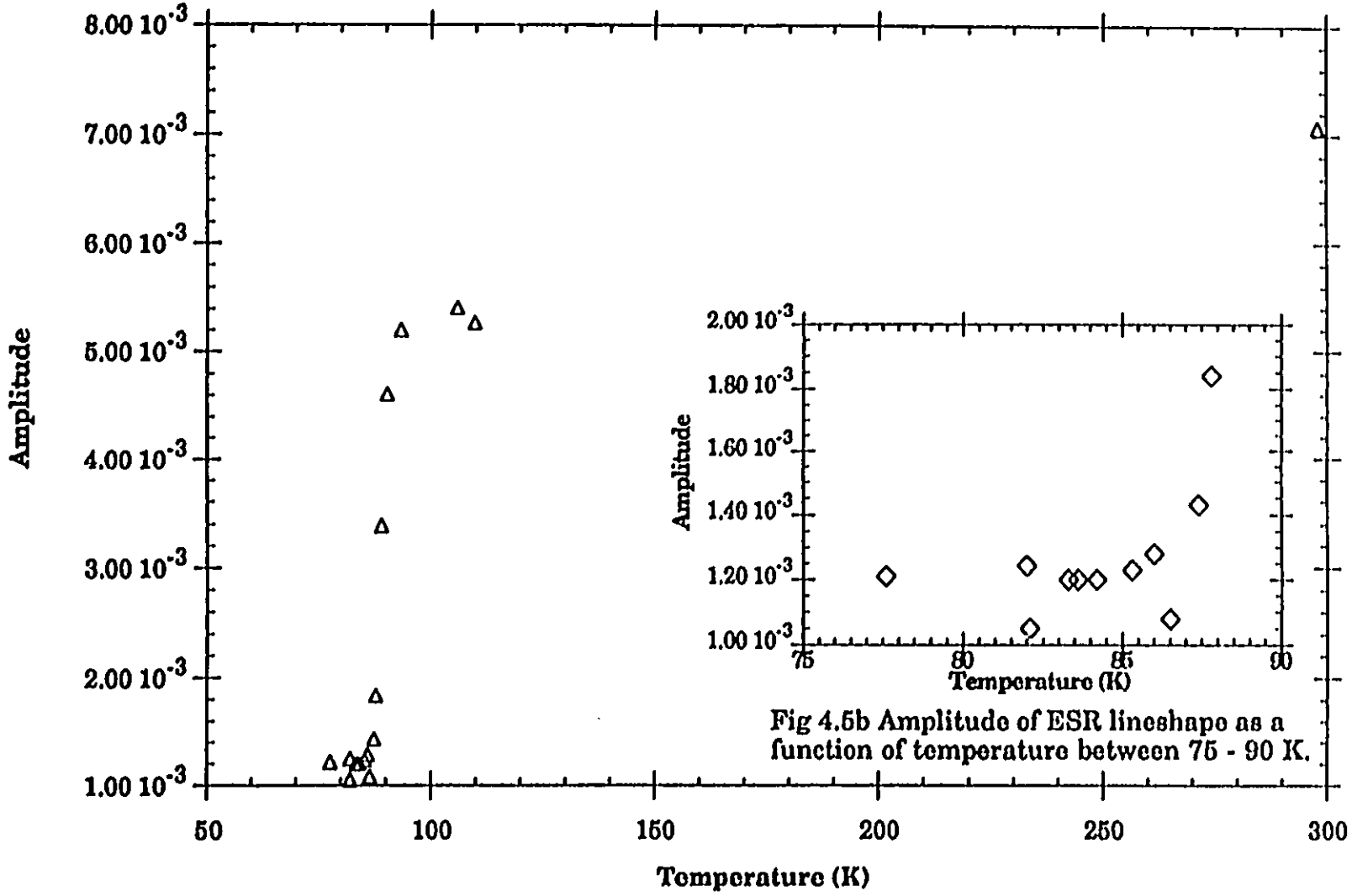

Fig 4.5b Amplitude of ESR lineshape as a function of temperature between 75 - 90 K.

Fig 4.5 Amplitude of ESR lineshape as a function of temperature.

In Mn_2SiS_4 there are two different sites for manganese which are unrelated by symmetry. As discussed earlier each atom is octahedrally coordinated, but each octahedra is distorted from the perfect octahedra in different directions. This would indicate that depending on the relative distortion the surrounding electric crystal field would differ from one manganese site to the other. Since there is a change in the local environment the signal of each manganese site could also differ. Since stoichiometrically there is an equal amount of Mn(4a) and Mn(4c) then the area under the curves of each LD, which is proportional to the number of spins, should be equal. A simple approximate form for the area under a LD is

$$\text{Area} = 3.63\, Y'_{max}\, \Delta H_{pp}^2 \quad [5]. \qquad 4.18$$

This equation is based on a normalized LD. In its use as a comparative measure it is more than adequate.

The area under the curve for a single LD as a function of temperature closely follows the variation of the amplitude as a function of temperature. Obviously this is due to the larger variation of the amplitude than the linewidth over the range of temperatures.

Goede et. al. [13] proposed that the Mn^{++} on the surface of a polycrystalline sample will have a Néel temperature different from the Mn^{++} ions within the crystallites. Above the highest T_n the ESR signal will be composed of 2 LD's having the same g value and hence the same Ho, but the linewidth will be different. This occurs because of the Mn ions on the surface have a reduced number of nearest and next nearest neighbours, which alters the effective spins of the Mn^{++} ions.

According to this model the two resultant LD lineshapes should have an area ratio which is proportional to the ratio of the number of spins

$$\frac{\text{Area}_{\text{Surface M}^{++}\text{ions}}}{\text{Area}_{\text{Bulk M}^{++}\text{ions}}} = 6\Delta d \qquad 4.19$$

where d is the average crystal diameter and Δ is the thickness of the surface region. In general Δ is assumed to be on the order of the lattice parameters.

Attempts to resolve the two ESR signals based on Goede's proposal did not yield any favorable results. At present there was not sufficient information to properly constrain enough parameters to get a meaningful output from the minimization process. Also due to the time restriction of a Masters degree this line of analysis was not pursued.

4.4 Conclusion:

The data acquisition system used performed adequately in the recording of the ESR signal. The configuration of the system contributed less than 1 % error to the final results. The software, written to control the LAB-PC board during acquisition, was relatively easy to use and produced consistent results. The analysis software, while sufficient for the current tasks, could be modified with ease of use and versatility in mind.

The analysis of the ESR spectra is summarized in the graphs shown in fig 4.4 and 4.5. The broadening of the resonance linewidth could be indicative of the increasing dipole fluctuation amplitudes or decreasing fluctuation frequencies [7,29]. Both of these effects are attributed to the same mechanism: the increase in spin-spin relaxation time. The peak of resonance broadening occurs just above the paramagnetic-ferrimagnetic transition temperature. As the temperature decreases the amplitude of the ESR spectra diminishes rapidly. This result is similar to Trounson et. al. [26] and, although they offer no precise explanation for this effect, they state that it coincides with a magnetic phase change.

At present there are no definitive theoretical explanations for the behavior of the resonance linewidth in broad ESR spectra. Despite ample experimental data there have been few attempts at a theoretical

interpretation of ESR linewidth broadening that go beyond the phenomenological models [13,21].

This technique of digitizing the ESR signal and then numerically analyzing the data has the potential to uncover or resolve important information that has been previously obscured. The testing of different hypotheses can be quickly accomplished once the physically correct numerical equation is obtained. The rendering of numerical approximations from theoretical constructs is beyond the scope of this thesis and is the next logical step towards understanding broad ESR signals.

CONCLUSION

The analysis of Mn_2SiS_4 has completely exposed the mechanisms that are responsible for its exceptional temperature dependent magnetic behavior, which was the spontaneous magnetization between 83 and 86.5 K. This behavior was discovered during low field magnetic susceptibility measurements performed by a SQUID magnetometer in the temperature range of 4.2 to 250 K.

The x-ray analysis indicated that Mn_2SiS_4 is an olivine with the lattice parameter of : a = 12.688, b = 7.427, c = 5.946 Å. This was later confirmed by neutron diffraction results. Mn_2SiS_4 has the orthorhombic symmetry Pnma. There are 8 Mn^{++} ions per unit cell which are divided into two sites unrelated by symmetry which give rise to two sublatticies.

A detailed analysis of neutron diffraction spectra, obtained at 29 different temperatures between 4.2 and 150 K, revealed information on the temperature dependence of: magnetic ordering, atom position, and lattice parameters. The results were that the Mn^{++} ions are antiferromagnetically aligned from 4.2 to 83 K. and at 83 K there is a transition to a weak ferromagnetic arrangement. This is due to the small angle canting of the two spin sublatticies which give rise to the observed spontaneous magnetization. At 86.5 K the Mn^{++} ions go though another transition from the weak ferromagnetic to a paramagnetic state.

From the specific heat measurements performed in Geneva, a lambda-type anomaly is seen at the order-disorder transition at 86.5 K. At 83 K there is a first order transition that is broadened by inhomogeneities. Further investigation of this transition produced a value for the latent heat of transition for the change in magnetic symmetry from Pnma to Pn'm'a.

The electron spin resonance measurements showed: a broadening of the linewidth as the transition to the ordered phase is approached, a maximum linewidth slightly above the transition temperature of 86.5 K,

and a rapid decrease in linewidth below the spontaneous magnetization region. This behavior may be associated with the increase in amplitude or the decrease in frequency of dipole fluctuations.

Through the results of all the experiments described in this thesis a comprehensive understanding of the rare magnetic behavior of Mn_2SiS_4 has been obtained. The next step in developing the techniques used in this research would be: 1) for the specific heat measurements, a more accurate thermometer must be obtained or the sensing voltage will have to be increased to provide higher resolution. Another possibility is to redesign or modify the existing system to function as a constant power adiabatic calorimeter similar to the one in Geneva. 2) for the neutron diffraction analysis, obtaining better documentation for the GSAS program. 3) For the ESR measurements, further development of theoretical models that explain experimental results.

REFERENCES

BOOKS:

[1] Abragam, A., Bleaney, B., Electron Paramagnetic Resonance of transition ions, Oxford University press, 1970.

[2] Bacon,G.E., Neutron Diffraction, 2nd ed., Clarendon Press, 1962

[3] Brown, P.J., Forsyth, J.B., The crystal structure of solids, Edward Arnold; Crane, Russak, 1973.

[4] Fake, G.E., Estle, T.L., The physical properties of Electron Paramagnetic resonance, 2nd ed., W.A. Benjamin, Inc., 1973.

[5] Poole jr, C.P., Electron spin resonance, 2nd ed., John Wiley & Sons, Inc. 1982.

[6] Poole jr, C.P., Farach, H.A., Theory of magnetic resonance, John Wiley & Sons, Inc., 1972.

[7] Owens, F.J., Poole jr, C.P., Farach, H.A., Magnetic resonance of phase transitions, Academic Press, 1979.

[8] Wertz, J.E., Bolton, J.R., Electon spin resonace: Elementary theory and practical applications, McGraw-Hill, Inc., 1972.

[9] White, R.M., Quantum theory of Magnetism, McGraw-Hill Inc., 1970.

[10] Morrish, A.H., The principles of magnetism, Robert Krieger Publishing Inc., 1965.

[11] Joshua, J.S., Symmetry Principle and Magnetic Symmetry in Solid State Physics, Adam Hilgar, 1991.

PAPERS:

[12] Lamarche, G., Rev. Sci. Instrum. **60**, 943 (1989).

[13] Goede, O., Back, D.,Heimbrodt, W., Kanis, M., EPR study of the antiferromagnetic phase transition in (Cd,Mn)S, Phys.stat.sol.(b) **151**, 311 (1989).

[14] Howard, S.A., Preston, K.D., Profile fitting of powder diffraction patterns, Rev. Mineral. **20**, 217-275 (1989).

[15] Ibers, J.A., Swalen, J.D., Paramagnetic resonance line shapes and magnetic parameters of polycrystalline substances, Phys. Rev. **127**,1914-1917 (1962).

[16] Vincent, H., Bertaut, E.F., Etude cristallographique et magnetique de Fe2GeS4 structures magnetiques a 85 et 4.2°K, J.Phys.Chem. solids **34**, 151-158 (1973)

[17] Vincent, H., Bertaut, E.F., Etude par diffraction neutronique de la structure nucleaire et magnetique de l'orthothiogermanate de manganese, Solid State Commun. **7**, 642-645 (1969).

[18] Fuhrmann J., Pickardt J., Structure of Mn2SiS4, Acta Cryst. **C45**, 1808-1809 (1989).

[19] Bachmann, R., DiSalvo, F.J. jr., Geballe, T.H., Howard, R.E., King, C.N.,Kirsch, H.C., Lee, K.N., Schwall, R.E., Thomas, H.U., and Zubeck, R.B., Heat capacity measurements on small samples at low temperatures, Rev. Sci. Instr. **43**, 2 , 205-214 (1972).

[20] Okamura, T., Torizuka, Y., Kojima, Y., Magnetic Resonance Absorption in Antiferromagnetic Materials, Phys. Rev. **82** (1951).

[21] Furdyna, J. K., ,Diluted Magnetic Semiconductors, J. Appl. Phys. **64** (1988).

[22] Lottermoser, Fuess, Magnetic structures of Orthosilicates, Phys. Stat. Sol.(a) **109**, 589-595 (1988).

[23] Larson, A. C., Von Dreele, R. B., GSAS Training and Technical manual (1990).

[24] Konyer, N. B., Root, J. H., Dualspec Powder Diffractometer Users Guide, (1992).

[25] Lamarche, A.-M., Lamarche, G., Church, C., Woolley, J. C.,Swainson, I., Neutron Diffraction Study of Magnetic Phases in Polycrystalline Mn_2SiS_4, to appear in J. Magn.Magn. (1994).

[26] Trounson, E.P., Bleil, D.F., Wangsness, R.K., Maxwell, L.R., Magnetic Reonance in Antiferromagnetic Materials near the Curie Temperature, Phys. Rev. **79**, 542-543 (1950).

[27] Lamarche, A.-M., private communicae.

[28] Sears, V.F., Neutron Scattering Lengths and Crosssections, AECL Research internal document.

[29] Guen, L., Glaunsinger, W.S.,Electrical, Magnetic, and EPR Studies of the Quarternary Chalcogenides $Cu_2A^{II}B^{IV}X_4$ Prepared by Iodine Transport, J. Sol. State Chem. 35, 10-21 (1980).

[30] National Instruments LAB-PC user manual, March 1990 edition, N.I. part number 320205-01.

[31] Junod, A., Wang, K.-Q., Triscone, G., Lamarche, G., Other Authors, Specific Heat, Magnetic Properties and Critical Behavior of Mn_2SiS_4 and Fe_2GeS_4, submitted to J. Magn. Magn.

Appendix A

Expansion of eqn 2.1 which is used in the program POWDER.

$$I_j = \left(\left(\left(\sum_{j=1}^{\#_n} Bn_j \sin(\alpha)\right)^2 + \left(\sum_{j=1}^{\#_n} Bn_j \cos(\alpha)\right)^2\right)_j + \left(\left(\sum_{p=1}^{\#_m} \mu_p \vec{q} \sin(\phi)\right)^2 + \left(\sum_{p=1}^{\#_m} \mu_p \vec{q} \cos(\phi)\right)^2\right)_j e^{-2dW_m Q_{su}}\right) \quad e^{-\frac{1}{2}dW_n^2 Q_{sum}}$$

Where

Bnj = coherent nuclear scattering factor,

$\alpha = 2\theta$, the scattering angle,

μ = the spin magnitude,

ϕ = the phase factor,

q = magnetic interaction vector, eqn 2.2

dW_m = the coefficient for the gaussian form factor.

dW_n = the rms vibrational ampitude (Å),

$Q_{sum} = Q^2$.

Appendix B

Below is the Minuit front end program that defines the theoretical parameters that model a lorentzian derivative lineshape and the least squares function which is minimized.

C Program designed to fit 3 lorentzian derivatives for ESR lineshapes.

```
      CHARACTER*8 DUMMY
      CHARACTER*12 COMFL1,DATFL1,OUTFL1,FITFL1
      EXTERNAL FCN
C     OPEN(5,FILE="CONS:")
C     OPEN(6,FILE="SCRN:")
      WRITE (6,10)
 10   FORMAT (//1X,'ENTER THE FILENAME YOU WISH TO ANALYZE.')
      READ(5,'(A)') DUMMY
      DATFL1 = DUMMY//".MIN"
      OUTFL1 = DUMMY//".OUT"
      FITFL1 = DUMMY//".FIT"
      OPEN (8,FILE=DATFL1)
      OPEN(11,FILE=OUTFL1)
      OPEN(15,FILE=FITFL1)
      WRITE (6,15) DATFL1,OUTFL1,FITFL1
 15   FORMAT (/1X,'DATA FILE: ',A14,' OUTPUT FILE:',A14,' FIT FILE:',
     *     A14)
      CALL MINTIO(8,6,11)
      CALL MINUIT(FCN,FUTIL)
      CLOSE (5)
      CLOSE (6)
      CLOSE (8)
      CLOSE (11)
      CLOSE (15)
      STOP
      END

C     ************************************************
      SUBROUTINE FCN(NPAR,G,F,P,IFLAG,futil)
      DOUBLE PRECISION UPPER1, SOWER1, UPPER2, SOWER2, X(2500), F, SUMEX
      DOUBLE PRECISION UPPER3,SOWER3
      DOUBLE PRECISION Y(2500),SUBT(2500), DIFF(2500),G(NPAR),P(NPAR)
      DOUBLE PRECISION CORREL, LOR1(2500), LOR2(2500), LOR3(2500)
      DOUBLE PRECISION AREA1, AREA2, MINFUNC
      INTEGER IFLAG, NPAR, ICOUNT
      FUTIL = 0
      IF (IFLAG .EQ. 1) THEN
        READ (8,*) ICOUNT
 110    FORMAT (T2,I3)
        WRITE (6,115)( ICOUNT)
        WRITE (11,115) (ICOUNT)
 115    FORMAT (1X,I4,1X,I4,1X,I4)
        DO 40 I = 1,ICOUNT
          READ (8,120) X(I),Y(I)
 120      FORMAT (T2,F12.6,T17,F10.6)
 40     CONTINUE
      ELSEIF (IFLAG .EQ. 2)THEN
C       NOTHING HAPPENS HERE!
      ELSEIF (IFLAG .GE. 3)THEN
        F = 0.0
        SUMEX = 0.0
        DO 200 J = 1 ,ICOUNT
          UPPER1 = ((16*P(1))*(X(J)-P(3)))/(0.5 * P(4))
```

```
        SOWER1 = (3+((X(J)-P(3))/(0.5 * P(4)))**2)**2
       UPPER2 = ((16*P(6))*(X(J)-P(S)))/(0.5 * P(9))
        SOWER2 = (3+((X(J)-P(S))/(0.5 * P(9)))**2)**2
       UPPER3 = ((16*P(10))*(X(J)-P(12)))/(0.5 * P(13))
        SOWER3 = (3+((X(J)-P(12))/(0.5 * P(13)))**2)**2
       SUBT(J) =(UPPER1/SOWER1) + (UPPER2/SOWER2) (UPPER3/SOWER3)
        DIFF(J) = Y(J) - SUBT(J)
      F = F + (DIFF(J))**2
      SUMEX = SUMEX + (Y(J))**2
200   CONTINUE
     IF (IFLAG .EQ. 3)THEN
      WRITE (15,124)
124     FORMAT (2X,'MAGNETIC FIELD',5X,'MEASURED',5X,'CALCULATED')
      DO 180 J= 1, ICOUNT
       UPPER1 = ((16*P(1))*(X(J)-P(3)))/(0.5 * P(4))
        SOWER1 = (3+((X(J)-P(3))/(0.5 * P(4)))**2)**2
       UPPER2 = ((16*P(6))*(X(J)-P(8)))/(0.5 * P(9))
        SOWER2 = (3+((X(J)-P(8))/(0.5 * P(9)))**2)**2
       UPPER3 = ((16*P(10))*(X(J)-P(12)))/(0.5 * P(13))
        SOWER3 = (3+((X(J)-P(12))/(0.5 * P(13)))**2)**2
       LOR1(J) = UPPER1/SOWER1
       LOR2(J) = UPPER2/SOWER2
       LOR3(J) = UPPER3/SOWER3
         WRITE (15,125) X(J),Y(J),SUBT(J),LOR1(J),LOR2(J),LOR3(J)
125       FORMAT (3X,F12.6,5X,F9.6,5X,F9.6,5X,F9.6,5X,F9.6,5X,F9.6)
180    CONTINUE
      WRITE (6,210) F
      WRITE (11,210) F
      WRITE (15,210) F
210     FORMAT (1X,'THE MEAN SQUARED ERROR IS ',2X,E15.7)
C       Assume that the average y-value is zero due to symmetry
C       so that (Y - Yavg) = Y
      CORREL = 1 - (F/SUMEX)
211     FORMAT (1X,'THE CORRELLATION FACTOR IS',2X,E15.7)
      WRITE (6,211) CORREL
      WRITE (11,211) CORREL
      WRITE (15,211) CORREL
    ENDIF
    ENDIF
    RETURN
    END
```

Appendix C

ESR Profiles

C1.....77.6 K

C2.....82.0 K

C3.....83.3 K

C4.....83.6 K

C5.....84.2 K

C6.....85.3 K

C7.....86.1 K

C8.....86.5 K

C9.....87.4 K

C10.....87.7 K

C11.....89.0 K

C12.....90.2 K

C13.....93.2 K

C14....105.7 K

C15....109.7 K

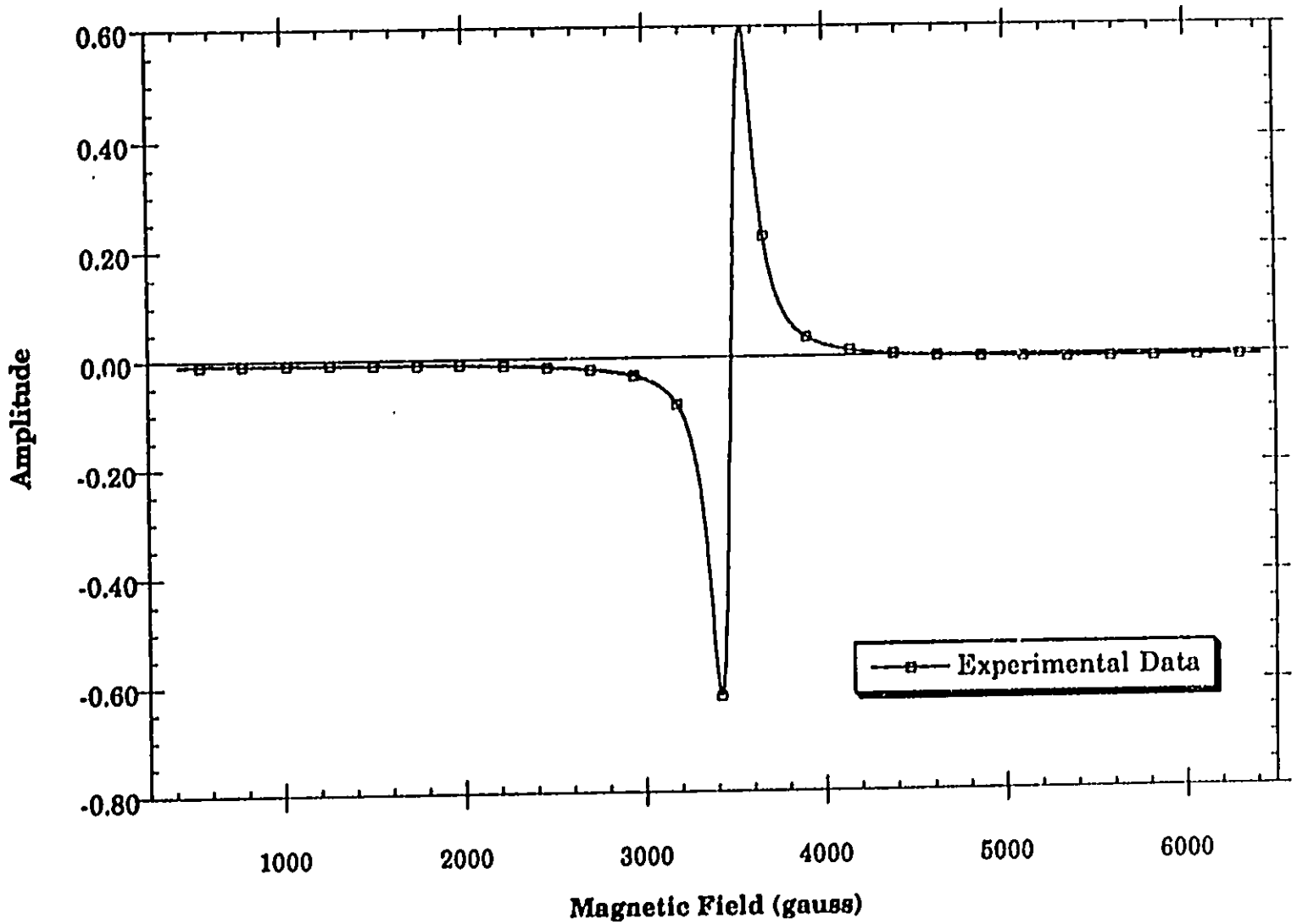

C1 ESR linshape of Mn_2SiS_4 at 77.6 K.

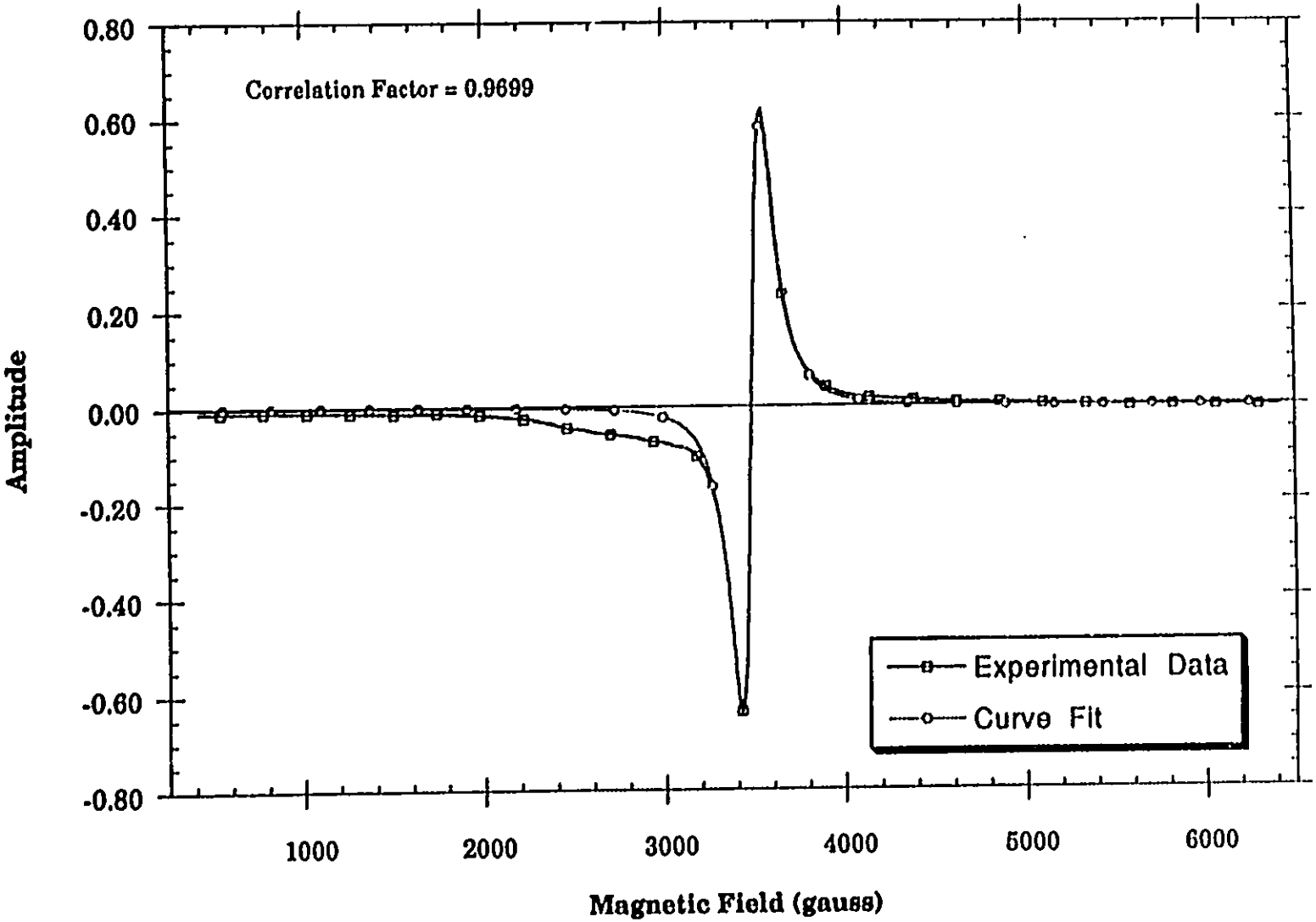

C2 ESR lineshape of Mn_2SiS_4 at 82.0 K fitted with 1 LD.

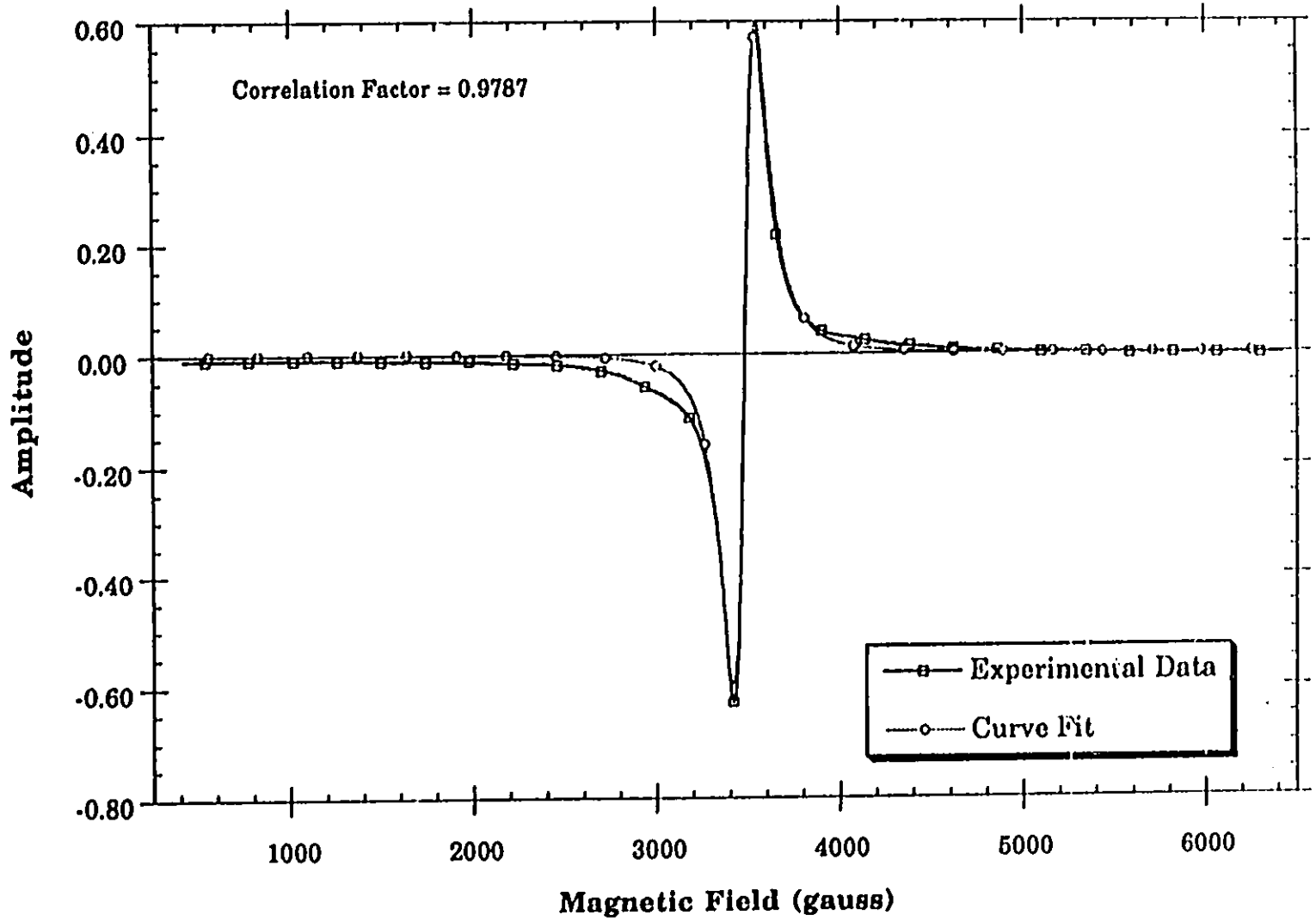

C3 ESR linshape of Mn_2SiS_4 at 83.3 K fitted with 1 LD.

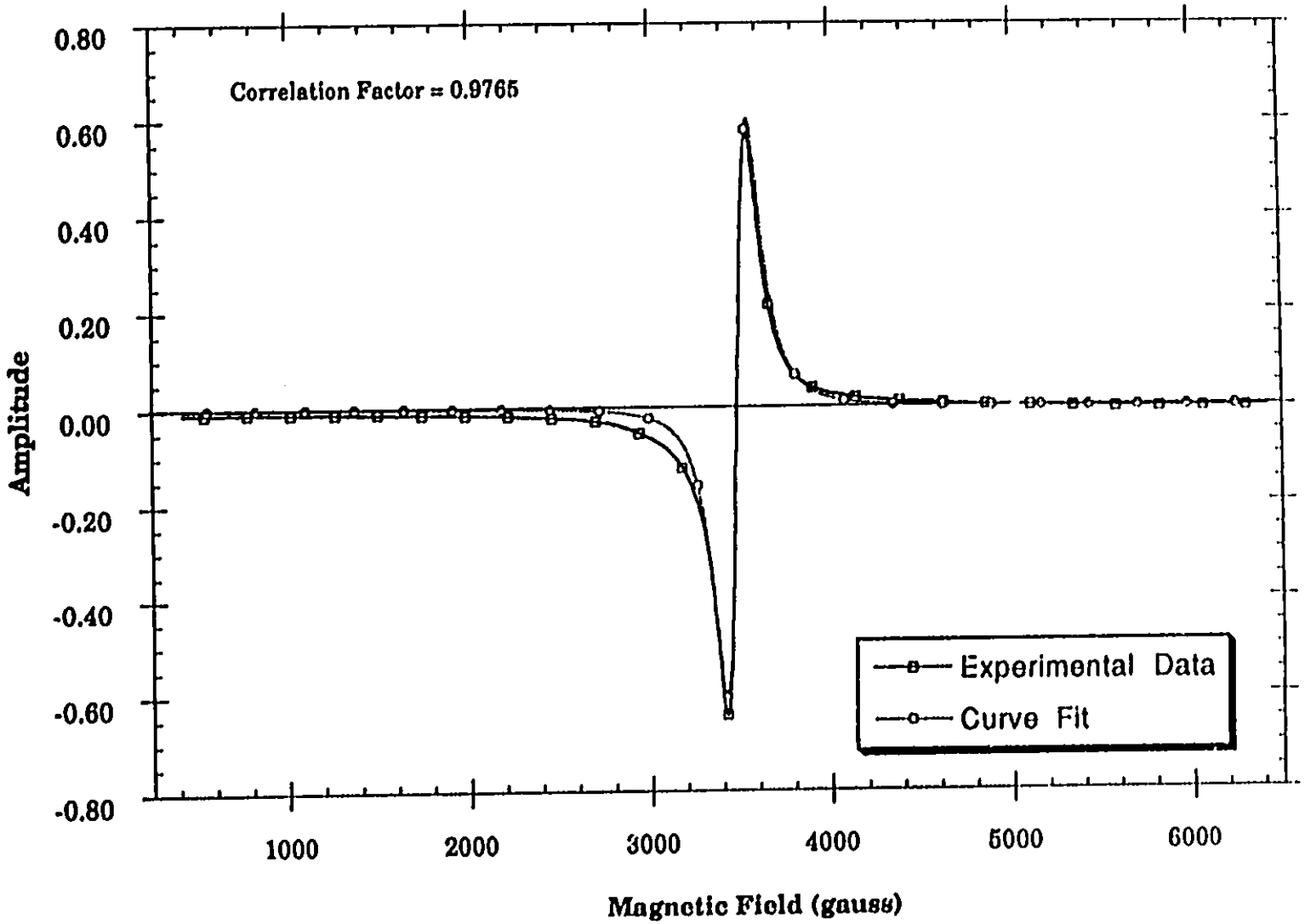

C4 ESR lineshape of Mn_2SiS_4 at 83.6 K fitted with 1 LD.

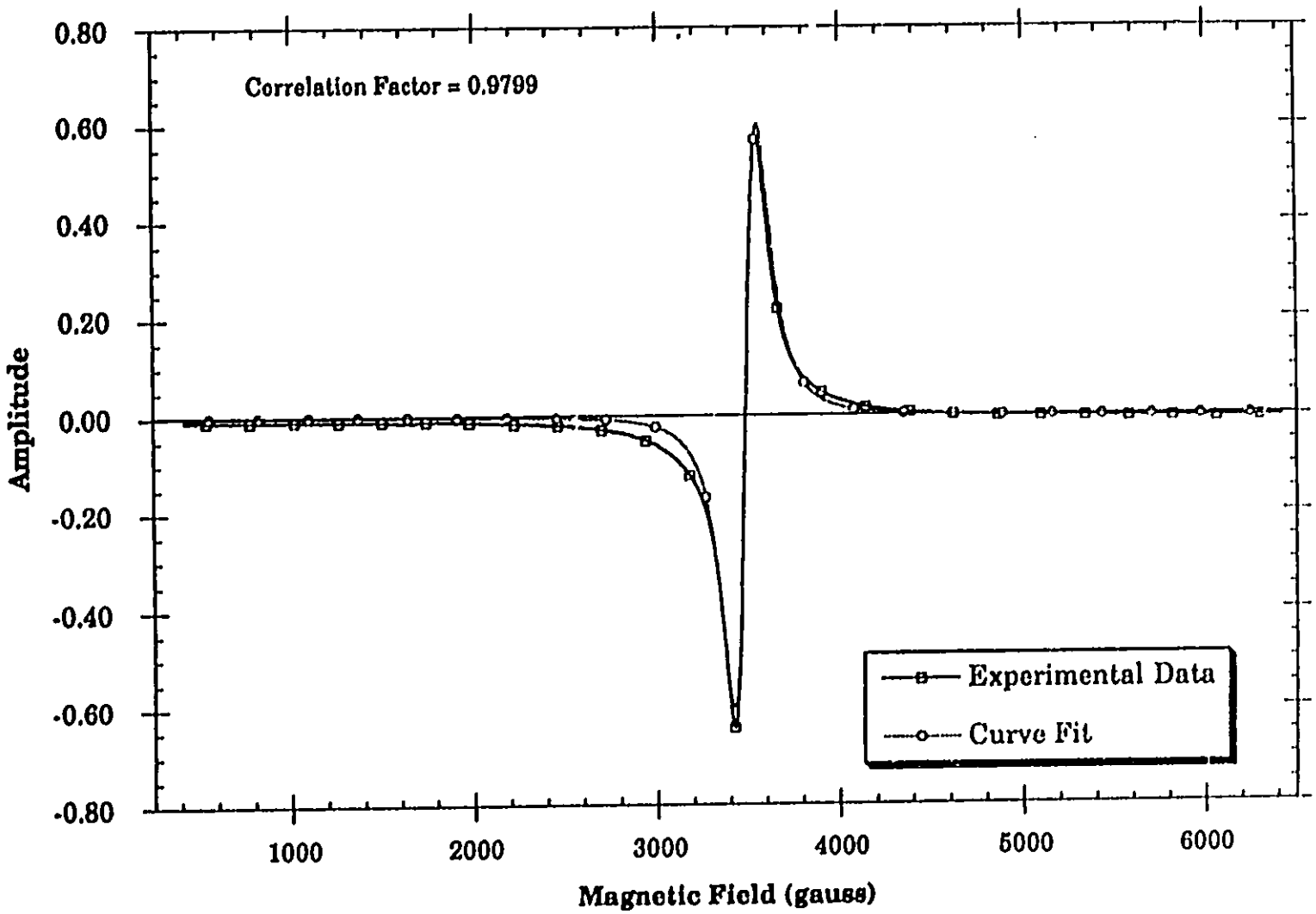

C5 ESR lineshape of Mn_2SiS_4 at 84.2 K fitted with 1 LD.

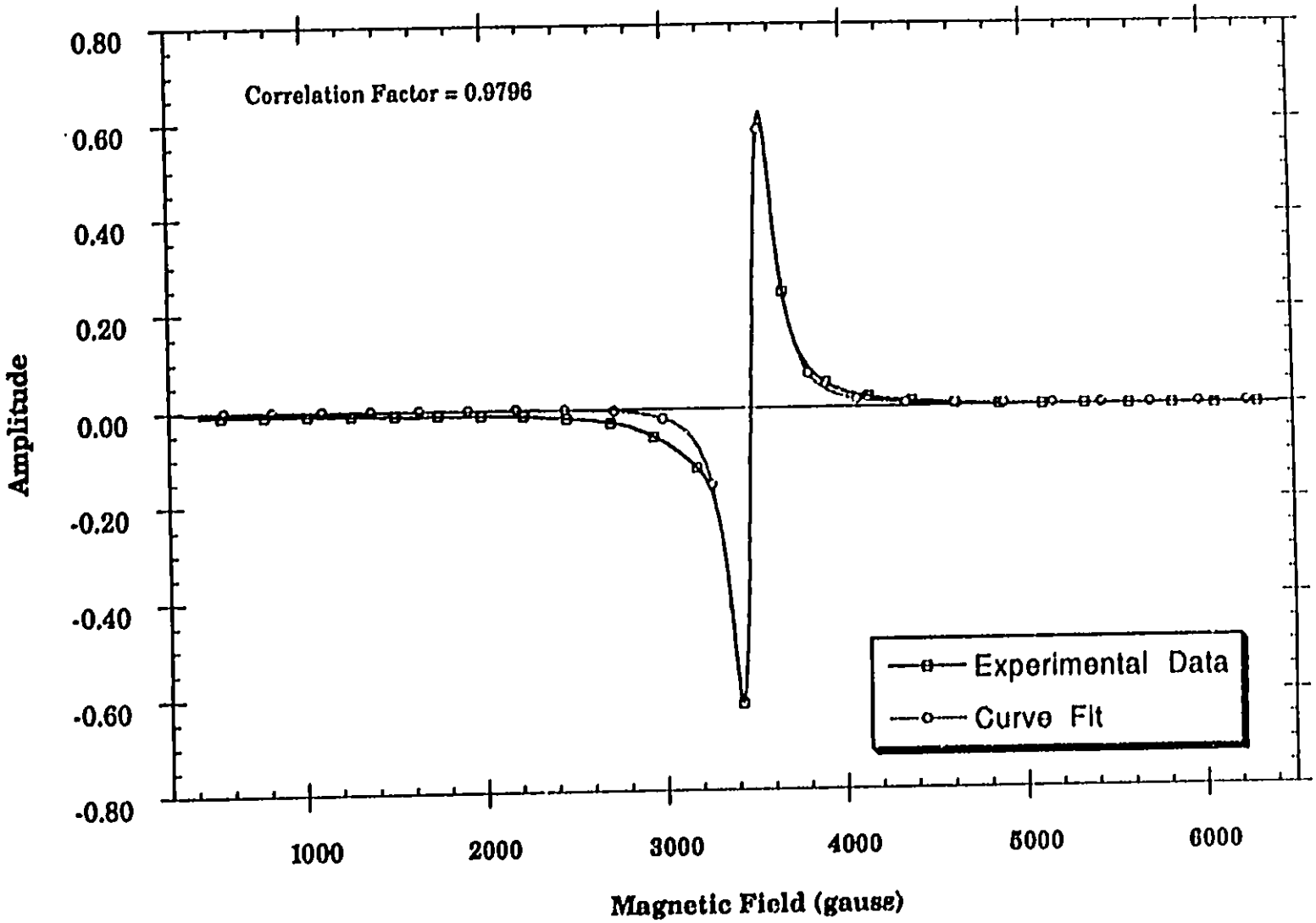

C6 ESR lineshape of Mn_2SiS_4 at 85.3 K fitted with 1 LD.

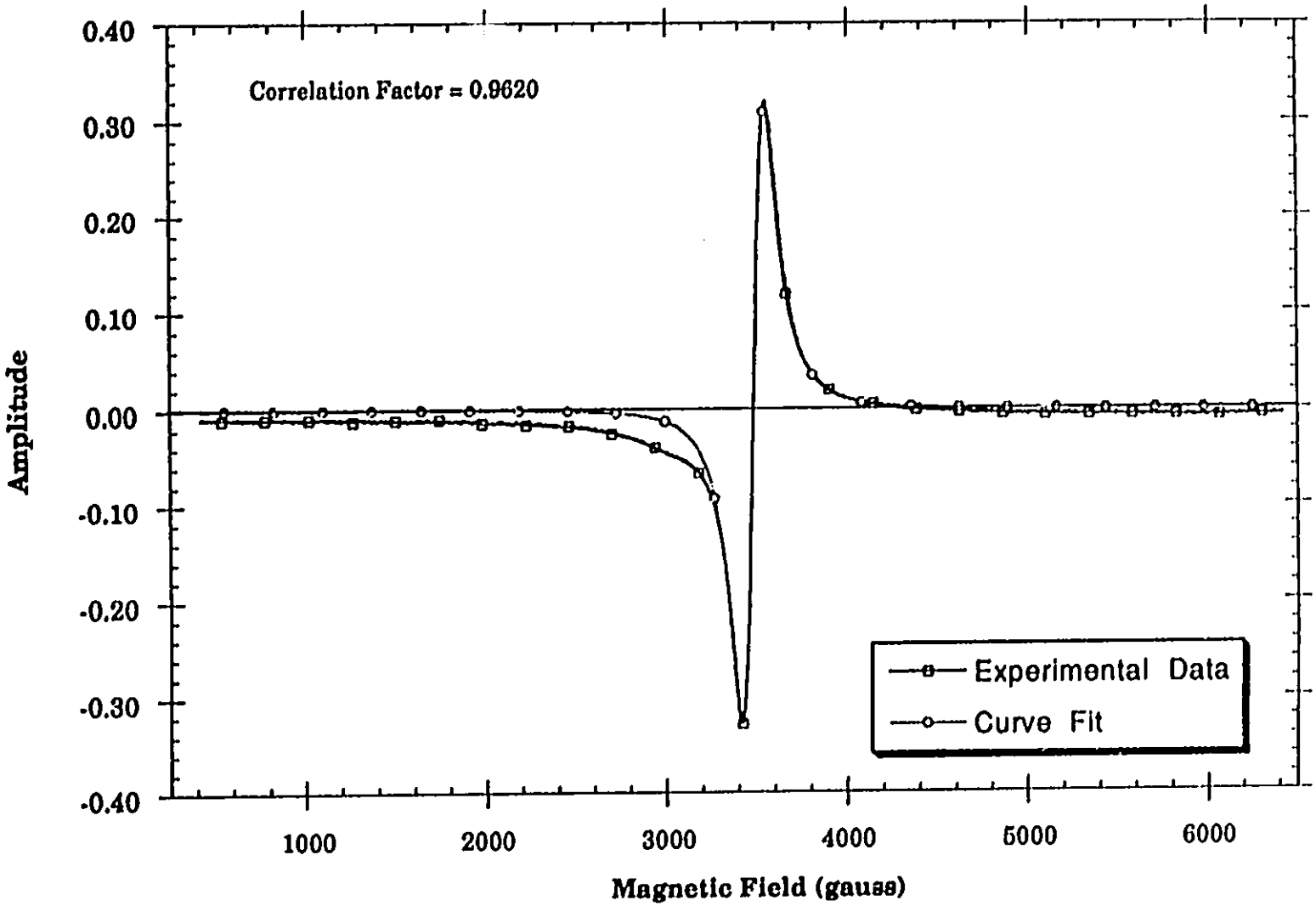

C7 ESR lineshape of Mn_2SiS_4 at 86.1 K fitted with 1 LD.

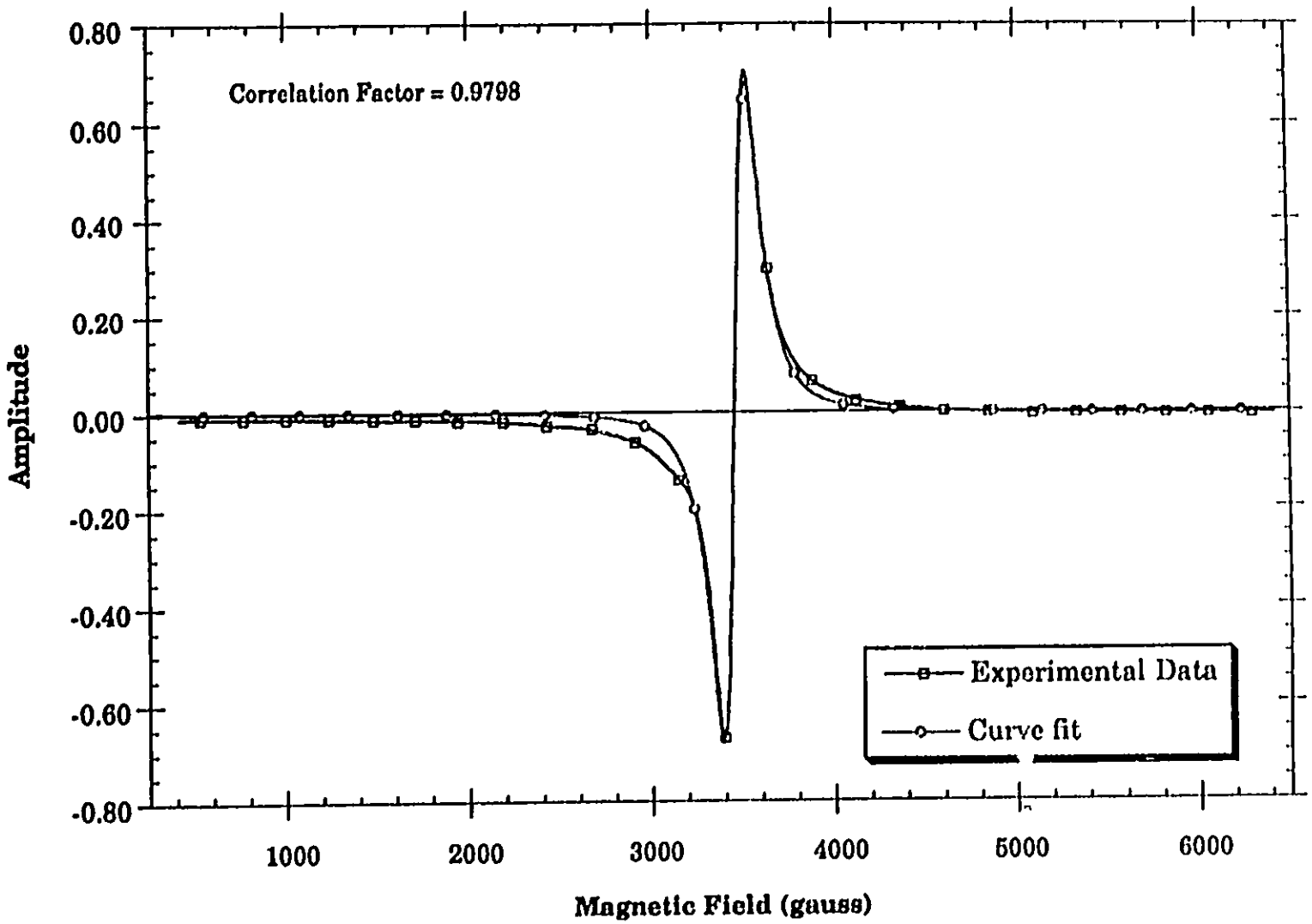

C8 ESR linshape of Mn_2SiS_4 at 86.5 K fitted with 1 LD.

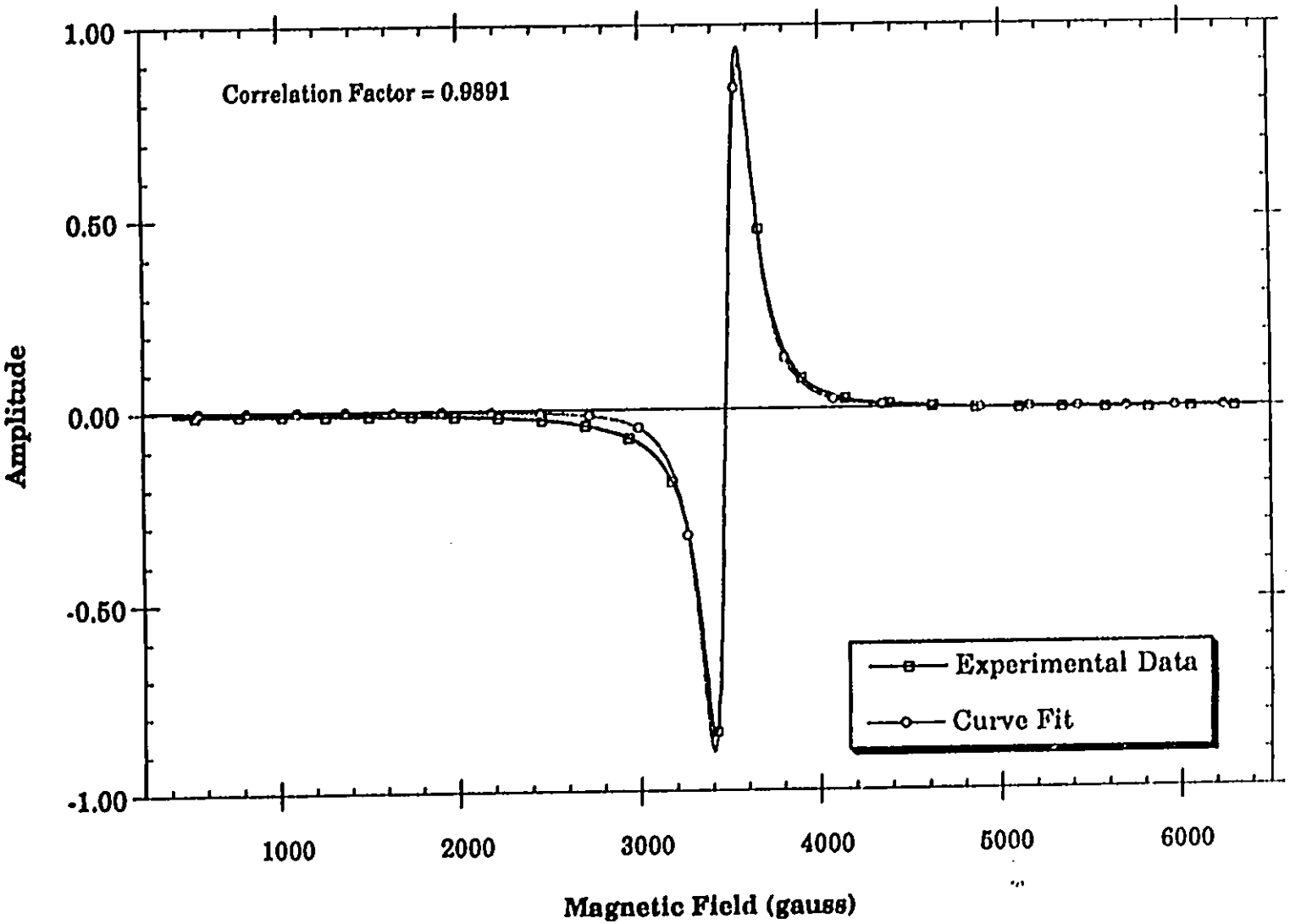

C9 ESR linshape of Mn_2SiS_4 at 87.4 K fitted with 1 LD.

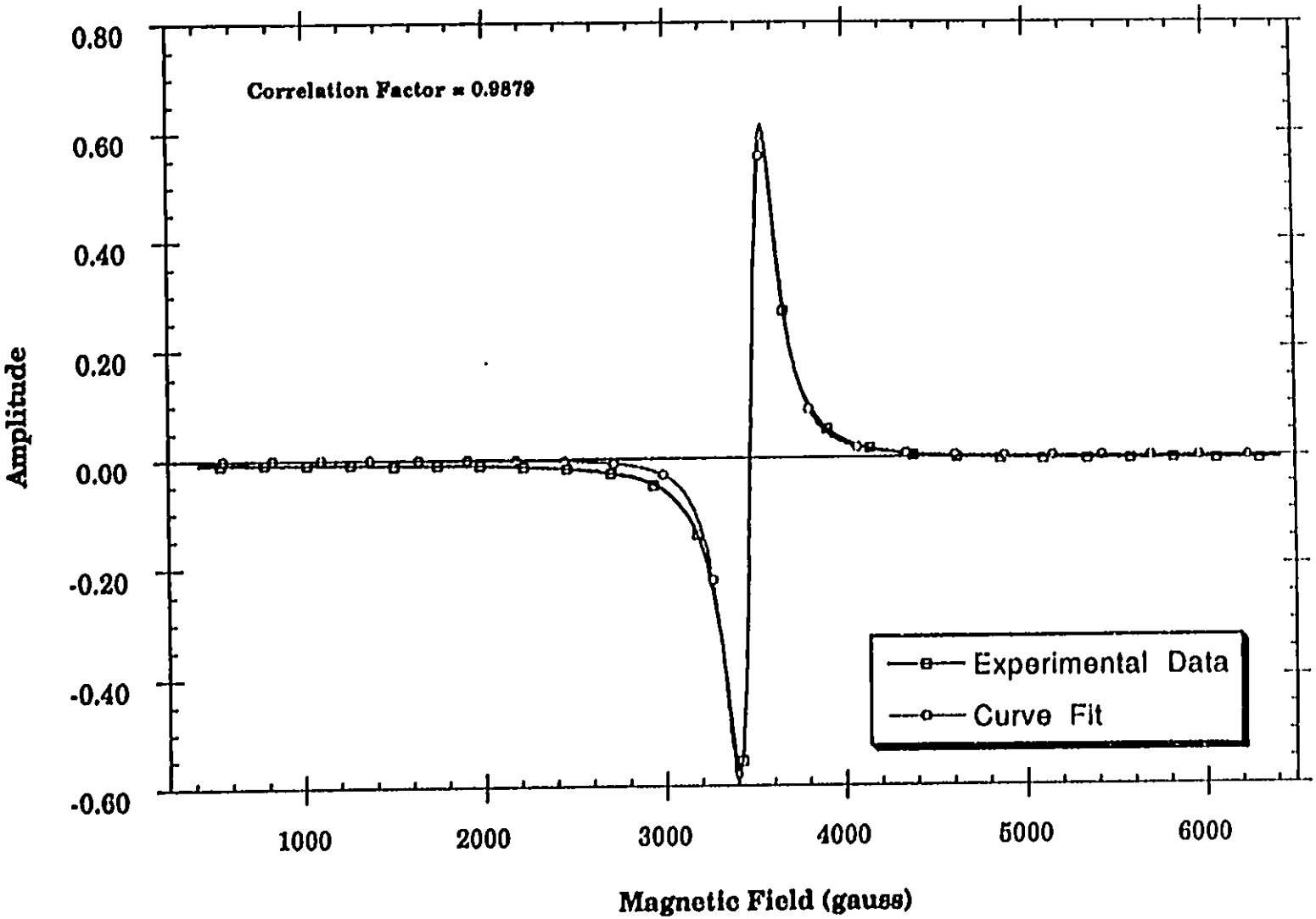

C10 ESR lineshape of Mn_2SiS_4 at 87.7 K fitted with 1 LD.

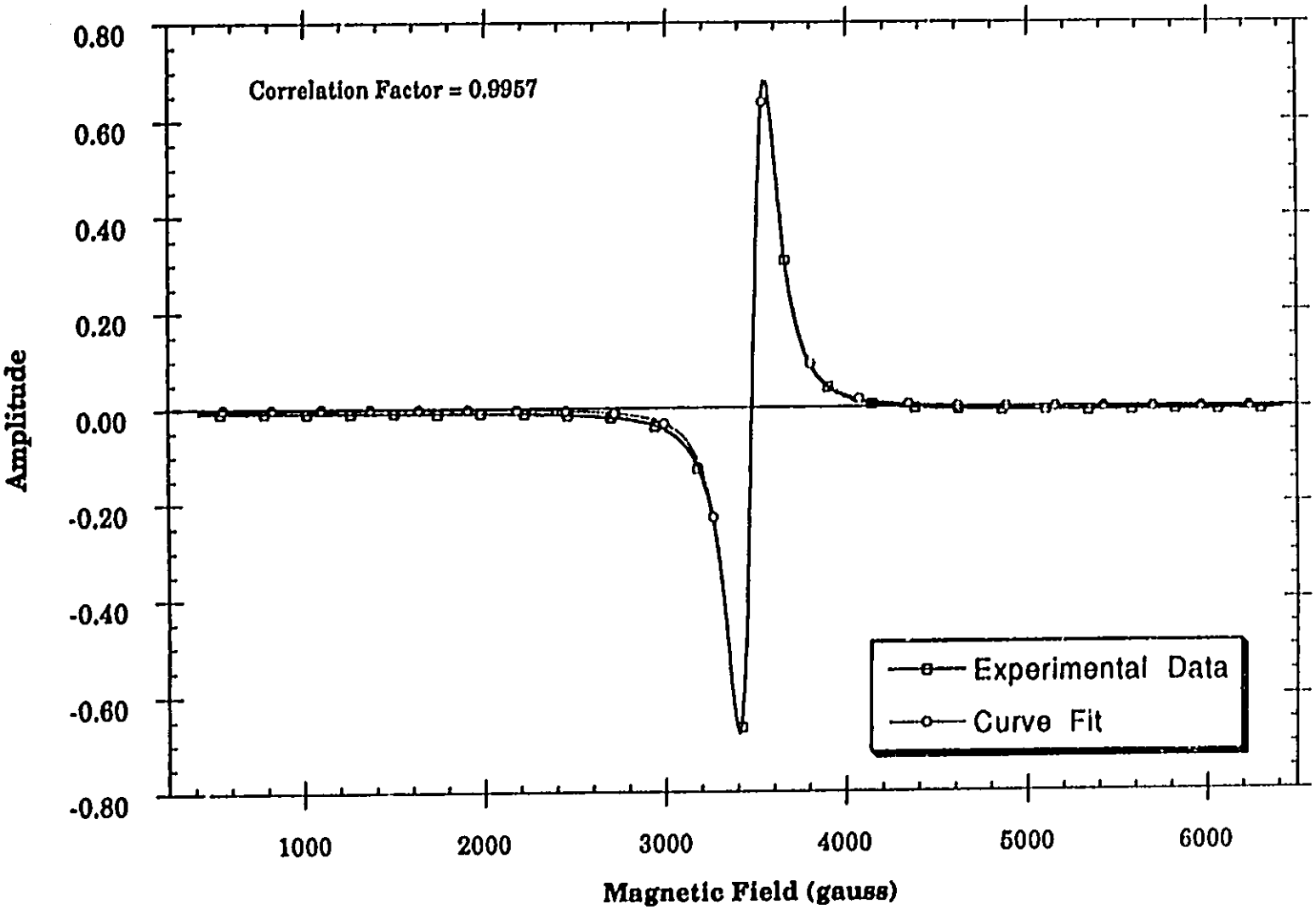

C11 ESR lineshape of Mn_2SiS_4 at 89.0 K fitted with 1 LD.

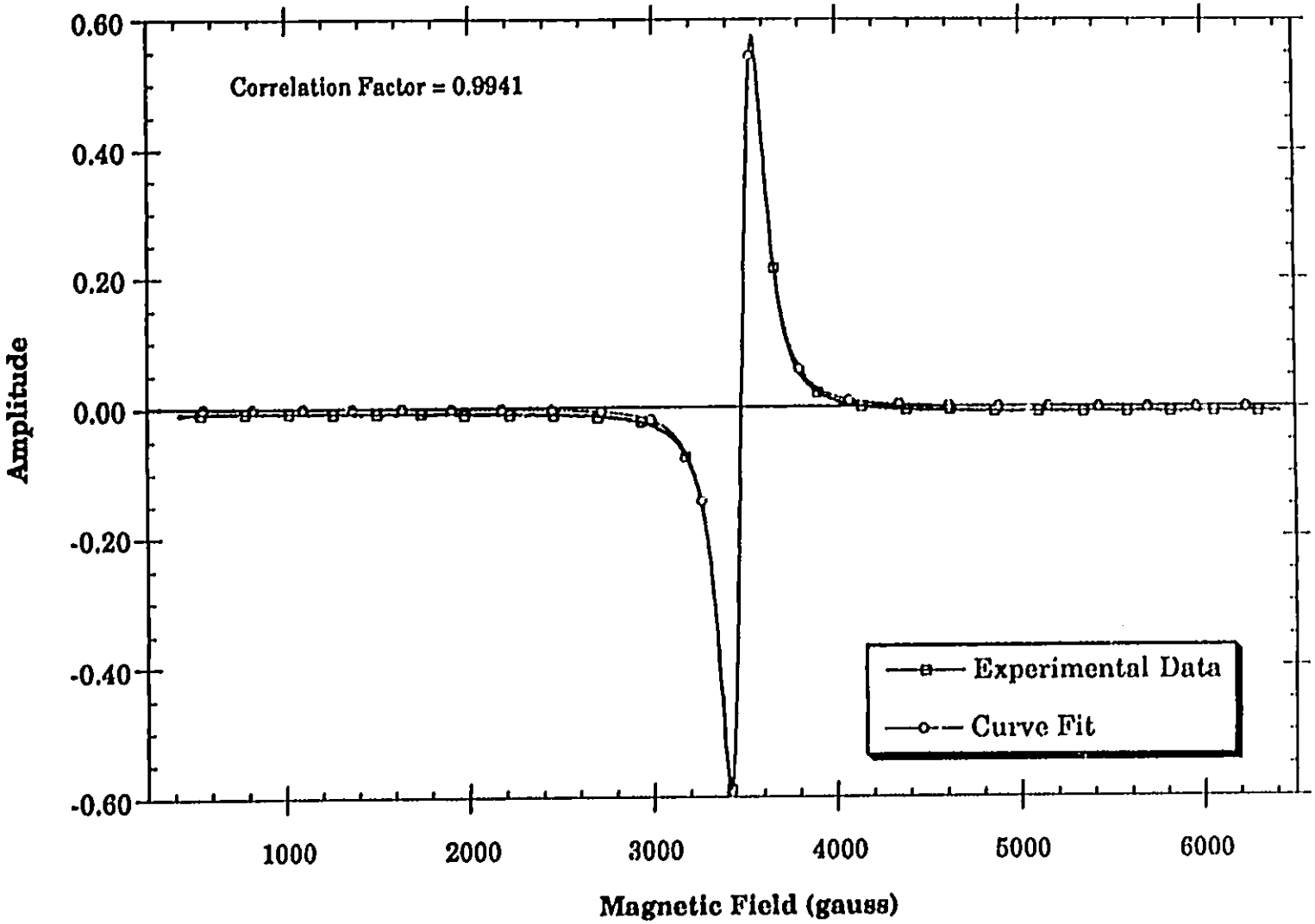

C12 ESR linshape of Mn_2SiS_4 at 90.2 K fitted with 1 LD.

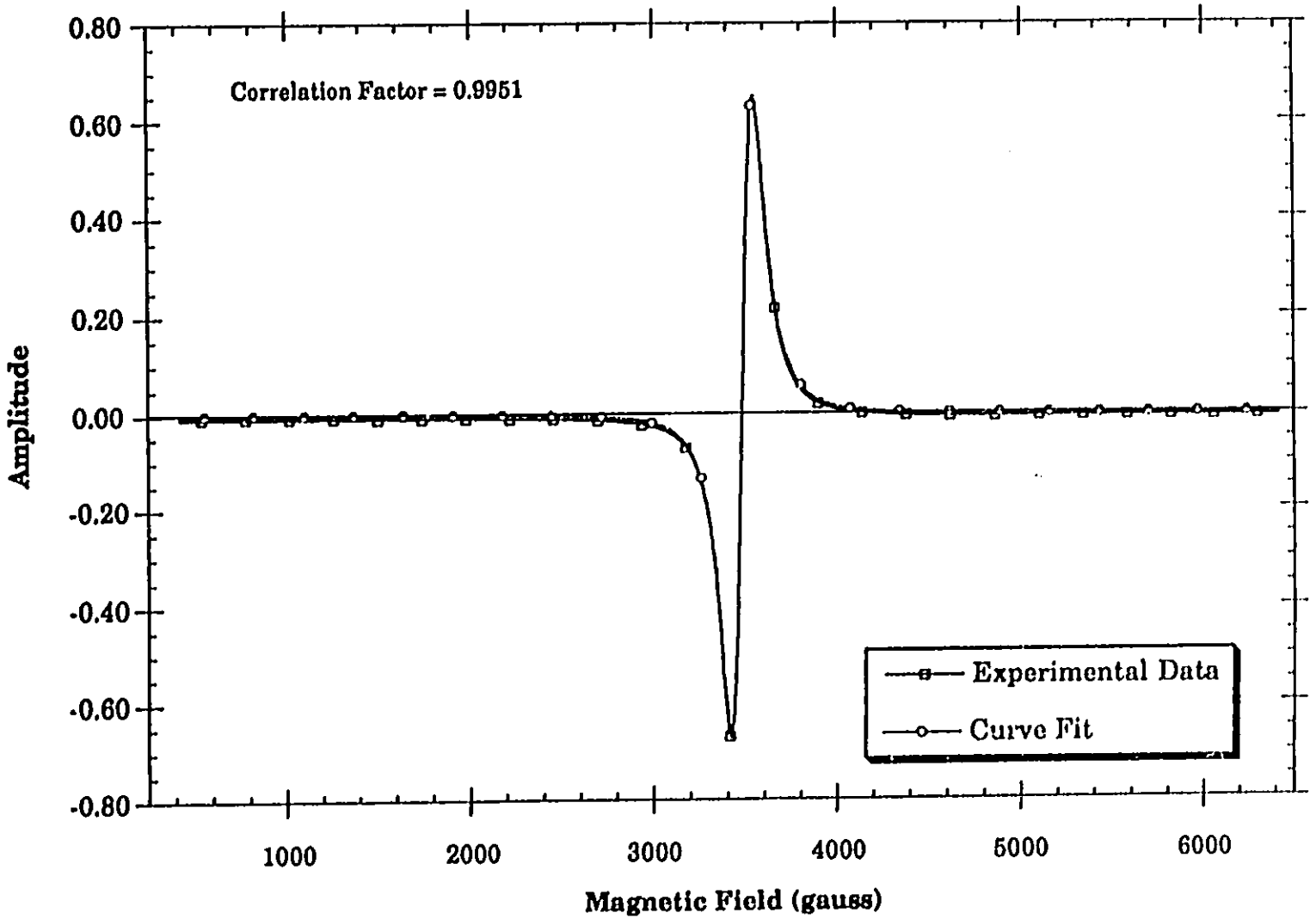

C13 ESR linshape of Mn_2SiS_4 at 93.2 K fitted with 1 LD.

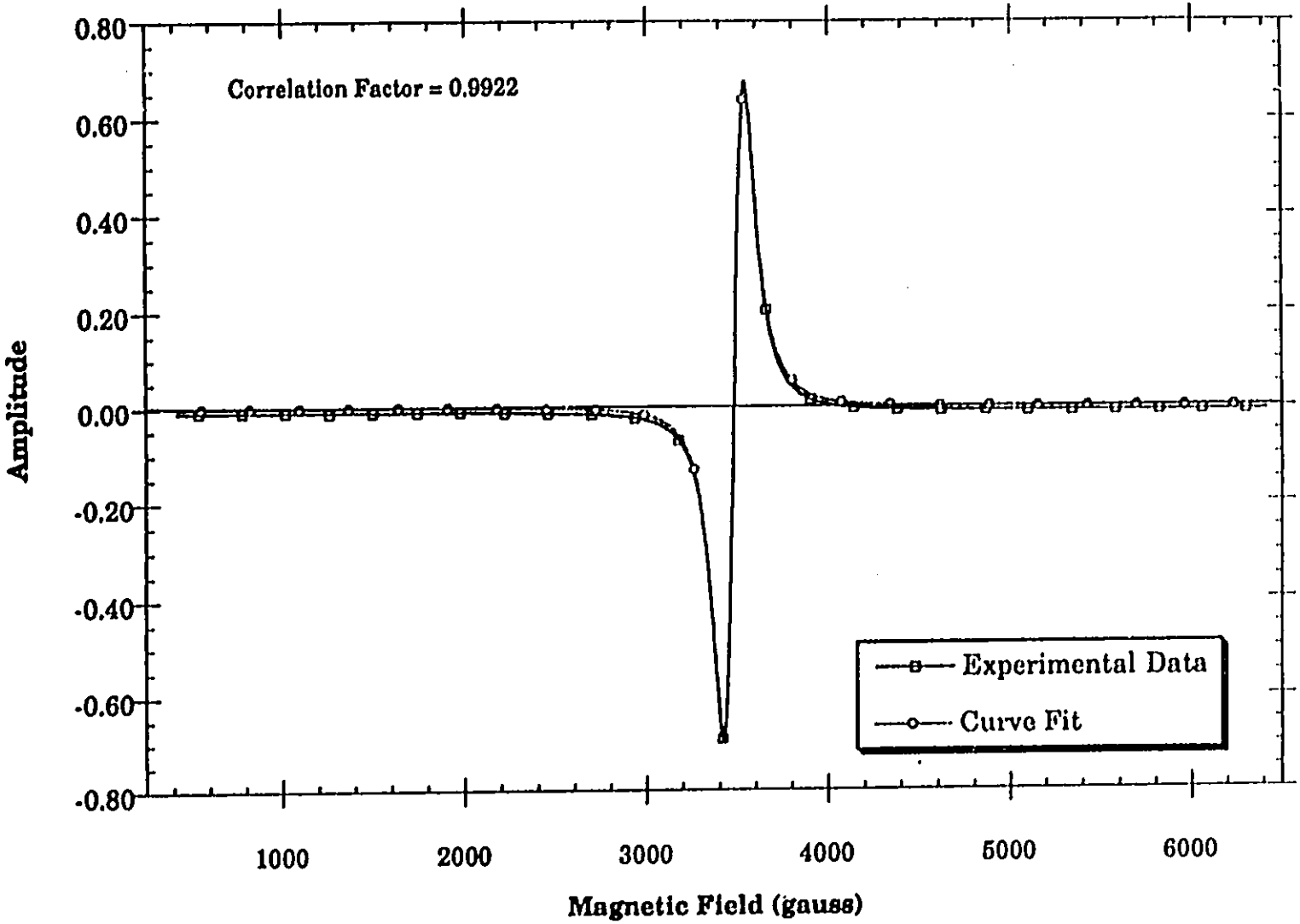

C14 ESR linshape of Mn_2SiS_4 at 105.7 K fitted with 1 LD.

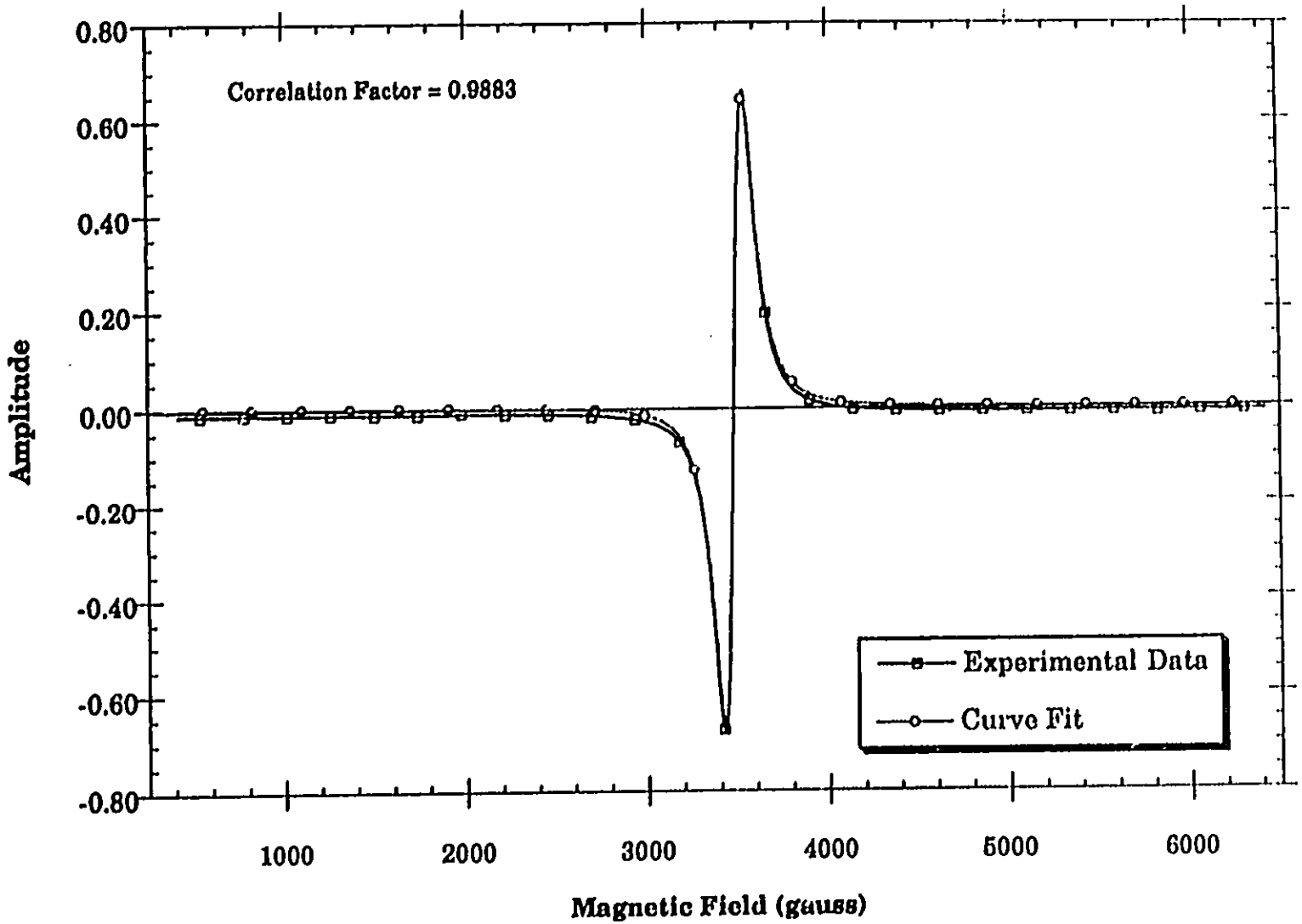

C15 ESR linshape of Mn_2SiS_4 at 109.7 K fitted with 1 LD.